ISSN: 2958-8995. 2958-8987
Doi: 10.59799/APPP6605
No: 6 Val:2 /8/ 2024

Journal of Natural and Applied Sciences URAL

A Quarterly Multidisciplinary Scientific Journal Issued by European Academy for Development and Research / Brussels and Center of Research and Human Resources Development Ramah- Jordan

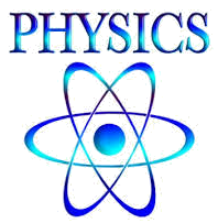

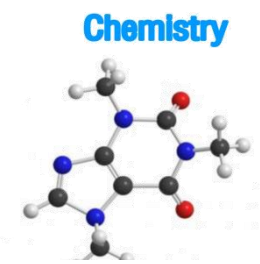

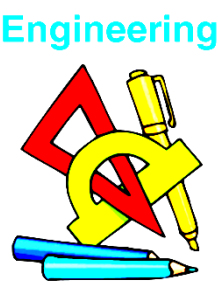

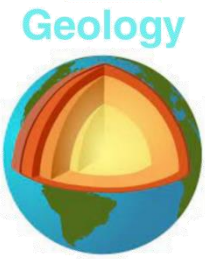

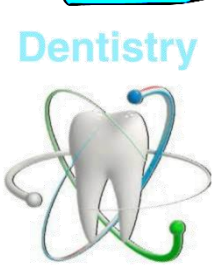

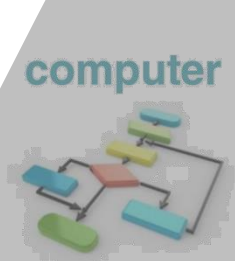

Editorial Team			
Prof. Dr. Ghassan Ezzulddin Arif	**Tikrit University\ College of Education for Pure Science's\ Department of Mathematics.**	**Iraq**	**Editor-in-Chief of the Journal**
Assist. Prof. Baraa Mohammed Ibrahim Al-Hilali	**University of Samarra\ College of Education\ Biology Department**	**Iraq**	**Managing Editor of the Journal**
Asst. inst. Alyaa Hussein Ashour	**University of Mashreq/ College of Medical Sciences Technologies Department of Medical Physics**	**Iraq**	**Editorial Secretary of the Journal**

Prof. Dr. Younis A. Rasheed	**Al-Iraqia University, College of Medicine**	**Iraq**
Assist. Prof. Dr. Hadeer Akram Al-Ani	**Dept. of Public Health Sciences UC Davis School of Medicine**	**USA**
Assist. Prof. Dr. Jawdat Akeel Mohammad Alebraheem	**College of Science Al-Zulfi Majmaah University, Al-Majmaah**	**KSA**
Assist. Prof. Dr. Almbrok Hussin Alsonosi OMAR	**Sebha University**	**Libya**
Assist. Prof. Dr. Saad Sabbar Dahham	**University of Technology and Applied Sciences**	**Sultanate oman**
Assist. Prof. Dr. Marrwa Abdullah Salih	**Tikrit University\ College of Education for Pure Science's\ Department of Mathematics.**	**Iraq**
Mr. Ans Ibrahim Mahameed	**Tikrit University\ College of Education for Pure Science's\ Department of Mathematics.**	**Iraq**

Advisory and Scientific Board			
Prof. Dr. Ahamed Saied Othman	**Tikrit University**	**Iraq**	**Head**
Prof. Dr. Salih Hamza Abbas	**University of Basrah**	**Iraq**	**Member**
Prof. Dr. Leith A. Majed	**University of Diyala**	**Iraq**	**Member**
Assist. Prof. Dr Ali Fareed Jameel	**Institute of Strategic Industrial Decision Modeling (ISIDM), School of Quantitative Sciences (SQS), University Utara (UUM), 06010 Sintok**	**Malaysia**	**Member**

Focus & Scope:

Journal of Natural and Applied Sciences URAL

Journal welcomes high quality contributions investigating topics in the fields of Biology, physics, computer science, Engineering, chemistry, Geology, Agriculture, Medicine, Mathematics, Pharmacy, Veterinary, Nursing, Dentistry, and Environment.

Publication specializations in the journal	
Biology	**Chemistry**
Physics	**Geology**
Computer	**Agriculture**
Engineering	**Mathematics**
Medicine	**Pharmacy**
Veterinary	**Dentistry Veternity,**
Environment	**Nursing**

The Journal is Published in English and Arabic

General Supervisor of the Journal

Prof. Dr. Khalid Ragheb Ahmed Al-Khatib

Head of the Center for Research and Human

Resources Development Ramah – Jordan

Managing Director:

Dr. Mosaddaq Ameen Ateah AL – Doori

Linguistic Reviewer Team

Prof. Dr. Lamiaa Ahmed Rasheed

Tikrit University/College of Education for Women

Asst. Prof. Ahmed Khalid Hasoon

Tikrit University/ College of Education for Women

Asst. Prof. Dr. Mohammad Burjess

Tikrit University/ College of Education

Administrative Title of the Journal:

Amman\ Jordan\ Wasfi Al-Tal \ Gardens

Phone: +962799424774

Supra Ring for Arithmetic Ring

Mohammed S. Jassim[1], Sinan O. Al-Salihi[2]

[1,2]Department of Mathematics, College of Education for Pure Science,
Tikrit University, Tikrit, Iraq

Supra Ring for Arithmetic Ring

Mohammed S. Jassim[1], Sinan O. Al-Salihi[2]

[1,2]Department of Mathematics, College of Education for Pure Science, Tikrit University, Tikrit, Iraq

Emails: [1]mohammed.s.lasim@st.tu.edu.iq; [2]somar@ tu.edu.iq

Abstract. In this paper, we will give proof of the below theorem :Any supra ring for the arithmetic ring is also arithmetic ring and study the converse of he this theorem, also we prove the theorem: The ring R is arithmetic ring if and only if $R_{s(M)}$ arithmetic ring for each maximal ideal M in R and some other propositions related them

Keywords: Multiplication ideal, Multiplication ring, Arithmetic ring, Integrally closed, Prüfer ring, Regular ideal, Invertible ideal.

1-Introduction.

All rings are commutative with 1. An ideal A of a ring R is called multiplication ideal if for every $B \subseteq A$ ideal there exists an ideal Csuch that $B = AC$, and a ring R is called a multiplication ring if all its ideals are multiplication ideals. We give proof the following theorems:

1-Any supra ring for the arithmetic ring is also arithmetic ring.

2- The ring R is arithmetic ring if and only if $R_{s(M)}$ arithmetic ring for each maximal ideal M in R.

3- Every arithmetic ring is integrally closed ring.

4- If R is arithmetic ring, then every supra ring for a ring R is arithmetic ring also.

5- The ring R is arithmetic ring if the ring $R_{s(M)}$ is arithmetic ring for each maximal ideal M in R.

2. Supra ring

Definition 2.1: The ring R is called arithmetical ring if each finitely generated ideal in R is multiplication ideal.

Definition 2.2 : $R`$ is said to be a supra ring for the ring $R$ if $R`$ it is any ring such that $R \subseteq R` \subseteq K$ where K is total quotient ring for the ring R .

Remark 2.3 : If R is integral domain and $R`$ is supra ring for $R$, then $R`$ is also integral domain and K is total quotient ring for $R`$ and it is for the ring R .

It is clear by Remark is based on the concept of ring $R_{s(P)}$. Therefore it is useful to give a brief idea about these rings [8] before giving the above proof.

Let X be multiplicative closed set and not contains zero, If P is prime ideal in R , we will write $S(P)$ instead of $S(R-P)$, then $S(P)$ is multiplication closed set in R, and we denote for $S(P)^{-1}R$ by $R_{s(P)}$ for ease of writing . Note that $R_{s(P)}$ for any prime ideal P is supra ring for the ring R . And also $M_{s(M)}$ is maximal regular and unique in the ring $R_{s(M)}$ for each maximal regular ideal M in R [8]. It's useful to note that $R_{s(P)} = R_s$ in case P is ideal not regular, where R_S is total quotient ring for R.

Proposition 2.4: Let R be a ring and let I be finitely generated ideal in R, if $I_{s(M)}$ is principal ideal for each maximal ideal M in R, then I is multiplication ideal.

Proof: Same steps of proof [9]

Definition 2.5: An element a in a ring R is said to be integral over another ring $R`$ if it satisfies a monic polynomial equation with coefficients in $R`$.

Definition 2.6: Let R be a subring of the ring $R`$, if each element in $R`$ is integral element on R, then we said that $R`$ is integral ring on $R$. Also, if the only elements of $R$ are $R`$ that is integral on R, we say that R is integrally closed in $R`$.

Definition 2.7[3]:A ring R is called a Prüfer ring if every finitely generated regular ideal is invertible.

Theorem 2.8 : Every arithmetic ring is integrally closed ring.

Proof : Let R be arithmetic ring, then R is by Prüfer ing, we know that every Prüfer ing is integrally closed ring [10].

Therefore arithmetic ring R is integrally closed ring.

Proposition 2.9 : If R is arithmetic ring, then every supra ring for a ring R is arithmetic ring also.

Proof : Let $R`$ be supra ring of arithmetic ring R this means

$R \subseteq R` \subseteq R_S$ where $R_S$ is total quotient ring of the ring $R$. To proof $R`$ is arithmetic ring, let $I = (a, b)$ be an ideal generated by a and b in $R`$, where $R`$ subset of R_S, so we can take the elements of I as elements located in R_S. Therefore it can be written as follows

$I = (\frac{a}{s}, \frac{b}{t})$ where $a, b \in R, \quad s, t \in S$

Since R arithmetic ring, then the ideal generated by two elements a and b, suppose $J = (a, b)$ is multiplication ideal then there exist 2x2-atrix M and coefficients in R and let

$M = \begin{pmatrix} r & w \\ u & v \end{pmatrix}$, such that

1- $(a, b) = (a, b)\begin{pmatrix} r & w \\ u & v \end{pmatrix}$

2- $Tr\ M = r + v = 1$

Now let $M` = \begin{bmatrix} r & \frac{s}{t}w \\ \frac{t}{s}u & v \end{bmatrix}$, it is clear that $\left(\frac{a}{s}, \frac{b}{t}\right) = (\frac{a}{s}, \frac{b}{t})\begin{bmatrix} r & \frac{s}{t}w \\ \frac{t}{s}u & v \end{bmatrix}$

and $TrM` = TrM = r + v = 1$, thus I is multiplication ideal in the ring R (proposition 4) in [7] . Therefor R is arithmetic ring (proposition 3) in [7].

The question about the converse of this result can be answered by formulating the following proposition:

Proposition 2.10: The ring R is arithmetic ring if the ring $R_{s(M)}$ is arithmetic ring for each maximal ideal M in R.

Proof : let M be a maximal ideal in R and let A and B be finitely generated ideal in R then $A_{s(M)}$ and $B_{s(M)}$ finitely generated ideal in the ring $R_{s(M)}$. Since $R_{s(M)}$ is arithmetic ring then $A_{s(M)} : B_{s(M)} + B_{s(M)} : A_{s(M)} = R_{s(M)}$ (see theorem 8) in [7].

This means $(A : B)_{s(M)} + (B : A)_{s(M)} = R_{s(M)}$. By proposition 3 in [7], we get $A : B + B : A = R$.

Therefore R is Arithmetic ring (theorem 8) in [7].

Theorem 2.11: The ring R is arithmetic ring if and only if $R_{S(M)}$ is arithmetic ring for each maximal regular ideal M in R.

Proof : By proposition (2.9) and proposition (2.11) .

References

[1] Al-Yassiri Akeel Ramadan Mehdi (2019) *Algebra (Ring Theory)*.

[2] Ali, M. M. (2021). A Remark on Arithmetical Rings. *International Journal of Algebra*, 15(4), 259-264.

[3] Anderson, D. D. (1976). Multiplication ideals, multiplication rings, and the. ring R (X). *Canadian Journal of Mathematics*, 28(4), 760-768.

[4] Anderson, D. D. (2000). Some remarks on multiplication ideals, II. *Communications in Algebra*, 28(5), 2577-2583.

[5] Alsuraiheed, T., & Bavula, V. V. (2019). Characterization of multiplication commutative rings with finitely many minimal prime ideals. *Communications in Algebra*, 47(11), 4533-4540.

[6] Anderson, D. D., & Pascual, J. (1987). Regular ideals in commutative rings, sublattices of regular ideals, and Prüfer rings. *Journal of Algebra*, 111(2), 404-426.

[7] Mohammed S. J., Sinan O. Al-Salihi (2024). Some ramarks on arithmetic rings, to apper.

[8] Larsen, M. D. and P. I. McCarthy, (1971) *Multiplicative Theory of Ideal*, Academic press, New York a London.

Digraph of Some Finite Commutative Rings with Identity

Delbrin K. Rabaty[1], Sinan O. Al-Salihi[2]

College of Education for Pure Sciences\ Tikrit University\ Tikrit – Iraq[1,2.]

[1]dk230007pep@st.tu.edu.iq

[2]somar@tu.edu.iq

Digraph of Some Finite Commutative Rings with Identity

Delbrin K. Rabaty[1], Sinan O. Al-Salihi[2]

College of Education for Pure Sciences\ Tikrit University\ Tikrit – Iraq[1,2.]

[1]dk230007pep@st.tu.edu.iq

[2]somar@tu.edu.iq

Abstract:

This study employed a unique approach to analyze the relationship between the vertices of a directed graph in order to investigate different characteristics of the directed graph of a finite commutative ring for short (R)=Z_n, n is a natural number. Specifically, we utilized a mapping function "$\varphi: R^2 \to R^2$ such that $\varphi(a,b) = (a + (-b), a.b)$". Where the path is analyzed and its distinctive characteristics are inferred, and introduced novel concepts for the ideal graph based on this new definition.

Keywords: Digraph, Ring, Path, Commutative Ring, Ideal.

1. Introduction

A diagram consisting of several points, usually shown as little circles or dots, connected by lines or curves, may be effectively used on paper to illustrate various structures related to real-world occurrences. For example, the points on the graph can represent various cities within a nation [1]. A line uniting two points on a graph that does not cross a third point might signify that there is direct air service between the two cities those points represent. Commutative ring theory is not only a fascinating and sophisticated subject in and of itself, but it also serves as a basis for algebraic geometry and complicated analytical geometry [2]. Cayley tables are utilized in group theory research, especially in the early phases of the study, to offer a straightforward visual representation of the group structure [3]. Although two tables are required to wholly describe the rings, since it have both an additive and multiplicative build. It's better to have a single visual depiction of a ring that keeps its build than two. Using graph theory, can make a digraph performance of a ring, as intended by Lipkovski in [4,5]. Istvan Beck developed the notion of linking a commutative ring to a graph [6]. He presented a diagram $\Gamma(\mathrm{R})$, whose vertices were R's elements, along with two separates . Therefore, the use of the graph theory was enough and sufficient for this purpose.

In this research, we represent the finite commutative ring with identity by the graph $\varphi(\mathrm{R})$ which we know in the form "$\varphi(\mathrm{R}): (x,y) \to (x + (-y), x \cdot y), \forall\, x, y \in \mathrm{R}$" for example [as Shown in Fig.1].

In section 2, the background information wanted to comprehend the article is mentioned.

In section 3, path and cycle and conclude through the graph of the ring a set of properties and corollary with proofs is studied.

In section 4, the focus will be the ideals and Some of them, and the pleasant properties will be seen that can be deducted and demonstrated by smoothly proven.

2. Background

Definition 2.1: A ring R is a nonempty set with two binary operations, addition " $+$ " and multiplication " $\cdot$ ", such that $\forall\ a, b,$ and c in R [7]:
1. $a + b = b + a$.
2. $(a + b) + c = a + (b + c)$.
3. $\forall a \in \mathrm{R}$ such that $a + 0 = a$.
4. $\forall a \in \mathrm{R}, \exists\ b \in \mathrm{R}$ such that $a + b = 0$.
5. $a(bc) = (ab)c$.
6. $c(a + b) = ca + cb,$ and $(a + b)c = ac + bc$.

If multiplication in a given ring R is abelian, then it said to be *commutative*. That is, $\forall\ x, y \in \mathrm{R}, xy = yx$. R is called have *identity* if there is $1 \in \mathrm{R}$ such that $x \cdot 1 = x, \forall x \in \mathrm{R}$. In general, R means a commutative ring with identity, except if else mentioned. Although graphing just finite rings is possible, results are given for all rings, except if else mentioned.

Definition 2.2: A *subring* of R is defined as S being a ring under the operation generated from R, if R is a ring and $\mathrm{S} \subset \mathrm{R}$. As a result, S will own the 0 from R, while S may or may not own the identity 1 [8].

Definition 2.3: If there is a nonzero x in a commutative ring R such that $ax = 0$, then an aspect *a* of that ring is referred to be a *zero divisor* $Z(\mathrm{R})$ [7].

Definition 2.4: If R is commutative, contains $1 \neq 0$, and has no zero divisor, then R is an *integral domain* [7].

Definition 2.5: The set of ordered pair (V, E) that satisfy the property, that $\mathrm{E} \subset \mathrm{V}^2$ of un-ordered pairs of V is called a *graph* G. The sets of *vertices* and *edges* of G are denoted by the letters V and E, respectively. An edge (x, y) joins vertices x and y [3].

Definition 2.6: A graph G is referred to as *directed* if its edges are ordered pairings of vertices. An arranged duo (a, b) is aimed from a to b [9].

Definition 2.7: A graph H is a *subgraph* of a graph G if every vertex and edge in graph H is also present in graph G [3].

Definition 2.8: The connected subgraph of G that is maximum in terms of the connectedness property is called a *maximal connected subgraph* (*component*) of G [9].

Definition 2.9: An alternating series of vertices and edges,
$v_1 e_1 v_2 e_2 \ldots v_n e_n v_{n+1}$ with $n \geq 0$, is called the *walk* in a graph. If $v_1 = v_{n+1}$ then the walk is *closed*. The walk's length is equal to the number of edges. Trivial walks are those that have no length [9].

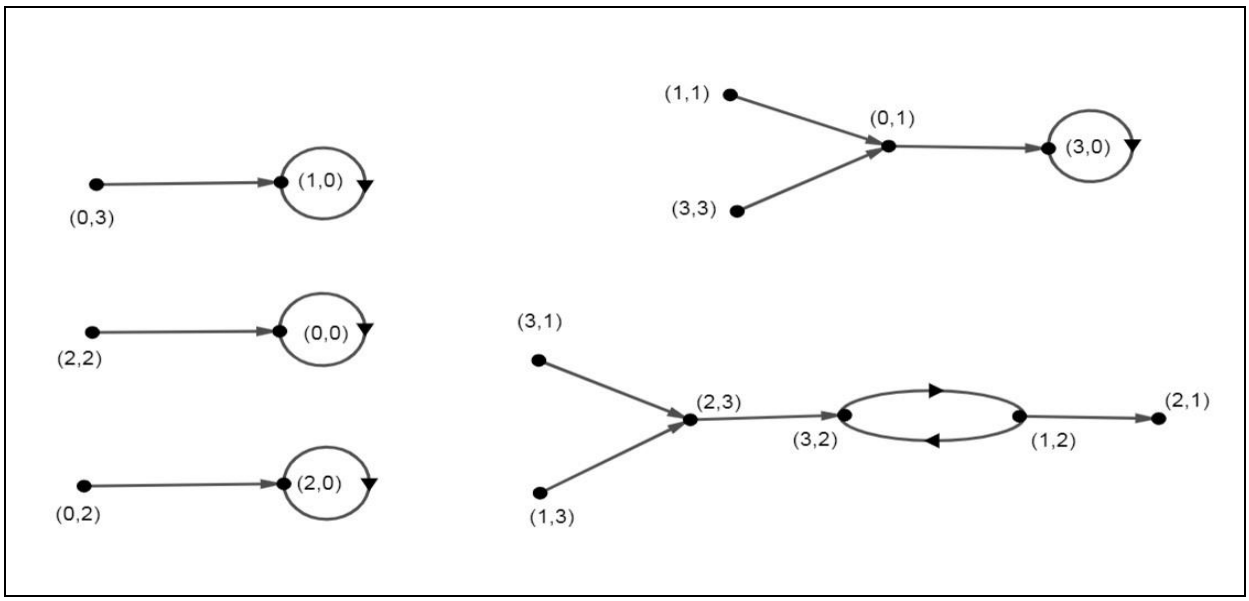

Figure 1: $\varphi(Z_4)$

3. Features of Path for Rings

The idea of a "path" is one of the core ideas of graph theory. A graph's path is a series of vertices joined by edges between every pair of neighboring vertices. Paths provide the systematic way of navigating from one vertex to another, revealing essential patterns and connectivity structures within a graph. In the directed graph the edges have a trend. A a path must follow the specified direction of the edges. Conversely, in an undirected graph, where edges do not have trend, a path allows movement between vertices in both directions.

Definition 3.1: A walk without recurring edges is called a *trail*. A walk without recurrent vertices is called a *path*. A *circuit* is a closed path. A *trivial circuit* consists of just one vertex and no edges. The uniqueness amidst a guided walk (path) and a walk (path) becomes crucial for digraphs [3].

Definition 3.2: Let (a_j, b_j), where $1 \leq j \leq m$ are vertices in $\varphi(\mathrm{R})$, then $(a_1, b_1) \rightarrow (a_2, b_2) \rightarrow \cdots \rightarrow (a_m, b_m)$ indicates a *directed walk* in $\varphi(\mathrm{R})$ from (a_1, b_1) to (a_m, b_m), and if (a_j, b_j) are different, then it is a *directed path*. (a_1, b_1) is said to be *upstream* from (a_m, b_m), and (a_m, b_m) is called a *downstream* from (a_1, b_1) [3].

Definition 3.3: If the walk exists between every pair of vertices in the graph, then it said to be *connected*. If there is no other linked subgraph of G that contains *C*, then *C* is a *connected component* of G [4].

Definition 3.4: We refer to an edge as *incident* to a vertex and the vertex as the edge's *endpoint* when an edge connects to it. An edge is referred to as a *loop* edge if it only has one terminus. *Multiple* or *parallel edges* are those that have two or more endpoints in common [4].

Definition 3.5: In a digraph, *in-degree* is the number of edges incident to a vertex, and the number of edges incident from the vertex is *out-degree* [4].

Remark: Note that the out-degree any vertex will always be one in $\varphi(\mathrm{R})$.

Definition 3.6: A non-trivial circuit that only has its start and end vertices repeated is called a *cycle* [5].

Proposition 3.1: A digraph's cycles are either the same cycle or they are separate cycles.

Proof: Suppose *H* and *T* be cycles in $\varphi(\mathrm{R})$. Given that $h \in V(H)$, h indicates several $t \in V(H)$, and given that $h \in V(T)$, h indicates several $t \in V(T)$. However, since t has a single outward degree, it only points to one vertex. Consequently, $h = t \in V(H)$ and $h = \in V(T)$. Maintaining this approach, it can be observed that every vertex outlet of h is an element in both $V(H)$ and $V(T)$. However, because $V(H)$ and $V(T)$ are both cycles, all of

their vertices are outlet from h. $V(H) = V(T)$ implies that H and T belong to the same cycle. This finding suggests that a digraph's cycles are either unique or exactly identical cycle.

Proposition 3.2: In the digraph $\varphi(\mathrm{R})$ there is no path connecting two different cycles.

Proof: Suppose *N* and *M* are distinct cycles in $\varphi(\mathrm{R})$ and $v \in V(N)$ and $w \in V(M)$. By contradiction, let's say that v is downstream from w for any $v \in V(N)$ and $w \in V(M)$. Furthermore, since w's outgoing degree is one, w is unable to point to any element that is not in *N*. Thus, v is not downstream from w as a result.
Let's say that some vertex x, which is external to *N* and *M*, is downstream of both v and w. This suggests that there is a contradiction in that x or any vertex downstream from x has out-degree > 1. So, it is impossible for v and w to be outlet of x. It follows that no exists path from v to w.

Proposition 3.3: Every connected component of $\varphi(\mathrm{R})$ has one cycle.

Proof: Let's say that C has several cycles. Take two examples of cycles in *C*, *N* and *M*. Since *N* and *M* are both in *C*, (proposition 3.2) is contradicted since there is a path of some $v \in V(N)$ to $w \in V(M)$. As a result, C is limited to one cycle.

Proposition 3.4: Suppose $(a,b) \to (h,t) \to (a,b)$ is an instar subgraph then $b = -t$

Proof: Since $(a,b) \to (h,t)$ connected, then $a + (-b) = h$.
Also, since $(h,t) \to (a,b)$ connected, then $h + (-t) = a$.
Therefore, $h + (-t) + (-b) = h \Rightarrow -t + (-b) = 0 \Rightarrow b = -t$.

Proposition 3.5: If $(a_i, b_i) \to (x,y)$, where $i = 1,2,\dots,n$, then $a_i + b_{i+1} = a_{i+1} + b_i$.

Proof: If $(a_i,b_i) \to (x,y)$, then $a_i + (-b_i) = x$, and $a_{i+1} + (-b_{i+1}) = x$.
Therefore $a_i + (-b_i) = a_{i+1} + (-b_{i+1}) \Rightarrow a_i + (-b_i) + b_i + b_{i+1} = a_{i+1} + (-b_{i+1}) + b_i + b_{i+1}$, then $a_i + b_{i+1} = a_{i+1} + b_i$.

Proposition 3.6: If $(x_1,y_1) \to \cdots \to (x_n,y_n)$ be a path in $\varphi(\mathrm{R})$ of length n, then $x_n = x_1 + \sum_{j=1}^{n-1}(-y_j)$, and $y_n = y_1 \prod_{j=1}^{n-1} x_j$.

Proof: Induction provides the proof.
For $n = 2$, it is true, by definition $x_2 = x_1 + (-y_1)$ and $y_2 = x_1 y_1$. We consider that the statement is correct of $n = k$, where $k \in Z^+$. i.e. $x_k = x_1 + \sum_{j=1}^{k-1}(-y_j)$ and $y_k = y_1 \prod_{j=1}^{k-1} x_j$. Next, we demonstrate that the assertion holds for $n = k+1$.
$x_{k+1} = x_k + (-y_k)$ and $y_{k+1} = x_k y_k$, (by definition of φ).
As per to the inductive thesis, $x_{k+1} = x_1 + \sum_{j=1}^{k-1}(-y_j) + (-y_k)$ and $y_{k+1} = y_1 x_k \prod_{j=1}^{k-1} x_j$. Therefore, $x_n = x_1 + \sum_{j=1}^{n-1}(-y_j)$ and $y_n = y_1 \prod_{j=1}^{n-1} x_j$.

Corollary 3.7: Let's assume the cycle $(x_1,y_1) \to \cdots \to (x_n,y_n) \to (x_1,y_1)$ of length n in $\varphi(\mathrm{R})$, then $\sum_{i=1}^{n} y_i = 0$.

Proof: When the length of a path equal to $n+1$, then by (proposition 3.6) $x_{n+1} = x_1 + \sum_{i=1}^{n}(-y_i)$, Furthermore $(x_{n+1},y_{n+1}) = (x_1,y_1)$ since, $(x_n,y_n) \to (x_1,y_1)$. This suggests that $x_1 = x_1 + \sum_{i=1}^{n}(-y_i)$. Therefore, $\sum_{i=1}^{n}(-y_i) = 0$, then $\sum_{i=1}^{n} y_i = 0$.

Corollary 3.8: Let $(x_1,y_1) \to \cdots \to (x_m,y_m) \to (x_1,y_1)$ is an m-cycle in $\varphi(D)$, and D is an integral domain, then $\prod_{i=1}^{m} x_i = 1$.

Proof: By (proposition 3.6), when the length of a path equal $(m+1)$, then $y_{m+1} = y_1 \prod_{i=1}^{m} x_i$. So, $(x_{m+1},y_{m+1}) = (x_1,y_1)$ since, $(x_m,y_m) \to (x_1,y_1)$. This suggests that $y_1 = y_1 \prod_{i=1}^{m} x_i$. Therefore, $\prod_{i=1}^{m} x_i = 1$.

Proposition 3.9: Allow (x_n,y_n) is the end point of a component with a cycle in $\varphi(D)$, then y_n is not equal to zero.

Proof: Let $(x_1,y_1) \rightarrow (x_2,y_2) \rightarrow \cdots \rightarrow (x_n,y_n)$ is a path in a component has a cycle in $\varphi(D)$, and (x_n,y_n) is the end point. To prove $y_n \neq 0$.
Suppose $y_n = 0$, then $(x_n,y_n) = (x_n,0)$. By definition of the ring, $(x_n,0)$ is upstream from itself, then (x_n,y_n) is a loop. Therefore, the path has not a cycle, and it is contradiction, then $y_n \neq 0$. [as shown in Fig. 2].

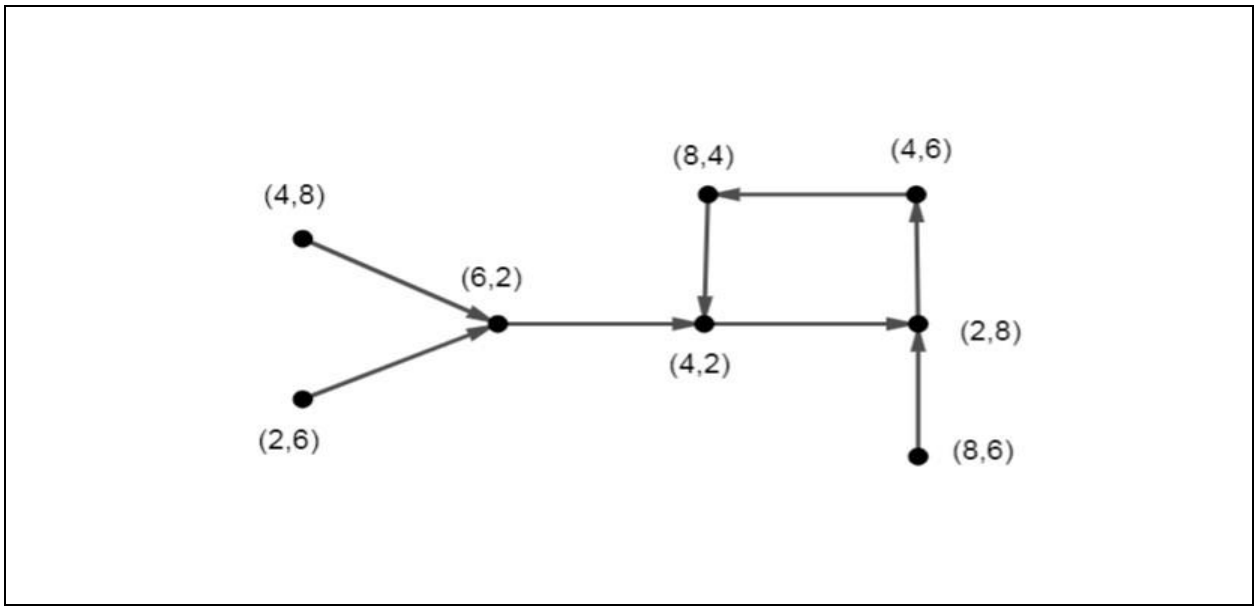

FIGURE 2: A Component Has Cycle In Digraph $\varphi(Z_{10})$

4. Digraphs of Ideals

The ideal of relating a commutative ring to a graph was introduced by Istvan Beck[6]. He introduced a graph, $\Gamma(\mathrm{R})$, whose vertices are the elements of R two distinct vertices x and y are adjacent if and only if $xy = 0$.

Definition 4.1: A *left ideal* of a ring R is defined as a subset I if

- I is an additive subgroup of R, and
- $\forall\, a \in \mathrm{I}$, and $x \in \mathrm{R}$, we have $xa \in \mathrm{I}$.

A *right ideal* is defined by substituting $ax \in \mathrm{I}$ for $xa \in \mathrm{I}$. Often just termed an ideal, a two-sided ideal is a left and right ideal [8].

Definition 4.2: A subring of R is *ideal*(I) if $\forall\, r \in \mathrm{R}, a \in \mathrm{A}, ra$ and ar are in A[10].

Definition 4.3: A *principle ideal* is an I of the ring R produced by a lone element $a \in \mathrm{R}$, and its represented by (a) or $\langle a \rangle$ where "$\langle a \rangle = \{r \cdot a : r \in \mathrm{R}\}$" [2].

Definition 4.4: The *maximal* I of the ring $(\mathrm{R},+,\cdot)$ is a nonzero I if $\mathrm{I} \neq \mathrm{R}$, and no proper ideal of a ring R containing I exists [2].

Definition 4.5: An ideal is called a *prime* if $\forall\, a, b \in \mathrm{R}$ such that $a \cdot b \in \mathrm{I}$, then either $a \in \mathrm{I}$ or $b \in \mathrm{I}$ [8].

Definition 4.6: If $(\mathrm{R}, +, \cdot)$ is a ring the *radical ideal* (*Jacobson ideal*) is denoted by $rad(\mathrm{R})$ or $J(\mathrm{R})$ where [10]:

$$rad(\mathrm{R}) = J(\mathrm{R}) = \cap \{M: M \text{ is a maximal idael of R}\}$$

Definition 4.7: [10] $\sqrt{\mathrm{I}}$ is a *nil radical* of I and is defined as,
$\sqrt{\mathrm{I}} = \{x \in \mathrm{R} : x^n \in \mathrm{I}, \text{for some } n \in Z^+\} = \cap \{p: p \text{ is a prime idael of R}\}$.

Proposition 4.1: If I is an ideal of R, then there is no one vertex in $\varphi(\mathrm{I})$, and one of its parts is not in I.

Proof: Assume that $a, b \in \mathrm{R}$, such that $a \in I, b \notin \mathrm{I}$, and $(a,b) \rightarrow (c,d)$, where $c, d \in \mathrm{I}$, exists. Then by definition of φ $a + (-b) = c$, and this leads to that $b = a + (-c)$. Since $a + (-c) \in \mathrm{I}$ by closure of I, $b \in \mathrm{I}$, which is contradictory. As a result, no vertex can link to $\varphi(\mathrm{I})$, and one of its parts is not in I.

Proposition 4.2: If I is a prime I within the ring R. Then $\varphi(\mathrm{I})$ is a $\bigcup_{i=1}^{n}(C_i)$ where C_i is all connected components of $\varphi(\mathrm{I})$ content in $\varphi(\mathrm{R})$.

Proof: Let's say there are some $a, b \in \mathrm{R}$ such that $a, b \notin \mathrm{I}$ and $(a,b) \rightarrow (x,y)$ where $x, y \in \mathrm{I}$. Then $a \cdot b = y$ by definition of φ. Thus $a \cdot b \in \mathrm{I}$. I is prime, hence this means that there is a contradiction because either a or b belong to I. As a result, no vertex can link to $\varphi(\mathrm{I})$ if both entries are not in I. By (proposition 4.1), no vertex that is not in $\mathrm{I} \times \mathrm{I}$ can be connected to the ideal digraph. Furthermore, since I is closed under ring operations, the vertices outlet of any element in I×I have to be in I×I as well. So, $\varphi(\mathrm{I})$ is a $\bigcup_{i=1}^{n}(C_i)$ in $\varphi(\mathrm{R})$.
About a prime ideal's digraph, there must be a union of linked components rather than just one connected component. As no component has more than one cycle, if $a \in \mathrm{I}, (a,0)$ will cycle on itself, resulting in at least |I| components (Proposition 3.3).

Example 4.1: Let Z_6 be the ring. Z_6 has two unique ideals, $\langle 2\rangle$ *and* $\langle 3\rangle$, because it is a principal ideal ring. In $\varphi(Z_6)$, the digraph $\varphi(\langle 2\rangle)$ consists of three connected components.[As Shown In Fig. 3].

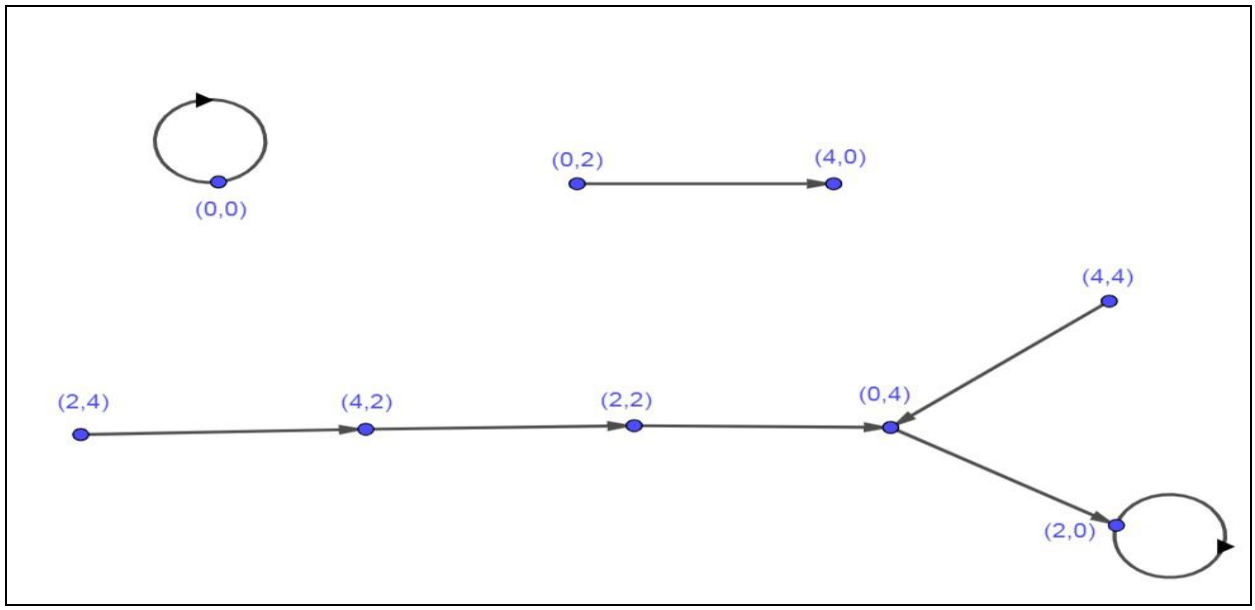

Figure 3: $\varphi(\langle 2\rangle)$ OF $\varphi(Z_6)$

Corollary 4.3: Define Z as the collection of R's zero-divisors. Given that Z is an ideal, $\varphi(Z)$ is a $\bigcup_{i=1}^{n}(C_i)$ where C_i is all connected components of $\varphi(Z)$ content in $\varphi(\mathrm{R})$.

Proof: Assume that $c, d \notin Z$ and that $c \cdot d \in Z$. Then, for some $x \in \mathrm{R}\backslash\{0\}$, $(c \cdot d) \cdot x = 0$, via associativity. Observe that since $d \notin Z, d \cdot x \neq 0$. Then, since $c \cdot (d \cdot x) = 0, c \in Z$, a paradox. Thus, Z is prime, and by (Proposition 4.2), $\varphi(Z)$ is a $\bigcup_{i=1}^{n}(C_i)$.

Remark: It is not necessary for K of R, $\varphi(K)$ to be a $\bigcup_{i=1}^{n}(C_i)$ in $\varphi(\mathrm{R})$ for a non-prime ideal.

Example 4.2 Let's look at (4) in Z_{12}. φ((4)) has several vertices attached to it that are not in $(4) \times (4)$, in contrast to prime ideals. [as Shown in Fig. 4].

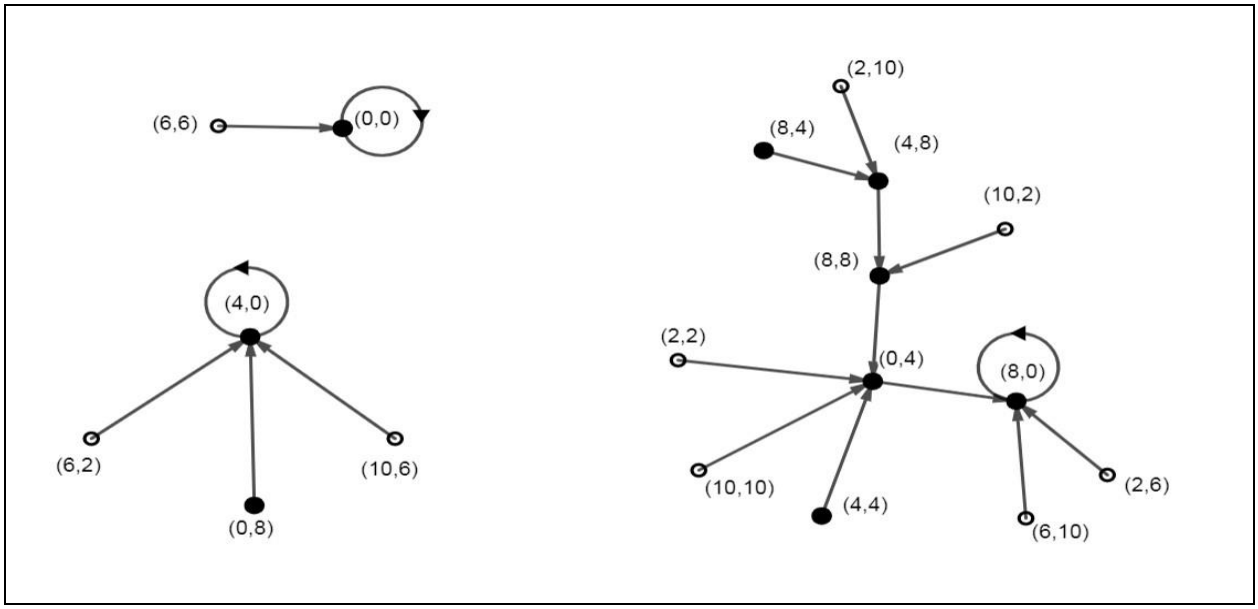

Figure 4: Section Of $\varphi(Z_{12})$ With $\varphi((4))$ Highlighted

Proposition 4.4: Let P_i is a prime I of R and let $\mathrm{I} = \bigcap_{i=1}^{n} P_i$. Then $\varphi(\mathrm{I})$ is a $\bigcup_{i=1}^{n}(C_i)$.

Proof: Let's say that a vertex $(a, b) \notin V(\varphi(\mathrm{I}))$ is linked to $\varphi(\mathrm{I})$. Hence, (a, b) must be a vertex in all $\varphi(P_i)$, as the digraph of each P_i is a $\bigcup_{i=1}^{n}(C_i)$. Because of this, a and b are in $\bigcap_{i=1}^{n} P_i$, which is I. Therefore, $a, b \in \mathrm{I}$, a paradox.

Corollary 4.5: $\sqrt{\mathrm{I}}$ of a ring R, creates a $\bigcup_{i=1}^{n}(C_i)$ in $\varphi(\mathrm{R})$.

Proof: By definition, nil rad $= \cap \{p: p$ is a prime idael of R$\}$. As a result, (Proposition 4.4) leads to the $\bigcup_{i=1}^{n}(C_i)$ in $\varphi(\mathrm{R})$.

Corollary 4.6: A ring's Jacobson radical, represented as $J(\mathrm{R})$, creates a $\bigcup_{i=1}^{n}(C_i)$ in $\varphi(\mathrm{R})$.

Proof: By definition, the intersection of every maximum I in a given R is denoted as $J(\mathrm{R})$. Primitive ideals are maximal aspirations. Thus, (corollary 4.3) leads to the conclusion.

Example 4.3: Suppose $\langle 6 \rangle$ in Z_{18}. Being non-prime I, it is included in the prime I $\langle 2 \rangle$ and $\langle 3 \rangle$. [as shown in Fig. 5].

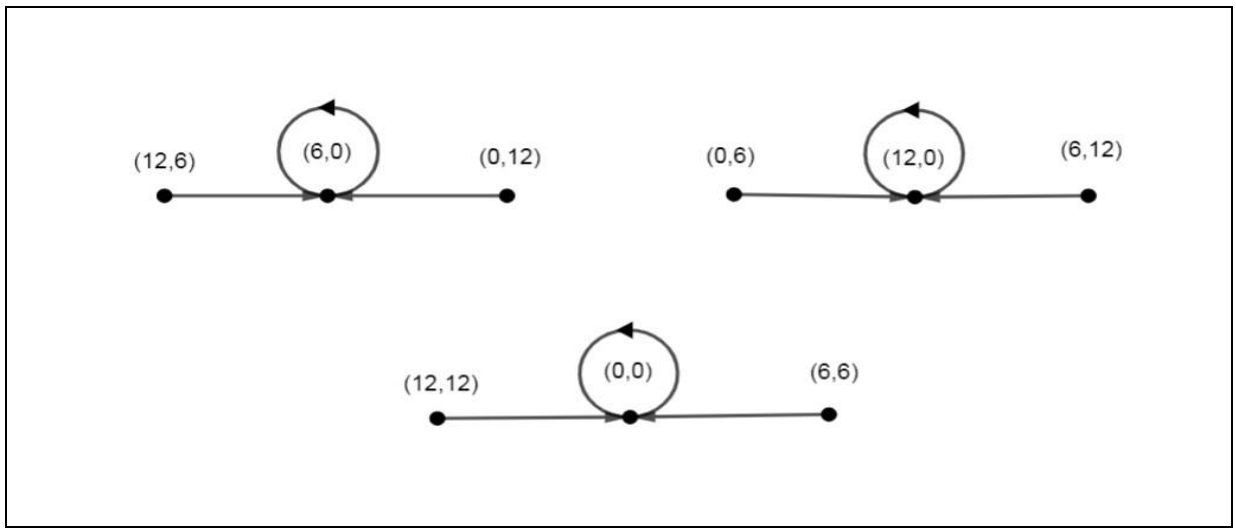

Figure 5: $\varphi((6))$ From $\varphi(Z_{18})$

5. Conclusion

The analysis of digraphs in commutative rings offers a significant insight into the structural connections inside these algebraic systems. By use directed graphs to represent components and processes, we are able to get valuable insights into the interconnections that exist inside the ring. The concept of a digraph in the context of a commutative ring is a valuable tool for visually representing and comprehending the relationships between elements and operations.

Our study yielded valuable results in the form of propositions. These propositions include the statement being disconnected, the out-degree of each vertex being equal to one, the absence of any component containing two cycles, the absence of common points between different cycles. And the presence of each cycle the total of the second coordinate of the vertices is zero $\sum_{i=1}^{n} y_i = 0$.

Conversely, the analysis of the ideals for these rings was conducted using a digraph, revealing that there is no connection between one component and another component. The prime ideal may be represented by a directed graph that is formed by combining all the components that include the elements of the ideal. Additionally, the relationship between the zero divisors of the ring and other relevant factors has been highlighted { $\varphi(Z)$ is a $\bigcup_{i=1}^{n}(C_i)$}. We highly encourage analyzing the digraph associated with these episodes, since many of them may be inferred from other elements, and the attributes of the episode can be interpreted via its corresponding digraph.

References:

[1] L. d. F. Costa and E. K. Tokuda, "A similarity approach to cities and features," *The European Physical Journal B,* vol. 95, no. 9, p. 155, 2022.

[2] A. Chambert-Loir, *(Mostly) Commutative Algebra*. Springer Nature, 2021.

[3] S. Hausken and J. Skinner, "Directed graphs of commutative rings," *Rose-Hulman Undergraduate Mathematics Journal,* vol. 14, no. 2, p. 11, 2013.

[4] C. Ang and A. Shulte, "Directed graphs of commutative rings with identity," *Rose-Hulman Undergraduate Mathematics Journal,* vol. 14, no. 1, p. 7, 2013.

[5] A. T. Lipkovski, "Digraphs associated with finite rings," *Publications de l'Institut Mathematique,* vol. 92, no. 106, pp. 35-41, 2012.

[6] D. KALAMANI and C. MYTHILY, "S-PRIME IDEAL GRAPH OF A FINITE COMMUTATIVE RING," 2023.

[7] J. Gallian, *Contemporary abstract algebra*. Chapman and Hall/CRC, 2021.

[8] R. Lal, *Algebra 2: Linear Algebra, Galois Theory, Representation Theory, Group Extensions and Schur Multiplier*. Springer, 2017.

[9] R. C. Alota and E. L. Enriquez, "On disjoint restrained domination in graphs," *Global Journal of Pure and Applied Mathematics,* vol. 12, no. 3, pp. 2385-2394, 2016.

[10] M. Jinnah and S. C. Mathew, "Ideal based graph structures for commutative rings," *Cubo (Temuco),* vol. 24, no. 2, pp. 333-341, 2022.

البيان الموجه لبعض الحلقات التبادلية المنتهية ذات المحايد

Delbrin K. Rabaty[1], Sinan O. Al-Salihi[2]

قسم الرياضيات/ كلية التربية للعلوم الصرفة/ جامعة تكريت/ تكريت-العراق

[1]dk230007pep@st.tu.edu.iq

[2]somar@tu.edu.iq

المستخلص:

استخدمت هذه الدراسة طريقة أخرى لتحليل العلاقة بين رؤوس الرسم البياني الموجه من أجل دراسة الخصائص المختلفة للرسم البياني الموجه للحلقة التبادلية المحدودة $R = Z_n$ حيث n عدد طبيعي. على وجه التحديد، استخدمنا في هذا البحث الدالة $\varphi: R^2 \to R^2$ بحيث $\varphi(a,b) = (a + (-b), ab)$ لكل من $a, b \in R$ لأرتباط الرؤوس المتجاورة. حيث يتم دراسة المسار واستخلاص خصائصه المميزة، كما و يتم تقديم أهم ما يميز الرسم البياني للحلقة المثالية منها المثالي البسيط و المثالي الابتدائي و غيرها من المثاليات الأخرى بناءً على التعريف المطروح قيد دراستنا.

DEVELOPPEMENT AND ANLYSIS OF BRAIN TUMOR SEGMENTATION AND CLASSIFICATION USING DEEP LEARNING ALGORITHMS

Ahmed Ramzi Rashid
College Of Political Science,

Mustansiriyah University, Baghdad, Iraq

ahmedramzi@uomustansiriyah.edu.iq

Ahmed Sedeeq Baker Northern Technical University / Technical Institute Al-Dour
ahmed.sb@ntu.edu.iq

Zaydon L. Ali

College Of Political Science,

Mustansiriyah University, Baghdad, Iraq

zaydonlatif@uomustansiriyah.edu.iq

DEVELOPPEMENT AND ANLYSIS OF BRAIN TUMOR SEGMENTATION AND CLASSIFICATION USING DEEP LEARNING ALGORITHMS

Ahmed Ramzi Rashid[0000-0003-3674-0097]
College Of Political Science,
Mustansiriyah University, Baghdad, Iraq
ahmedramzi@uomustansiriyah.edu.iq

Ahmed Sedeeq Baker Northern Technical University / Technical Institute Al-Dour
ahmed.sb@ntu.edu.iq

Zaydon L. Ali [0000-0003-3480-7198]
College Of Political Science,
Mustansiriyah University, Baghdad, Iraq

Abstract

Among brain tumors, gliomas are the most common and aggressive, having extreme variations in shape, size, and appearance. Automatic and reliable segmentation methods are important because the large amount of data produced by MRI prevents manual segmentation in a reasonable time. In this study we aim to develop a deep learning model using a 2D UNet and 3D UNet with adaptations in the preprocessing, training and testing strategies. In addition to this, we created an ensemble of multiple models trained with different hyper-parameters that are used to reduce random errors from each model and yield improved performance. Given the limited computational power, 2D UNet and 3D UNet architectures are implemented where each model performs better than the other in its own aspects. Furthermore, the ensemble provides better results. This added attention helps locate the brain more accurately, while improved data augmentation and regularization boosts the performance. We also employ 2DUNet and Mobile-UNet with regularized weighted-class loss function for tumour segmentation. The best results are shown by 3DUNet with 97.2% accuracy, 97.1% specificity and 96.8% sensitivity for detection and 3DUNet with a dice score of 96% and 83% IoU for segmentation.

Keywords: — Brain tumour, Attention network, U-Net, BraTS2020, Multi- scale features, Deep supervision

INTRODUCTION

Weather conditions determining starts with a steady perception of the situation with the air for a specific site and its environmental elements. Temperature, gaseous tension, dampness, precipitation, dissipation, mugginess, wind speed, wind course, and other barometrical elements should be checked and recorded. The World Meteorological

Association offers the establishment for noticing stages like radars, satellites, and surface climate perceptions, which help in the observing of different climate factors. The Public Maritime and Environmental Organization (NOAA) is the sole approved backer of serious weather conditions watches and admonitions in the US, and it is generally viewed as the forerunner in precise weather conditions estimates and lifesaving alerts.

Weather conditions stations incorporate a thermometer and an indicator. Different sensors evaluate environmental factors, for example, wind speed, wind heading, dampness, and precipitation sum. These hardware are put at different areas to evaluate the air boundaries of that area. Climate information is gathered by 15 satellites, 100 fixed floats, 600 floating floats, 3,000 planes, 7,300 boats, and around 10,000 land-based stations, as indicated by the WMO. The Mechanized Surface Noticing Framework is the name given to the authority weather conditions stations used by the Public Weather conditions Administration (ASOS). As they fly through the air, radiosondes measure environmental properties like temperature, tension, and stickiness. Wind speed and heading can be gotten by following radiosondes in flight.

Various meteorologists and cautioning focuses gave themselves to this concentrate throughout the past hundred years, making progresses in observational innovation, heightening physical science, air climate communications, the environmental limit layer and air-ocean interface, sea reactions, and estimating strategies [11]. In any case, huge issues with prescient capacities persevere, especially with TC beginning, power, and hazard determining. As a rule, the most unmistakable hurricane dynamical estimate models have low precision, inferable from incorrect vortex introduction of TCs, deficient depiction of muddled actual cycles, and coarse goal [12,13].

As per some exploration, erroneous portrayals of the air-sea energy stream under very high wind speed conditions would make it challenging to imitate the power of TCs effectively [14]. Moreover, there is a wide agreement that upper sea input has huge effect on TCs, albeit hardly any functional mathematical estimate models consider it, diminishing model execution [15,16]. Moreover, different strategies, as measurable models, can't of managing the confounded and nonlinear connection between TC-related factors; subsequently, their conjecture results should be upgraded further [17–18]. Researchers have as of late explored the utilization of AI (ML) to examine satellite, radar, in-situ information, and different sources to further develop TC anticipating abilities. In light of their purposes, AI calculations can be arranged as man-made brainpower (man-

made intelligence) in three ways: highlight choice, gathering, and relapse or grouping [19]. Feature selection algorithms can use attribute selection to exclude extraneous attributes from tasks, increasing task effectiveness and model correctness. A typical Exhaust disintegration strategy, for instance, can handle spatio-fleeting issues that the exemplary tensor deterioration calculation can't [20]. A grouping calculation, which can consequently segment an example dataset into numerous classifications, is one of the early methodologies utilized in design acknowledgment and information mining. This has various purposes in enormous information examination. The limited blended model (FMM) [21], progressive grouping [22], and K-implies technique are instances of normal bunching calculations.

In this thesis, we assembled a weather prediction model that successfully anticipate the weather. Our model is concerned with meteorological data in the form of time series, and those data are changed with information where meaningful information is derived using data mining techniques. The data mining system is used to uncover hidden patterns and connect them to the many parameters associated with meteorological conditions. The data now displays a series across time, and weather prediction can be well considered by applying time series mining. Several automated prediction systems on the market are being investigated for providing incorrect information to customers. Several prediction systems on the market lack capabilities and appropriate interface designs. As a result, individuals believe that all prediction systems are the same. To eliminate these misconceptions, our technology will deliver appropriate degrees of prediction while occupants are away from their home. This system will be especially beneficial to people who work irregular hours at their jobs and take frequent vacations. Eventually, a flawed prediction system is destructive to people's assets; it has turned into a drama with people's trust. As a result, we see it as a possibility for working on this platform.

PROPOSED SYSTEM

Our goal was to compare the capabilities of 2D network structure to that of 3D network structure without sacrificing too many computational resources for 3D models while still retaining significant accuracy in an image segmentation challenge. To validate the credibility of a 2D network's performance in comparison to a 3D model, we expand our best proposed model in 3D form, as illustrated in Figure 3, to assess the trade off. As a result, our team project's roadmap is as follows: the goal was to improve the performance

of our benchmark, U-net, by extending the structure of the model with attention and deep supervised mechanisms. To challenge U-dominance net's in image segmentation.

Methodology

With the advent of deep learning in the image recognition domain, a lot of neural net architecture based on convolution neural net are launched every year, hence the accuracy of these algorithm is increasing day by day. Initially these recognition tasks were confined to real world pictures like human, animals and other object and much was not done in the medical domain. However, in recent years a lot of these models are also used for medical domain. A prominent problem statement in this domain is detection and segmentation of Brain Tumors. We implement several architectures used in classification and segmentation for our problem of Brain Tumor Detection and Segmentation and evaluate their performance, additionally we combine image processing and data augmentation techniques to improve quality of data and make our models more generalized. We have worked on two models which are popular for segmentation task because of their complex architecture design, specifically 2D UNet and 3D UNet, which are discussed in this section.

Dataset

We used the BraTS 2015 dataset to train our segmentation model. 1550 MRI image slices of T1 modality were used for training and 165 images were used for testing. The ground truth consisted of 4 classes: Background, Tumour core (TC), Whole tumour (WT) and Enhancing Tumour (ET). The images have been converted to JPG format. Sample images of the input and segmentation ground truth in the dataset are shown below.

(a) Input image **(b)** Ground truth

Figure 1: Segmentation dataset

The location dataset is comprised of uninhibitedly accessible MR pictures separated into two classifications: ordinary and danger. The photos in the assortment were gathered and shared on the web by field experts like specialists and radiologists. There are 253 photographs on the whole, with each picture gathered from a worker patient. Subsequently, the dataset has a disconnected construction. The growth photographs complete 155, while the ordinary examples absolute 98. The picture goal is temperamental, and the picture quality is poor. The photographs were saved in JPG

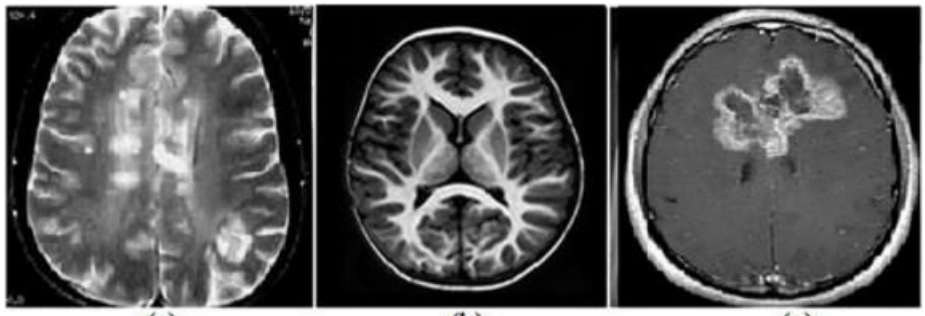

design. These are a few instances of photographs from the dataset's orders.

Figure 2: (a) and (b) normal samples, (c) a tumor sample

Data Preparation

Dataset used in our project is BRATS 2018 [2]. It contains brain MRI of high grade glioma (HGG) patients as well as low grade glioma (LGG) patients, a total amounting to 210 HGG patients and 75 LGG patients. They are stored in nii.gz format,the dataset was handled with the help of SimpleITK module of python. A single MRI has 4 channels, each channel consists of 155 slices and each individual slice is of the dimensionality 240x240. For the 2D UNet, we created three batches, each with 70 MRIs, each MRI is first loaded in the form of a numpy array, and concatenated and rearranged to form a 5 dimensional data (N, 155, 240, 240, 4), N represents the number of patients in each batch. One batch is used for training, and other two for testing. Furthermore, each slice contains redundant information (background) and the volume has few slices which do not have any segmentation. So we have cropped each slice of the volume, as well as reduced few slices of the volume. Finally, for each batch, we get the image in the format (N, 95, 192, 192, 4). The ground truth consists of segmented volume with the labels : 0 for background, 1 for edema, 2 for enhancing tumor, and 3 for non enhancing tumor. At the time of training, one hot encoding was used to split a single segmented volume into 4 channels. Thus, the 2D UNet was trained in a fashion to take in one 4 channel 2

dimensional slice and produce 4 channel 2 dimensional output, each representing segmentation of one of the four channels. As for the 3D UNet, the approach towards dealing with the data completely changes, since now we tend to exploit the correlation between each slice of a mode of MRI as well. For this, after loading the MRI in the form of 5 dimensional numpy array, for a given 4 channel (155, 240, 240, 4) volume, we extract out a (16,160,160,4) volume such that the extracted volume has atmost 95% background and not more, i.e. at least 5% of the segmented ground truth. This is carried out by an iterative algorithm explained as follows :

1) Random (x,y,z) corresponding to 160x160x16x4 volume selected from one hot encoded volume.

2) Check for number of pixels labelled 0 (Background)

3) Check if these pixels account at most 95% of the total pixels.

4) If 95% and current iteration < max iterations, vary the centre coordinates (x,y,z) of the sub volume to get a new one hot encoded volume. Go to step 2. If current iterations > max iterations, go to step 6. 6) Use the same (x,y,z) to get the subvolumes from all the 4 channels. Repeat for each MRI data sample.

Models

We have worked on two models which are popular for segmentation task because of their complex architecture design, specifically 2D UNet and 3D UNet, which are discussed in this section.

2D UNet model

Because of its expertise in conducting image localization by anticipating image pixels by pixel, U-net was originally designed and first utilized for biomedical image segmentation. Its architecture is roughly equivalent to an encoder network followed by a decoder network. Unlike classification, where the final result of the deep network is all that matters, semantic segmentation and regression require not just discrimination at the pixel level, but also a way to project the discriminative features learned at different stages of the encoder onto the pixel space.

1Batch normalization is also implemented in order to diminish the reliance of gradients on the scale of the parameters also to make model less delicate to hyperparameter tuning.

• The encoder is the first half in the architecture diagram, It is usually pre-trained but we had trained this model on our dataset and then applied convolution blocks followed by a maxpool down sampling to encode the input image into feature representations at multiple different levels.

• The decoder is the architecture's second half. The goal is to semantically project the encoder's learned discriminative features (lower resolution) onto the pixel space (higher resolution) to obtain a dense regression. Up sampling and concatenation are used in the decoder, followed by normal convolution operations.

• Instead of Tanh, logistic, arctan or Sigmoid as activation function it uses ReLU function which reduce likelihood of vanishing gradient problem.

• It is faster to train than other deeper designs. Figure 2 depicts the UNet architecture, which consists of two 3 3 convolutions, followed by Rectified Linear Unit (ReLu) and 22 maximum pooling operations with a stride of 2 for the down sampling path. In the Up sampling path, a 2 2 transposed convolution operation was performed to reduce the feature channels. The UNet architecture also includes convolution path Skip connections [5].

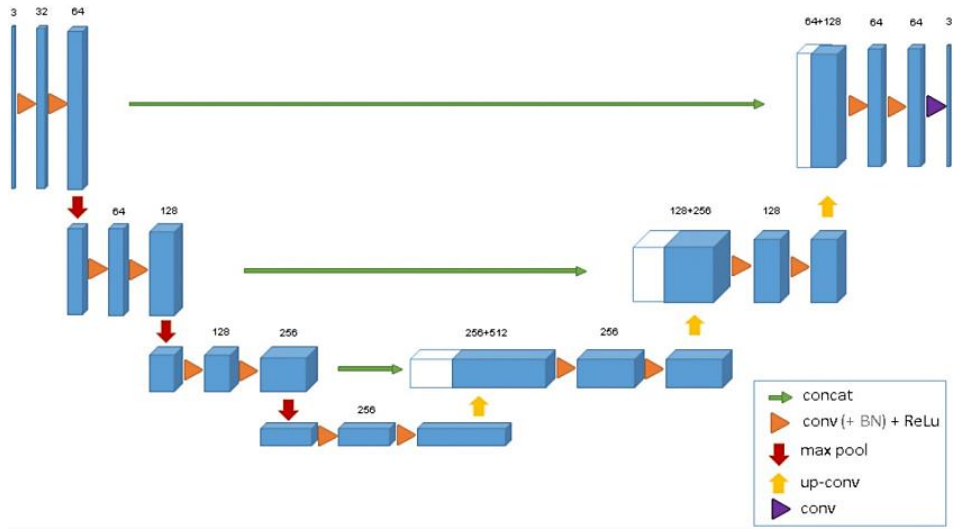

Figure 3:3D UNet model

This connection is used to skip the features from the contracting path to the expanding path in order to recover the spatial feature lost during down sampling operations as shown in figure 4. So, the regression is very fast and accurate when compared with other regression methods. We'd like to up sample it to match the size of the equivalent concatenation blocks from the left. The gray and green arrows indicate where we

concatenate two feature maps together. In this regard, the primary contribution of U-Net is that while up sampling in the network, we also concatenate the higher resolution feature maps from the encoder network with the up sampled features in order to better learn representations with following convolutions.

3D UNet model

Methods for segmenting brain tumors include both generative and discriminative approaches. The most significant advance in this field was made by [2], a 3D CNN that utilizes multi-scale characteristics via parallel paths and integrates a fully connected conditional random field (CRF) to eliminate false positives [10]. FCN is the main architecture for many semantic segmentation tasks. Furthermore, residual connection is used in the UNet, which is called Res-U-Net[4]. This is called DeepLab. DeepLabV3 is another form of DeepLab. They used few convolutional layers in the decoder path. The 3D UNet [6] model essentially makes use of the fact that there exists correlation among the slices of a volume, and thus rather than operating with 2D slices, it essentially operates with 3D volumes by the means of 3D Convolution. 3D U-Net architecture is quite similar to 2D U-Net architecture except for the fact that it takes 3D volumes as input and processes them with corresponding 3D operations, in particular, 3D convolutions, 3D max pooling, and 3D up-convolutional layers.

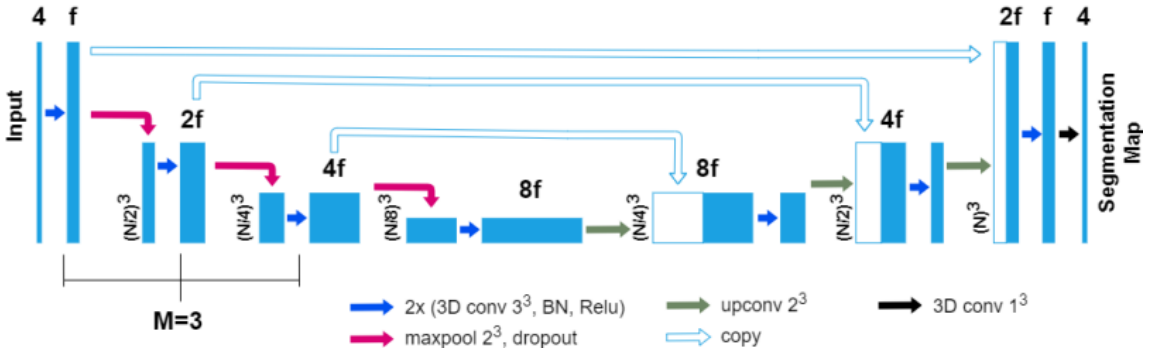

Figure 4: 3D UNet model

The encoder path of the architecture consists of several blocks. The first block consists of 2 convolution layers with number of filters being 32 and 64 respectively, kernel size being (3,3,3). The second block is essentially max pooling block with a stride of 2 and pool size of (2,2,2) to reduce the size from (None,64,160,160,16) to (None,64,80,80,8). The pattern of block 1 and block 2 is repeated, i.e., block 3 and 5 are similar to block 1 but with filter numbers 128,256 and 256,512 respectively, and block 4 and 6 is same as

block 2. The output of block 6 has the shape (None,256,20,20,2). The next block 7 consists of 2 convolution layers with kernel size (3,3,3) and filter numbers being 256 and 512, to obtain an output with shape (None,512,20,20,2).

RESULT AND DISCUSSION

Data

The dataset being referred to is the Multimodal Cerebrum Growth Division Rivalry 2019 (Imps 2019). This assortment contains fMRI pictures of cerebrum growths. It covers 259 glioblastoma (GBM/HGG) and 76 lower grade glioma (LGG) preoperative multimodal X-ray pictures with obsessively affirmed determination and accessible endurance insights. The identification dataset is comprised of openly accessible MR pictures partitioned into two classifications: typical and harm. The photos in the assortment were gathered and shared on the web by field experts like specialists and radiologists. There are 253 photographs on the whole, with each picture gathered from a worker patient. Subsequently, the dataset has a disconnected construction. The growth photographs absolute 155, while the ordinary examples complete 98. The picture goal is unsteady, and the picture quality is poor. The photographs were saved in JPG design. These are a few instances of photographs from the dataset's characterizations.

Prepossessing

The BraTS dataset contains 3D images with a resolution of (240x240x155). Due of computational constraints, the data was reduced to 64x64x41. Because the network does not know if a tumor is HGG or LGG when it receives an input, the two tumor types are mixed into a single dataset. The data is then mixed and divided into three categories: train (70%), validation (15%), and test (15%).

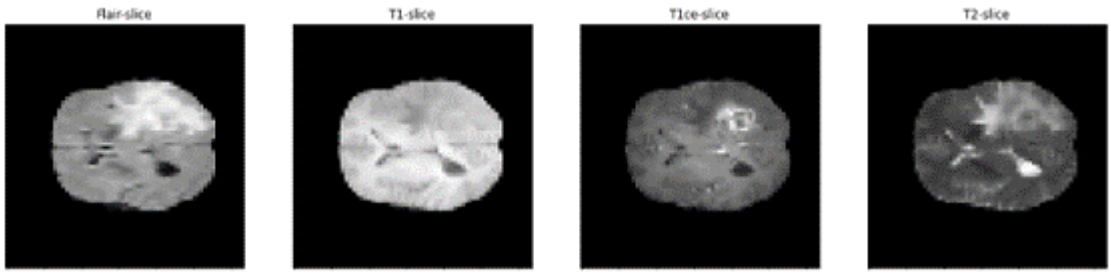

Figure 5: The 4 different type of MRI scans. The images are generated by using BRATS 2019 data

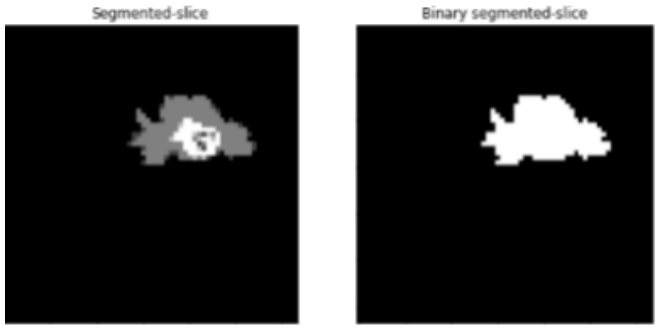

Figure 6: The segmentation masks provided by the dataset, and the binary mask used in this research. The images are generated by using BRATS 2019 data.

The information is then standardized by separating all qualities in the 3D picture by the most elevated esteem and switched over completely to a 2D cut design: every 3D picture was changed over completely to 41 64x64 2D cuts. Moreover, each 2D cut has four channels, one for every one of the four sorts of X-ray checks (T1, T1Gd, T2, and T2-Energy), for a sum of 41 4x64x64 2D cuts for each X-ray filter. Before cutting the information, it was standardized by isolating all qualities by the most elevated esteem in the 3D picture. The division covers were changed over similarly as the 3D pictures, bringing about a 1x64x64 division veil. Besides, as found in figure 4, the division veils were switched over completely to a twofold organization: 0 for every pixel behind the scenes and 1 for any pixel in a cancer.

Models Output

Classification

MRI images of various sizes were resized to 224x224 pixels and normalized. Various transforms as augmentation. Additionally, we perform augmentation techniques to artificially increase the diversity of our dataset in order to increase the dataset size. Transforms like Vertical Flip=0.5, Horizontal Flip=0.5, Random Brightness Contrast=0.3, Shift Scale Rotate=0.5, Shift Limit=0.2, Scale Limit=0.2, Rotate Limit=20° were applied to improve model stability and generalize its ability.

In our experiments, we compare the models using the following metrics: Accuracy (Acc), Sensitivity (Se), Specificty (Sp), F1 score (F1) and Precision (Pr) computed from the confusion matrix with True Positives (TP), False Positives (FP), True Negatives (TN) and False Negatives (FN).

Figure 7: Computed metrics for different implemented models

Architecture	Acc	Se	Sp	F1	Pr
3DUnet	**0.972**	**0.968**	**0.971**	**0.942**	**0.925**
2DUNet	0.889	0.8438	0.9231	0.8852	0.931
Googlenet	0.908	0.846	0.963	0.903	0.965
VGG16	0.931	0.886	0.944	0.949	0.951
Alexnet	0.947	0.893	0.952	0.956	0.941

Segmentation

The segmentation models were implemented in Tensorflow and were run on Tesla K80 GPU for hardware acceleration. The models were trained for a total of 50 epochs with weighted categorical cross entropy as the loss function and with LR scheduling for the optimizer. The weights applied to each class were: Background (1.0), Whole tumour (4.0), Tumour core (15.0) and Enhanced Tumour (10.0). Segmentation models are best understood using the dice and Intersection of Union (IoU) scores. Additionally, the class-wise accuracies are also computed and tabulated.

Table 1 summarizes and compares the metrics obtained for the different implemented models. It is observed that 3DUNet outperforms the other models in all the metrics obtaining a highest dice score of 96% and an IoU score of 83%. 2DUNet had a comparatively lower dice score than UNet as they weren't able to learn the contours very well. Figure 8 shows a graphical comparison of Table 2.

Table 1: Computed metrics for different implemented models

Architecture	Accuracy	Dice	IoU	Background	TC	WT	ET
3DUnet	**0.97**	**0.96**	**0.83**	**0.98**	**0.82**	**0.82**	**0.89**
2DUNet	0.93	0.90	0.78	0.93	0.78	0.76	0.87
PSPNet	0.87	0.87	0.72	0.88	0.73	0.71	0.74
Encoder-Decoder	0.89	0.82	0.71	0.90	0.72	0.71	0.75

Table 2: Comparison of metrics with existing literature

Paper	TC	WT	ET
3DUnet	**0.82**	**0.82**	**0.89**
[8]	0.81	0.72	0.58
[16]	0.88	0.83	0.77
[11]	0.89	0.75	0.72

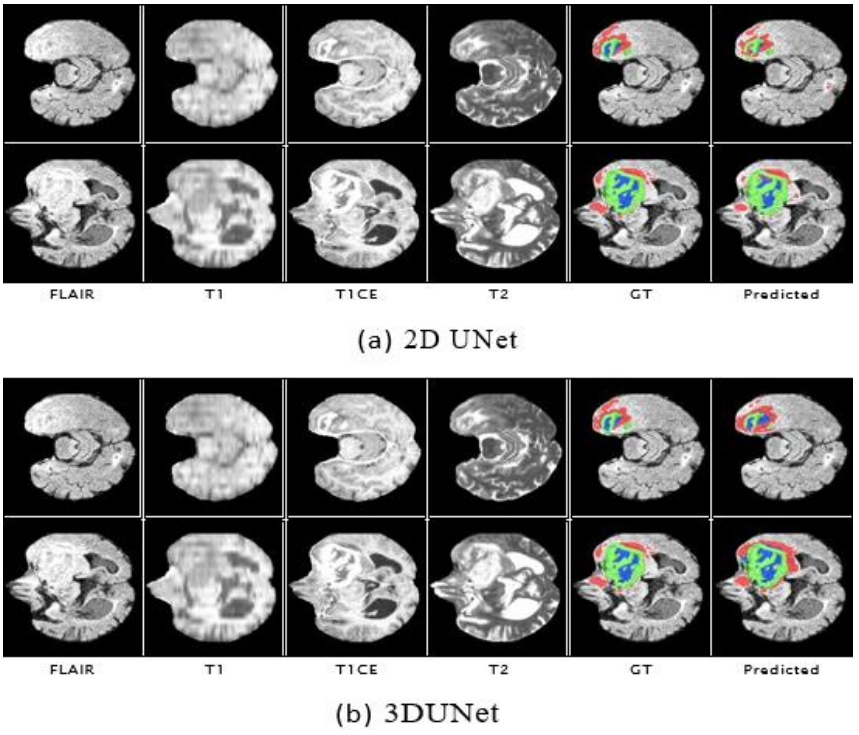

Figure 8: Segmentation results for BraTS 2020 training dataset,

We implemented brain tumour detection and segmentation using state-of-art architecture. We observed that spatial attention with regularized training improved the robustness of classification task using the proposed 2DUNet model. Including hyper column to aggregate the features and residual connections to reduce the negative tendencies improved the performance of the model. We also developed 3DUnet model for segmentation with results better than its contemporary architectures. This was achieved using weighted loss function due to the unbalanced pixel ratio in classes. We observed that the results can be improved with data augmentation indicating the need to increase

the data collection process for a more generalized model. Hence, we establish the superiority of artificial intelligence in tumour detection which can be of great importance for medical community in real-time emergency diagnostics. In the future, efforts can be focused on the combining detection and segmentation into a single architecture, hence mobilizing the diagnosis with more accuracy. The results of segmentation can be used as priori distribution for classification and vice- versa. Combining multi-modal imaging data from multiple views, along with joint registration is prospective direction to work along. This way, the detection models can be made more robust and fast for quick diagnostic results.

CONCLUSION

We implemented brain tumour detection and segmentation using state-of-art architecture. We observed that spatial attention with regularized training improved the robustness of classification task using the proposed 2DUNet model. Including hyper column to aggregate the features and residual connections to reduce the negative tendencies improved the performance of the model. We also developed 3DUnet model for segmentation with results better than its contemporary architectures. This was achieved using weighted loss function due to the unbalanced pixel ratio in classes. We observed that the results can be improved with data augmentation indicating the need to increase the data collection process for a more generalized model. Hence, we establish the superiority of artificial intelligence in tumour detection which can be of great importance for medical community in real-time emergency diagnostics. Subsequently, in the Imps 2020 test for mind cancer division, the expansion of UNet as a spine with the mix of consideration component and profound management, 3DUNet, conveys the best outcome. Furthermore, 3D organization plans for clinical picture division presently can't seem to be completely used because of time imperatives. Later on, we will focus on bringing down model intricacy by utilizing 2D model designs to diminish redundancies, using the potential outcomes of a 3D model engineering, and trying different things with misfortune capabilities to address class irregularity for ideal model execution.

REFERENCES

[1] Bhagyashri Asodekar and Sonal Gore. “Brain Tumor Classification Using Shape Analysis of MRI Images”. In: SSRN Electronic Journal (Jan. 2019). doi: 10. 2139/ssrn.3425335.

[2] Babak Ehteshami Bejnordi et al. “A brain tumor segmentation framework based on outlier detection”. In: . Medical image analysis 8.3 (2004), pp. 275– 283.

[3] Liang-Chieh Chen et al. “DeepLab: Semantic Image Segmentation with Deep Convolutional Nets, Atrous Convolution, and Fully Connected CRFs”. In: IEEE Transactions on Pattern Analysis and Machine Intelligence 40.4 (2018), pp. 834–848. doi: 10.1109/TPAMI.2017.2699184.

[4] Jun Cheng et al. “Correction: Enhanced Performance of Brain Tumor Classification via Tumor Region Augmentation and Partition”. In: PLoS ONE 10 (Dec. 2015). doi: 10.1371/journal.pone.0144479.

[5] Jun Cheng et al. “Enhanced Performance of Brain Tumor Classification via Tumor Region Augmentation and Partition”. In: PLoS ONE 10 (Oct. 2015). doi: 10.1371/journal.pone.0140381.

[6] A Gooya et al. “Joint segmentation and deformable registration of brain scans guided by a tumor growth model”. In: Medical Image Computing and ComputerAssisted Intervention – MICCAI 6892 (2011), pp. 532–540.

[7] Abdu Gumaei et al. “A Hybrid Feature Extraction Method With Regularized Extreme Learning Machine for Brain Tumor Classification”. In: IEEE Access 7 (2019), pp. 36266–36273. doi: 10.1109/ACCESS.2019.2904145.

[8] Mohammad Havaei et al. “Brain Tumor Segmentation with Deep Neural Networks”. In: CoRR abs/1505.03540 (2015). arXiv: 1505 . 03540. url: http : //arxiv.org/abs/1505.03540.

[9] Kaiming He et al. Deep Residual Learning for Image Recognition. 2015. arXiv: 1512.03385 [cs.CV]. [10] Mustafa R. Ismael and Ikhlas Abdel-Qader. “Brain Tumor Classification via Statistical Features and Back-Propagation Neural Network”. In: 2018 IEEE International Conference on Electro/Information Technology (EIT). 2018, pp. 0252– 0257. doi: 10.1109/EIT.2018.8500308.

[10] Konstantinos Kamnitsas et al. “DeepMedic for Brain Tumor Segmentation”. In: Brainlesion: Glioma, Multiple Sclerosis, Stroke and Traumatic Brain Injuries. Ed. by Alessandro Crimi et al. Cham: Springer International Publishing, 2016, pp. 138–149. isbn: 978-3-319-55524-9.

[11] Alex Krizhevsky, Ilya Sutskever, and Geoffrey E Hinton. “ImageNet Classification with Deep Convolutional Neural Networks”. In: Advances in Neural Information Processing Systems. Ed. by F. Pereira et al. Vol. 25. Curran Associates, Inc., 2012. url: https://proceedings.neurips.cc/paper/2012/ file/c399862d3b9d6b76c8436e924a68c45b-Paper.pdf.

[12] Geert Litjens et al. “A survey on deep learning in medical image analysis”. In: Medical Image Analysis 42 (Dec. 2017), pp. 60–88. issn: 1361-8415. doi: 10.1016/j.media.2017.07.005. url: http://dx.doi.org/10.1016/j. media.2017.07.005. [14] McKinney PA. “McKinney PABrain

tumours: incidence, survival, and aetiology". In: Journal of Neurology, Neurosurgery & Psychiatry (2004).

[13] Krishna Pathak et al. "Classification of Brain Tumor Using Convolutional Neural Network". In: (2019), pp. 128–132. doi: 10.1109/ICECA.2019.8821931.

[14] Sérgio Pereira et al. "Brain Tumor Segmentation Using Convolutional Neural Networks in MRI Images". In: IEEE Transactions on Medical Imaging 35.5 (2016), pp. 1240–1251. doi: 10.1109/TMI.2016.2538465.

[15] Olaf Ronneberger, Philipp Fischer, and Thomas Brox. U-Net: Convolutional Networks for Biomedical Image Segmentation. 2015. arXiv: 1505.04597 [cs.CV].

[16] Karen Simonyan and Andrew Zisserman. Very Deep Convolutional Networks for Large-Scale Image Recognition. 2015. arXiv: 1409.1556 [cs.CV].

[17] Zahra Sobhaninia et al. Brain Tumor Segmentation by Cascaded Deep Neural Networks Using Multiple Image Scales. 2020. arXiv: 2002.01975 [eess.IV].

[18] Zahra Sobhaninia et al. Brain Tumor Segmentation Using Deep Learning by Type Specific Sorting of Images. 2018. arXiv: 1809.07786 [cs.CV]

Spectrophotometric Determination of Metoclopramid Hydrochloride by Oxidative Coupling Method in Pharmaceutical Formulations

Nour Alaaalddin Hussein *[1], Hussein Abood Idham [2] , Aliya hussien ahmed[3]

[1,3] College of Education for Girls, Kirkuk University.

[2] Imam Jaafar AI- Sadiq University/Kirkuk ,Dept. of Medical Lab. Technique

**Corresponding author: husainabood88@gmail.com*

Spectrophotometric Determination of Metoclopramid Hydrochloride by Oxidative Coupling Method in Pharmaceutical Formulations

Nour Alaaalddin Hussein *[1], Hussein Abood Idham [2] , Aliya hussien ahmed[3]

[1,3] Dept. of Biology , College of Education for women Kirkuk University, Iraq.

[2] Dept. of Medical Lab. Technique, Imam Jaafar AI- Sadiq University , Iraq.

**Corresponding author: husainabood88@gmail.com*

Abstract:

Using oxidative coupling with N,N-diethyl paraphenylin diamin in the presence of sodium Nitroproside, an oxidizing substance in an alkaline environment, a green dye was formed that dissolved in water and had the highest intensity of absorption at λmax 703 nm. This method of spectrophotometric determination of metclopramid hydrochloride was developed. Beer's law has been followed by the technique, with a molar absorbance of $1.4278*10^4$L.mol^{-1}cm^{-1} sandal within the region of focus of 2–22 mg.ml^{-1}. At 0.02481 mg.cm^{-2} for the index value, 0.2258 µg.ml^{-1} for the detection limit, and a a correlation value of 0.9882 and a relative standard deviation of the technique stays below 3.53%. Using both the direct and conventional addition procedures, the suggested approach was effectively used to determine the amount of metoclopramid hydrochloride in tablets; the recovery percentage varied from 97 to 103%.

Keywords : Metoclopramid hydrochloride, Nitroproside, Spectrophotometer.

1. Introduction

The following structural frame describes the 4-amino-5-chloro-N-(2-diethylaminoethyl)-2-methoxybenzimide mono hydrolysis, which is the scientific name for metoclopramide hydrochloride as shown in figure (1) :

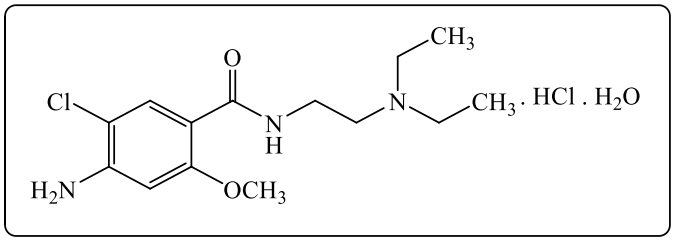

Fig.(1): Structure of metoclopramide hydrochloride

It is a mainly white powder, odorless and quickly soluble in water [1]. It is one of the compounds that is highly receptive to light, so its pharmaceutical preparations are kept in dark containers away from light [2]. This pharmaceutical compound was discovered in 1960 and was prescribed to patients, children and adults, as it is used to prevent Vomiting due to the effect of medications that inhibit the growth of malignant tumors [3]. Various analytical techniques have been used for the determination, including the spectrophotometric method [4,5,7,8], HPLC [6,7,8], and flow-injection technique [6,7,9].

2.Experimental Part

2-1. Techniques

Measurements of spectrophotometry possessed been conducted using the GBC Cintra 6 UV-Visible Visible.

2-2. Chemicals and reagents used

Every chemical and a reagent for analysis utilized in this study is pure and provided by the businesses BDF, Merck, and SDI.

2-3. Preparation of solutions

2-3.a-Standard MCP solution, (1000 µg/ml)

Volumetric flasks contain a volume that has been diluted with distilled water to 100 milliliters after 0.1 gm of MCP was dissolved in the quantity of water.

2-3.b- N,N-diethyl paraphenylin diamin reagent solution (0.02 M)

The preparation of this solution included dissolving 0.2623g of N,N-diethyl paraphenylin diamin in 100 ml with distilled water.

2-3.c-Sodium nitroprosidesolution (0.02 M)

In order to create this solution, 0.2619 grams in 100 milliliters of distilled water inside A flask with volumetric measurements containing dissolved sodium hydroxide.

2-3.d- Sodium hydroxide solution (0.1M)

Volumetric flasks have a volume that was diluted to 100 ml using distilled water after 0.4 g of NaOH was dissolved in that quantity.

2-3.e- Solution of MCP tablets formulation 100 µg/ml

Tablet solution 100 µg.ml-1: Prepare this solution by weighing 10 tablets (10µg Metochlopromaide.HCl/ Tablet) carefully, and after grinding and mixing them, a weight equivalent to 0.01 grams of pure metoclopramide hydrochloride is taken from them and well stirred until dissolved in a little quantity of ethanol. After sifting the mixture and transferring it into a 100 ml volumetric vial, With the use of a 100 ml volumetric vial and distilled water, the capacity was brought to 100 ml. The syrup solution, which included 5 ml of 5 µg of Metochlopromaide.HCl/5 ml, was extracted.

3. Preliminary Investigations

1 ml of sodium nitroproside solution with an accumulation of $1x10^{-2}$ M was added to 2 ml of metoclopramide hydrochloride solution with a concentration of 100 µg.ml^{-1}, then 1.5 ml of the reagent solution N,N-diethyl para-phenylenediamine with a concentration of $1x10^{-2}$ was added, and 3 molar, and a pink-colored product is formed show the oxidation reaction between the drug and the oxidizing agent. Once the additions are completed, when 1.5 ml of sodium hydroxide in an amount of 0.1 molar is added and the solution is left for 10 minutes, a green-colored product was formed. When the colored product's absorption spectrum was compared to the pseudo solution (after being diluted to the proper amount inside a volumetric vial of 25 ml, distilled water), it was discovered that The product with color demonstrated the greatest absorption occurring at 703 nm in wavelength, while the pseudo solution gave no absorption in this range.

4. Optimization of the Experimental Condition

In order to get a colored solution with high absorption the optimal conditions were studied and selected that result in the product generated in the aqueous solution having the maximum absorption.

4-1. Effect of oxidizing agent concentration

This research set out to ascertain the ideal concentration of oxidizing agent, sodium nitroproside (0.02 M), by filling volumetric flasks with varying volumes (0.2–3) of oxidizing agent, 1 ml of reagent solution (0.02 M), and 2 ml of MCP (100 µg/ml). After that, 1.5 ml of (0.1M) NaOH was poured, and when the capacity reached 25 milliliters, distilled water was added. The volume of 1 milliliter was used in the studies that followed since it was the ideal quantity due to its greatest absorbance.

Table(1): Impact of an oxidizing substance quantityOh dear.

ml of 0.01 M Potassium persulphate	Abs.	ml of 0.01 M Potassium persulphate	Abs.
0.2	0.388	1.5	0.489
0.5	0,420	2	0.432
0.7	0.452	2.5	0.409
1	0.501	3	0.399

4-2. Impact of coupling reagent quantity

The impact of the coupling reagent amount was investigated by filling volumetric flasks with varying volumes (0.5– 4(ml) of N,N-diethyl para-phenylenediamine reagent (0.02 M) and 1.5ml of sodium nitroproside (0.02 M). After that, After adding 1.5 milliliters of 0.1M NaOH, distilled water was added to reduce the volume to 25 milliliters.

Table(2): Impact of coupling reagent quantity

ml of Reagent 0.01M	*Abs.*	*ml of Reagent 0.01M*	*Abs.*
0.5	0.107	2	0.510
0.7	0.098	2.5	0.502
1	0.499	3	0.488
1.5	0.506	4	0.478

the outcomes are shown Since it produced the greatest absorption, the volume of 1.5 ml was determined to be the ideal quantity and used in the studies that followed.

4-3. The base's effect

The optimal pH was determined to be 11.6 and 1.5 ml of solution NaOH was used in the trials that followed. The impact of base was investigated by adding NaOH solution (0.3 – 4) ml of 0.1 M. The table(3) displays the findings.

Table (3): The base's effect

ml of base 0.1 M	*Abs.*	*PH*	*ml of acetic acid 0.5 M*	*Abs.*	*PH*
0.3	0.342	10.69	2	0.442	11.62
0.7	0.492	11.21	2.5	0.431	11.68
1	0.498	11.39	3	0.422	11.76
1.5	0.532	11.57	4	0.397	12.03

4-4. Impact of time of oxidation

The time it takes for sodium nitroproside to oxidize metoclopramide hydrochloride was measured using a series of 25 ml volumetric flasks. 2.5 milliliters of the solution, 1 milliliter of sodium nitroproside (1x10-2 M) and 2 milliliters of metoclopramide hydrochloride (100 $\mu g.ml^{-1}$) were added to each container. After 1.5 ml of 0.1 M sodium hydroxide was added, 25 ml of distilled water was used to dilute the reagent, N,N-diethyl para phenylenediamine. The results shown in Table (4) demonstrate that the solutions' absorbance at a wavelength of 703 nm was then assessed in comparison to their pseudo solutions. This table shows that the oxidation may be completed in 10 minutes, and the subsequent experiments used this technique.

Table (4): Impact of Time of Oxidation.

Time	5	10	15	20	25	30	40	45	50	60
Abs.	0.474	0.471	0.489	0.505	0.501	0.492	0.480	0.476	0.474	0.471

4-5. The additions' sequence

A series of experiments were conducted to examine the impact of altering the order in which reactants are added on the colored product's absorption. The table (5) presents the findings of additional tests that were conducted using the

addition II sequence, which was shown to yield the largest absorption of the colored product.

Table (5): The additions' sequence

Order *number*	*Order of addition*	*Abs.*
1	D + R + O + A	0.388
2	D + O + R + A	0.510
3	R + O + D + A	0.322
4	O + R + A + D	0.211
5	O + R + D +A	0.388

4-6. The temperature impact

This study looked at how temperature (between 5 and 60 °C) affected the colored product's absorption; the findings are shown in table (6).

Table (6): **Temperature's impact**

Temp.	5	10	15	20	25	30	35	40	45	50	60
Abs	0.512	0.523	0.536	0.539	0.543	0.541	0.529	0.505	0.464	0.443	0.425

4-7. The stability of the colored product throughout time

It was determined how long the colored result would be stable by mixing 0.7 ml of p-bromoaniline with 1 ml of MCP (100µg/ml), 1.5 ml of sodium nitroproside solution, and 1.5 ml of 0.1 M NaOH. The volume is increased to 25 milliliters in volumetric flasks with distilled water within, and the colored product's absorption value is monitored for at least 40 minutes. The results may be shown in table (7).

Table (7): The stability of the colored product throughout time

Time min	5	10	15	20	25	30	35	40	45	50	60
Abs.	0.511	0.512	0.511	0.512	0.510	0.511	0.511	0.511	0.510	0.508	0.505

4-8. The solvent's impact

Instead of using water for the dilution process, an alternative solvent was used to examine the impact of the solvent on the resulting colored product. The results from the table (8) that include water gives less absorption than the rest of the solvents, while methanol gives the highest absorption. Due to its high price and lack of availability in the markets, they resort to using water due to its abundant use and cheap price.

Table (8): The solvent's impact

Solvent	***Absorbance***	λ_{max}, ***nm***
Ethanol	0.521	703
Methanol	0.342	698
Water	0.725	700

5. Last spectrum of absorption

When MCP is coupled with N,N-diethyl paraphenylenediamine in an alkaline medium with a pH of 11.6 and a temperature of 25 C0, a colored product is formed. The product's spectrum is compared to that of the corresponding blank reagent, which has a few absorbance at λmax and a maxim absorption at 703 nm, as shown in figure (2).

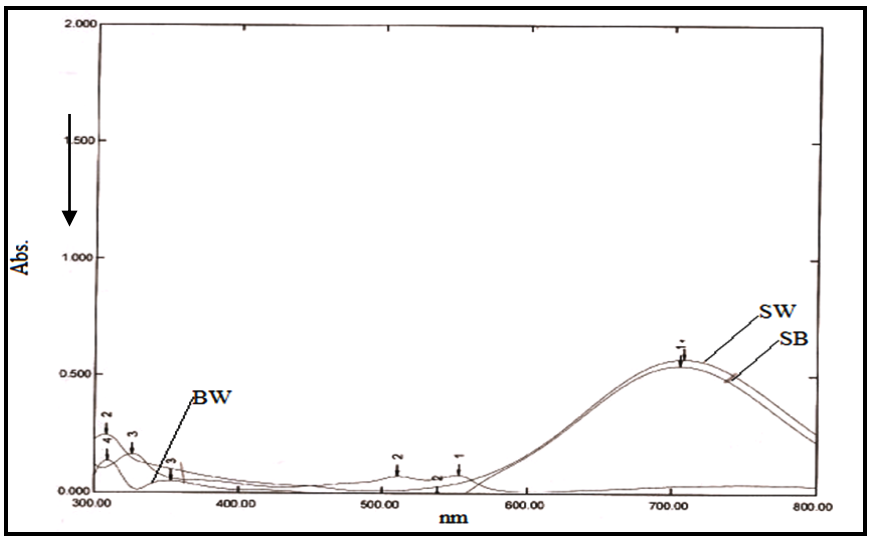

Fig. (2): Last spectrum of absorption of the Determntion PYR

BW: MCP's absorption spectra in comparison to a blank reaction.

SW: MCP's absorption spectra in comparison to distilled water.

SB: Blank reagent absorption in comparison to pure water.

6. The process for creating a calibration chart

A set of 25 ml volumetric vials were filled with progressively larger contents (0.5-5.5 ml). At a wavelength of 703 nm, the absorbance each answer was evaluated in comparison to the pseudo solution. The concentration of beer in metoclopramide hydrochloride solution ranges from 2 to 22 µg/ml-1. Deviation from Beer's law occurs at concentrations of more than 22 $\mu g.ml^{-1}$. The molar absorbance value was determined to be 14278.29 $L.mol^{-1}. cm^{-1}$, with an association value of 0.9882. The Sandel significance value was found to be 0.02481 $\mu g.cm^{-2}$. The calibration curve and absorption spectra that conform to the law are shown in figures (3) and (4).

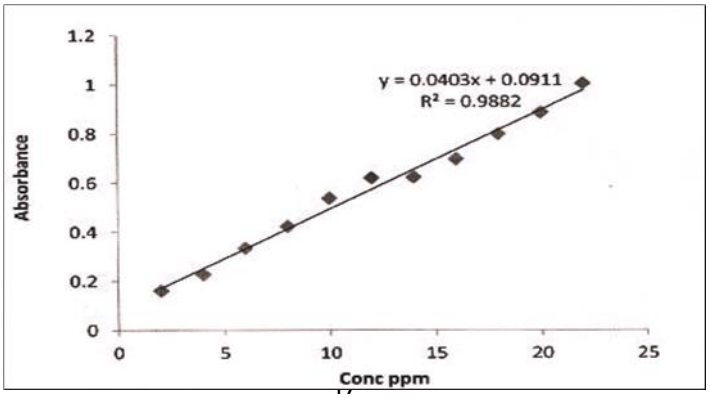

Fig.(3): Calibrating curve for figuring out MCP

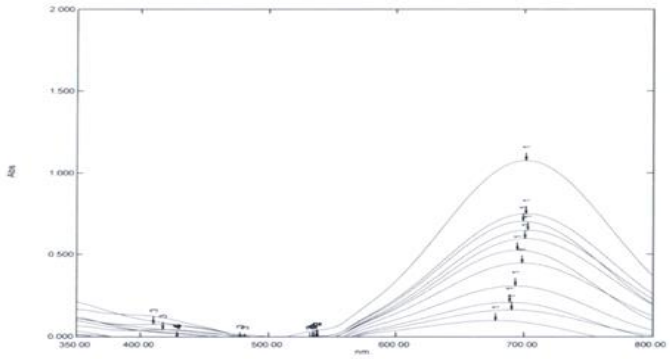

Fig.(4): Range of absorptions of concertation (2 - 22) µg/ml for CPZ

7. Precision and accuracy

The method's accuracy and compatibility were determined under authorized ideal circumstances by averaging five readings for each of three distinct numbers (4, 12, 18) µg.ml^{-1} to compute the recall and relative standard deviation. The approach was found to be very accurate and to have good agreement, as shown by the recall rate of 99.54% and the proportional standard deviation being below 3.86%. The results are shown in table (9).

Table (9): Precision and accuracy

Conc. of Chlorpromazine .HCl µg /ml	***RE%***	***Recovery%***	***Average of Recovery%***	***RSD%***
4	- 2.929	97.05	99.54	3.53
12	- 3.25	101.32		3.86
18	1.244	100.25		0.877

8. Limit of Detection

The lower concentration of 2 µg.ml^{-1} was measured five times under ideal conditions at 703 nm in order to determine the detection limit. The table (10) displays the results.

Table (10): Limit of detection

Conc. of Chlorpromazine .HCl µg /ml	$\overline{X}$	*S*	*D.L µg/ml*
2	0.1129	1.7002	0.2258

9. The Nature of the Merchandise that is Created

Job's approach, the molar method, and the nature of the previous green color product were all used. The normal MCP solution and N,N-diethyl paraphenylene diamine reagent solution concertation in both methods is equivalent to 0.001 M. In Job's approach, various quantities (1–9) ml of the reagent solution and various volumes (1–9) ml of the medication solution were divided among several 25 ml volumetric flasks. Purified water was used to adjust the quantities after the addition of 1.5 milliliters of NaOH solution and 1 milliliter of sodium nitroproside. In reference to the blank, the absorbance was measured at 703 nm. ..reaction. The ratio is 1:1, as shown in figure (5).

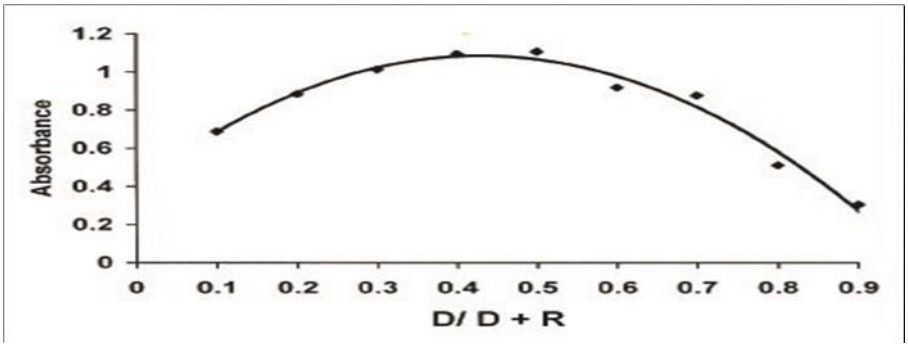

Fig.(5): The process used in the work to create the product by combining MCP and reagent oxidative.

Making use of many 25 ml volumetric bottles, 2 ml of the drug solution was put into every bottle along with 0.5–5 ml of the reagent solution, 1.5 ml of the mixture of oxidizing agents, 2.5 ml of N,N-dihydrate, and sodium nitroproside. This procedure is known as the molar ratio technique. Sodium hydroxide in 1.5 ml and ethylene paraphenylene diamine. Once the container was precisely filled with distilled water, In contrast to the fictitious solution, At a wavelength of 703 nm, the absorbance of each solution was measured. It was established that the ratio was reached (1:1) and the molar ratio corresponded with the technique of continuous modifications, as shown in Fig.(6).

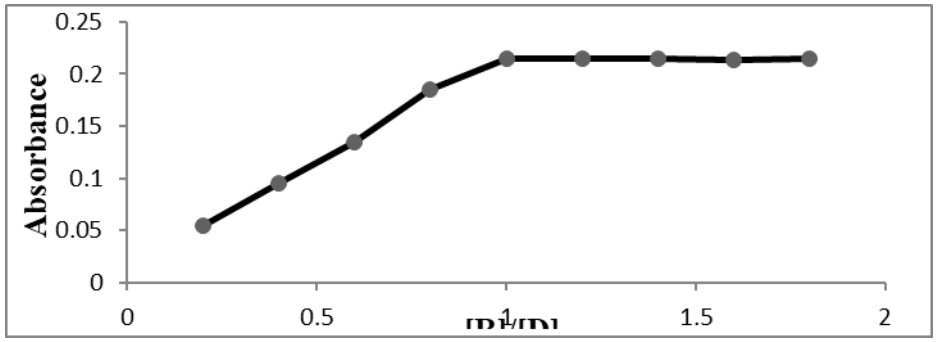

Fig. (6): Oxidative coupling of MCP with reagent using the molar ratio technique of generated product

The suggested reaction equation is as shown in scheme (1) :

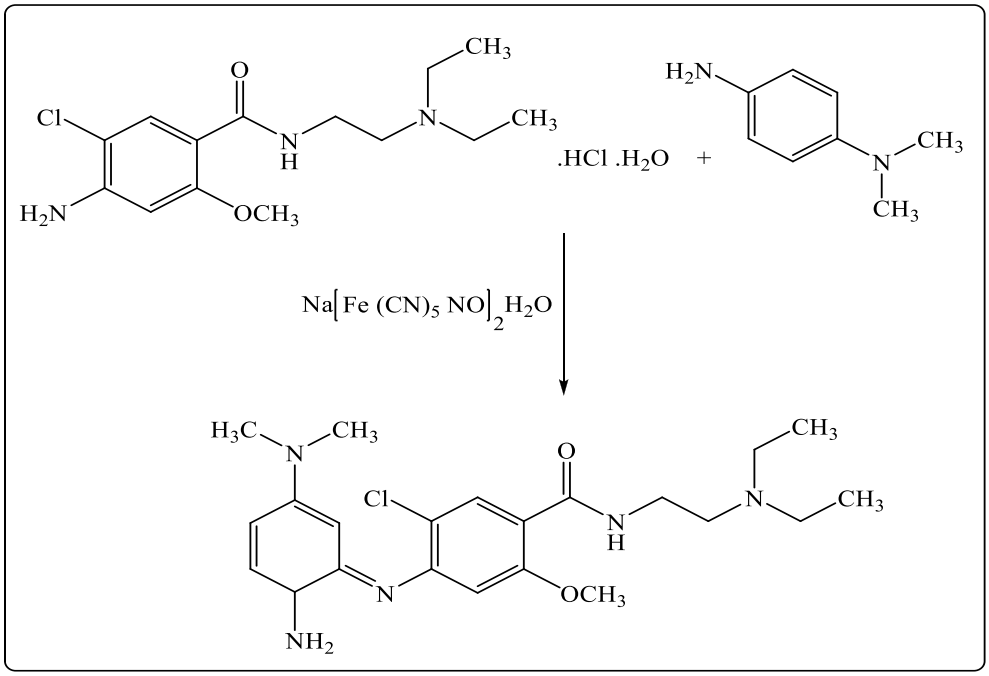

Scheme.(1): Structure of (E)-4-((6-amino-3-(dimethylamino)cyclohexa-2,4-dien-1-ylidene)amino)-5-chloro-N-(2-(diethylamino)ethyl)-2-methoxybenzamide

10. Applications

10-1. Direct method

With this procedure, a pharmaceutical formulation (100µg/ml) in various quantities (0.7, 1.2, 1.6) moved to a volumetric measure flask with a 25 ml volume. The resultant concentration (2, 12, 18) was then measured and used to generate a calibration curve. Five measurements of the absorbance at 703 nm were made The outcomes of the recuperation computation and RSD are shown in table (11).

Table (11): Direct method

Conc. of MCP (µg/ml)	*Abs. of standard MCP*	*Metoclopramide (Tablet)*		*Metoclopramide (Syrup)*	
		Abs.	*Recovery*	*Abs.*	*Recovery*
2	0.162	0.185	103.21	0.155	99.52
12	0.621	0.615	100	0.611	99.31
18	0.697	0.685	100	0.681	100.12

The effectiveness of the suggested approach in identifying the chemical metoclopramide hydrochloride in pharmaceutical compositions containing it is shown in the above table.. The recovery rate value for pills (tablet) was 101.07 and syrup (syrup) was 99.65.

10-2. The conventional adds technique

The objective of the efficiency statement for the proposed approach is to validate its precision and exhibit the interference-free use of the standard method for calculating the added MCP in the pharmaceutical product Largacatil. It discussed how Using a picture wavelength of 703 nm, compare the absorption of each solution to the reference solution. The table (12) present the finding, volumetric 25 ml bottles should be filled with a predetermined quantity (0.3, 0.5) of lotion pharmaceutical record solution concentration of 100 µg.ml-1. One should take care of a concentration of 250 µg.ml-1. and add quantities increasing to (0, 0.3, 0.5, 1, 1.4) ml of the solution MCP.

Table (12): The conventional adds technique

Type of Drug	*Metoclopramide Present mg/ml*	*Metoclopramide measured mg/ml*	*Recovery*
Metoclopramide (10 mg/ tablet)	2	2.2	101.204
	6	6.19	101.66
Metoclopramide (5 mg/ 5ml/Syrup)	2	2.23	100
	6	6.13	100.81

The figure (6) present the finding.

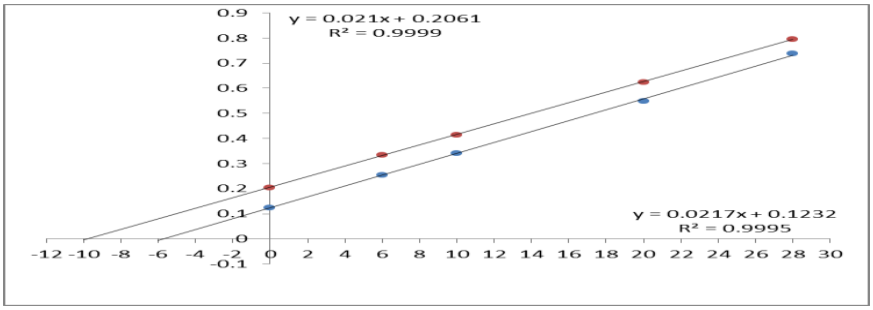

Fig .(6): Standard additions method

The above table's findings show that, within an allowable error range, the standard additions technique and the direct approach agree well, suggesting that the method is suitable and interference-free.

11.Conclusions

The results obtained validate the simplicity, speed, and excellent sensitivity of the suggested approach for MCP determination. In an alkaline media containing sodium nitroprosidein, MCP and N,N-diethyl paraphenylenediamine reagent undergo oxidative coupling to generate a green dye that is stable and soluble in water, with a maximum absorption at 703 nm. With a recovery of 97–103%, this approach may be effectively employed for calculating MCP in pharmacological formulation without the need for temperature control, organic solvents, or solvent extraction.

Reference

1- Husain, S., Kifayatullah, M., & Sekar, R. (2001). Simultaneous determination of mefenamic acid and paracetamol in pharmaceutical preparations by 1 H-Nuclear Magnetic Resonance Spectroscopy.

2- Gorog, S. (2018). Ultraviolet-visible spectrophotometry in pharmaceutical analysis. CRC press.

3- Sc, S. (2009). Martindale: the complete drug reference.

4- Javanbakht, M., Shaabani, N., & Akbari-Adergani, B. (2009). Novel molecularly imprinted polymers for the selective extraction and determination of metoclopramide in human serum and urine samples using high-performance liquid chromatography. Journal of Chromatography B, 877(24), 2537-2544.

5- Al-Abachi, M. Q., & Al-Ward, H. S.(2002). Spectrophotometric Micro Determination of Metoclopramide Hydrochloride in Pharmaceutical preparations via.

6- Cossu, M., Sanna, V., Gavini, E., Rassu, G., & Giunchedi, P. (2008). A New Sensitive Reversed-phase High-performance Liquid Chromatography Method for the Quantitative Determination of Metoclopramide in Canine Plasma. Analytical letters, 41(5), 767-778.

7- Foda, N. H. (1994). Quantitative analysis of metoclopramide in tablet formulations by HPLC. Analytical letters, 27(3), 549-559.

8- Amin, A. S., & Ragab, G. H. (2003). Spectrophotometric methods for the determination of anti-emetic drugs in bulk and in pharmaceutical preparations. Analytical sciences, 19(5), 747-751.

9- Shunli, F., Zhihao, W., Lei, Z., & Chao, L. (2002). Chemiluminescence determination of metoclopramide. Analytical letters, 35(9), 1479-1489.

التقدير الطيفي لعقار ميتوكلوبرامايد هيدروكلوريد بطريقة الاقتران التأكسدي في المستحضرات الصيدلانية

نور علاء الدين حسين[1] , حسين عبود ادهام[2] ,علياء حسين احمد [3]

[3,1] قسم علوم الحياة, كلية التربية للبنات , جامعة كركوك , العراق.

[2]قسم تقنيات المختبرات الطبية جامعة الامام جعفر الصادق فرع كركوك , العراق.

المستخلص :

باستخدام الاقتران التأكسدي مع ن،ن- ثنائي إيثيل بارافينيلين ديامين في وجود نيتروبروسيد الصوديوم، وهو عامل مؤكسد، في وسط قلوي، تم تكوين صبغة خضراء تذوب في الماء ولها أعلى كثافة امتصاص عند λmax 703 نانومتر. تم تطوير طريقة التحديد الطيفي الضوئي للميتكلوريد هيدروكلوريد الميتكلوريد.وقد اتبعت هذه التقنية قانون بير، حيث بلغ الامتصاص المولي 1.4278* 10^4لتر.مول$^{-1}$.سم$^{-1}$ صندل في نطاق تركيز 2-22 ملغم.مل$^{-1}$ عند 0.02481 مجم.سم$^{-2}$ لقيمة المؤشر، و0.2258 ميكروجرام.مل$^{-1}$ لحد الكشف، ومعامل ارتباط قدره 0.9882، يبقى الانحراف المعياري النسبي للتقنية أقل من 3.53%. باستخدام كل من إجراءات الإضافة المباشرة والتقليدية، تم استخدام النهج المقترح بفعالية لتحديد كمية الميتوكلوبراميد هيدروكلوريد في الأقراص؛ وتراوحت نسبة الاسترداد من 97 إلى 103%.

The Extent of Radiation Safety Knowledge Among Non-Radiology Personnel

Haneen Abass Alrubaie [1]* Raneen Salam [2] Aysar Keiteb [3] Alyaa hussein ashour[4]

[1]Al-Nahrain University, Al-Nahrain Renewable Energy Research Center, Jadriya, Baghdad, Iraq

[2] Al-Nahrain University, Al-Nahrain Renewable Energy Research Center, Jadriya, Baghdad, Iraq

[3] Department of Radiology, College of Health & Medical Technologies, Baghdad 10047, Iraq

[4] University of Mashreq, College of Medical Sciences, Technologies Department of Medical Physics

*Corresponding author: Haneen Abass Alrubaie

E-mail: **haneenabassabed1@gmail.com**

The Extent of Radiation Safety Knowledge Among Non-Radiology Personnel

Haneen Abass Alrubaie [1]* Raneen Salam [2] Aysar Keiteb [3] Alyaa hussein ashour[4]

[1]Al-Nahrain University, Al-Nahrain Renewable Energy Research Center, Jadriya, Baghdad, Iraq

[2] Al-Nahrain University, Al-Nahrain Renewable Energy Research Center, Jadriya, Baghdad, Iraq

[3] Department of Radiology, College of Health & Medical Technologies, Baghdad 10047, Iraq

[4] University of Mashreq, College of Medical Sciences, Technologies Department of Medical Physics

*Corresponding author: Haneen Abass Alrubaie

E-mail: **haneenabassabed1@gmail.com**

Abstract

The utilization of ionizing radiation for diagnostic and therapeutic objectives proves beneficial to a vast number of individuals. Various radiation modalities, such as X-rays, are accessible. While radiation offers benefits in the management and detection of various medical conditions, it is also linked to certain avoidable hazards for patients, healthcare professionals, and technicians. Nevertheless, it is possible to reduce the hazards associated with radiation and ensure the safety of both patients and workers. This study aimed

to evaluate the level of knowledge among individuals who are not radiologists regarding radiation protection.

Keywords: Ionizing radiation, X-ray, Safety of radiation.

1. Introduction

The term radiation encompasses a broad range of diverse energy types [1], which has proven to be advantageous for medical care. By producing intricate anatomical images, this technology has the potential to better diagnoses, reduce unnecessary medical procedures, and consequently improve treatment outcomes [2]. The utilization of ionizing radiation for diagnostic and therapeutic purposes is beneficial to a vast number of individuals worldwide [3]. The United Nations estimated that about 3.6 billion radiological tests are conducted each year for diagnostic purposes, and 7.5 million patients receive treatments annually, including radiotherapy [4]. The general population receives an average radiation dosage of 2.5 mSv per year, with medical exposure accounting for about 15% of this dose [5, 6]. With the expansion of medical imaging, the exposure of interventional radiologists and other workers in the radiology department to ionizing radiation has increased due to the use of imaging modalities. Within the United Kingdom, around 100 to 250 deaths are recorded annually as a direct consequence of cancer caused by exposure to radiation in medical settings [7]. Therefore, health care professionals have a responsibility to give patients accurate and fundamental information about all radiological procedures and processes, including their potential negative impacts [8]. The physician should respond to patient inquiries on radiation hazards, as long as

their expertise is sufficient and current. Undergraduate training at medical colleges includes instruction on radiation-related knowledge. Physicians significantly underestimate the accurate hazards connected with the appropriate utilization of medical imaging equipment and the radiation dangers they entail. The predominant demographic exposed to artificial radiation sources in work settings consists of those employed in healthcare facilities. The individuals encompassed in this group are radiologists, radiation oncologists, other physicians who utilize X-rays and radionuclides in their medical practices, licensed practitioners such as dentists, pediatricians, and chiropractors who are authorized to employ X-rays, radiographers and radiological technologists who aid in the creation of images and patient care, radiological physicists, installers, repairmen, as well as inspectors and regulators [9, 10]. There are a few reported studies on the level of radiation knowledge and radiation safety awareness amongst medical staffs in other countries [11-15]. The aim of the present study was to assess the knowledge of non-radiologists about radiation protection.

2. Background of X-ray

Discovered in 1895 by Wilhelm Konrad Rontgen while studying electron beams in electrical discharges, X-rays have since become an indispensable tool in medical diagnostics. Due to their ionizing capabilities, these particles have the ability to prompt neutral atoms to emit electrons. This process has the potential to cause harmful biochemical changes in genes, chromosomes, and cellular structures as they pass through live tissues. This ionization mechanism serves

as the foundation for efficient radiation therapies that specifically target cancerous cancers [16].

X-rays play a crucial role in medical imaging by enabling the evaluation of internal anatomical structures such as bones and organs. They are frequently used to detect fractures, infections, and foreign items that are stuck inside the body. Additionally, contrast chemicals such as iodine or barium can be employed to augment the visibility of X-rays in certain organs or tissues [17].

Overall, X-rays are a powerful tool in modern civilization with a wide range of uses, both in medicine and other fields. This is because X-rays can penetrate materials and provide detailed images of internal structures [18].

3. Subjects and Methods

Between November and December, a questionnaire survey with teen questions was given to 100 staff of the Red Crescent, Tarmiya, and Kazemiya hospitals.

Closed-ended questions about the profession and familiarity with the fundamentals of radiation protection made up the poll. Verifying the medical staff's knowledge on particular radiation protection themes was the aim of the survey questions table 1.

QUESTIONNAIRE OF RADIATION SAFETY

Case number:

Name: Age:

Gender: Occupation:

1) What is your profession?
   - Physician
   - Nurse
   - Ray diagnostics technician-x
   - Other
2) What type of department you work at?
   - Anesthesiology
   - Oncology
   - Radiology
   - Emergency
3) What is the length of your service?
   - Less than 1 year
   - 1-5 years
   - 6-10 years
   - 11-15 years
   - More than 16 year
4) Is there a radiation committee at the hospital wh work?
   - Yes
   - No
5) Are you adequately informed concerning the scop responsibilities of radiation safety committee?
   - Yes
   - No
6) Are there periodic trainings on radiation safety at the hospital where you work?
   - Yes
   - No
7) Information provided during the trainings efficient to raise awareness on radiation safety?
   - Yes
   - No
8) Is there a specific guideline or document on radiation safety at the hospital where you work?
   - Yes
   - No
9) Do you regularly use a pocket dosimeter?
   - Yes
   - No
   - If not, what's the reason?
     - I don't have a dosimeter
     - I keep forgetting it
     - I don't think it provides accurate measurements
10) Which of the following explains the ALARA principle?
   - As Low as Reasonably Achievable
   - Allowable Administered Radiation
   - Assurance Limits Applied to Radiation

Table 1: A sample questionnaire

4. Results

Table 1 lists the demographic information gathered from a survey of medical professionals who work in radiation environments. The results showed that 75% of the participants were employed in state hospitals, 25% in private hospitals, 0% in high school, 65% in college and university settings, 26% in postgraduate settings, and 9% in doctorate programs. Among the participant occupational groupings were doctors (18%), technicians (10%), nurses (31%), and other 41 Healthcare professionals working in radiology made up 10% of the participants, followed by anesthesiologists (27%), oncologists (3%), and emergency surgeons (11%). The participants' work experience was divided into four categories: less than one year (19%), one to five years (47%), six to ten years (23%), and more than sixteen years (2%).

Table 2. Demographic characteristics of the healthcare professionals who participated in the study

		Number	Rate (%)
type of hospital	state	75	75%
	private	25	25%
Education	high school	0	0%
	undergraduate	65	65%
	postgraduate	26	26%
	PhD	9	9%
Occupation	physician	18	18%
	nurse	31	31%
	raydiagnostics	10	10%
	other	41	41%
Department	Anesthesiology	27	27%
	Oncology	3	3%
	radiology	10	10%
	emergency surgery	11	11%
experience	less than 1years	19	19%
	1_5 year	47	47%
	6_10 year	23	23%
	11_15 year	9	9%
	more than 16 years	2	2%
total		100	100%

creating a radiation safety manual and conducting routine training in hospitals, Examining the responses to the questions about this topic, (87%) of the

participants said that the hospital where they worked had a radiation safety committee, and (44%) said they were aware of the committee's duties and purview. Conversely, a majority of the participants (53%), indicated that a radiation safety document was present of the participants, (41%) percent said that the hospital where they work offers regular training on radiation safety , as shown in the figure's(1−4) .

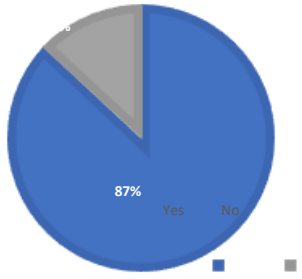

Fig 1: Is there a Radiation Committee at the hospital where you work?

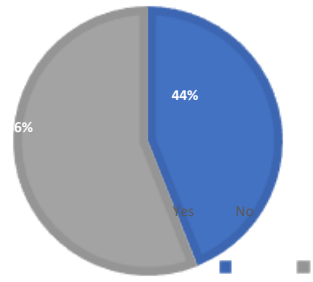

Fig 2: Are you adequately informed concerning the scope and responsibilities of radiation safety committees you work?

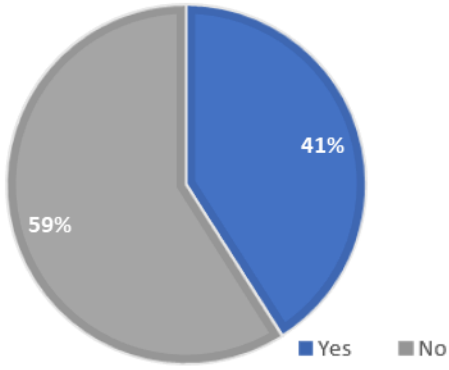

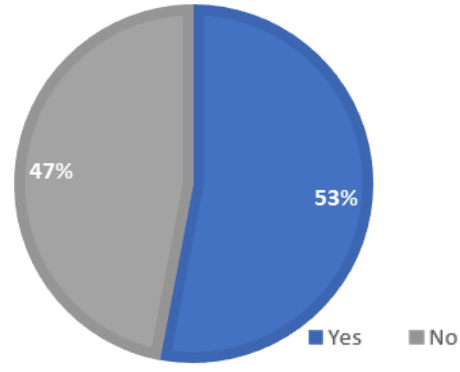

Fig 3: Are there periodic trainings on radiation safety at the hospital where you work?

Fig 4: Is the information provided during the trainings efficient to raise awareness on radiation safety?

The Act specifies the use guidelines for dosimeters, which are required in radiation areas. Questions about the usage of dosimeters and safety precautions were raised as a result. of the participants, 40% reported using a pocket dosimeter often, whereas 60% said they did not use one at all. of the 60 participants who reported not using a dosimeter, the most common reasons given were forgetting to wear the device (41.6%), not owning a dosimeter (33.3%), and believing that the measurements the dosimeter provided were erroneous (25.1%).

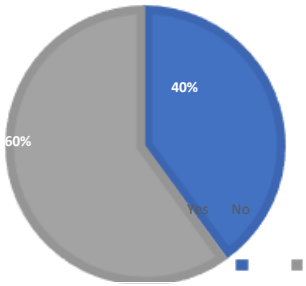

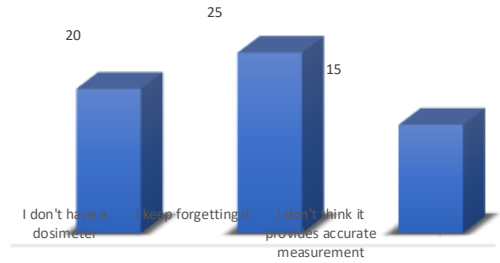

Fig 5: do you regularly use a pocket?

Fig 6: if not, what's the reason

60 % of the participants were unaware that the lowest radiation dose was what was meant by the ALARA (as low as reasonably attainable) principle.

5. Discussion

Every diagnostic or therapeutic technique that uses ionizing radiation has patient and staff safety as a top focus. When dealing with medical personnel exposed to ionizing radiation, they have to follow the As Low as Reasonably Achievable (ALARA) guidelines. This involves carrying out the scans at the potentially lowest ionizing radiation dosages possible in order to get the intended diagnostic outcome [19]. We are making an effort to ascertain the level of radiation protection awareness among the medical staff of a few Baghdad hospitals, as a result of the daily clinical practice and the inaccurate and occasionally contradictory information provided by the medical staff. Non-physicians, such as nurses, medical technicians, and auxiliary staff members, were specifically included in the study group. This resulted from these medical personnel' frequent interactions with patients both before and during ionizing radiation operations. As per the initial assumptions, the research group need to exhibit diversity with respect to both the location and duration of service. The results gathered offered intriguing insights into medical professionals' beliefs, knowledge, and proficiency in radiation safety.

It is not unexpected that staff members in radiology departments have a thorough understanding of the entire range of ionizing radiation effects given their specialized training. The comparatively high level of radiation protection knowledge in emergency rooms, across all staff ranks (medical, nursing, and support), is noteworthy. This seems to be because these individuals frequently interact with imaging diagnostics labs, which leads to an improved comprehension of radiological techniques. However, there are very few

explanations for why oncology staff members know so little about the characteristics of ionizing radiation. The fact that a sizable portion of all patients receiving a diagnosis in any medical facility are referred for diagnostic exams by cancer units makes this even more unexpected. The low level of general radiography technique knowledge among nursing staff is another intriguing finding. It is especially intriguing when considering the treatment, they give hospitalized patients and how actively they participate in getting ready for planned imaging tests. The high percentage of accurate responses to the majority of questions among employees with $1-4$ years of service as well as those with $11-15$ years of service is noteworthy. It's concerning that personnel with six to ten and more years of employment have such a low level of understanding. This appears to be caused by the dearth of radiological protection trainings and senior workers' resistance to adopting new work practices.

Training in radiation safety is only required for employees who have been exposed to radiation on the job. The study population's awareness of ionizing radiation was found to be quite limited, according to the analysis. However, it's noteworthy that 60% of respondents gave accurate responses, indicating that they had a reasonable understanding of the possible cancer risks associated with high ionizing radiation exposure. Sadly, it appears that mainstream sources, rather than specialized publications and trainings, are where this knowledge is obtained.

6. Conclusions

While radiation diagnostics plays a vital role in the therapeutic process, protection-related matters are often treated casually. In an era of growing health consciousness in society and an increase in legal claims against medical personnel, a comprehensive understanding of radiation protection is becoming an essential component of professional expertise for not only radiologists and radiation therapists but also other specialists and support staff. The survey's conclusion emphasizes the need for thorough and systematic education on radiological protection for all healthcare professionals.

7. Reference

[1] Mubeen, Syed Mohammed, Qamar Abbas, and Nighat Nisar. "Knowledge about ionizing and non-ionizing radiation among medical students." *J Ayub Med Coll Abbottabad* 20.1 (2008): 118-121.

[2] Scans, C. T. "and Medical Benefits." *Environmental Health Perspectives* 120.3 (2012).

[3] Algohani, Khaled Awdah, et al. "Awareness of radiation protection measures among radiologists and non-radiologists." *The Egyptian Journal of Hospital Medicine* 70.3 (2018): 371-375.

[4] UNSCEAR (United Nations Scientific Committee on the Effects of Atomic Radiation). "Sources and effects of ionizing radiation." *Report to the General Assembly with scientific annexes* 1 (2000).

[5] Wootton, R. "The POPUMET regulations: careless radiology costs lives." *British journal of hospital medicine* 45.3 (1991): 133.

[6] National Radiological Protection Board. *Patient dose reduction in diagnostic radiology*. National Radiological Protection Board, 1990.

[7] Shiralkar, S., et al. "Doctors' knowledge of radiation exposure: questionnaire study." *Bmj* 327.7411 (2003): 371-372.

[8] Finestone, Aharon, et al. "Do physicians correctly estimate radiation risks from medical imaging?" *Archives of Environmental Health: An International Journal* 58.1 (2003): 59-62.

[9] Martinez, Ten. "Operational radiological protection at medical installations." *Occupational radiation protection: Protecting workers against exposure to ionizing radiation. Proceedings of an international conference*. 2003.

[10] Vohra, Apurva. "Awareness and Knowledge of Risk in Radiation Exposure among Health Care Professionals: A Hospital Based Survey." (2016).

[11] Yunus, N. A., et al. "Assessment of radiation safety awareness among nuclear medicine nurses: a pilot study." *Journal of Physics: Conference Series*. Vol. 546. No. 1. IOP Publishing, 2014.

[12] Eksioglu, Ayse Secil, and Çigdem Üner. "Pediatricians' awareness of diagnostic medical radiation effects and doses: are the latest efforts paying off?" *Diagnostic and interventional radiology* 18.1 (2012): 78.

[13] Shiralkar, S., et al. "Doctors' knowledge of radiation exposure: questionnaire study." *Bmj* 327.7411 (2003): 371-372.

[14] Soye, J. A., and A. Paterson. "A survey of awareness of radiation dose among health professionals in Northern Ireland." *The British journal of radiology* 81.969 (2008): 725-729.

[15] Lee, Christoph I., et al. "Diagnostic CT scans: assessment of patient, physician, and radiologist awareness of radiation dose and possible risks." *Radiology* 231.2 (2004): 393-398.

[16] Warren, Bertram Eugene. *X-ray Diffraction*. Courier Corporation, 1990.

[17] Whittig, L. D., and W. R. Allardice. "X-ray diffraction techniques." *Methods of Soil Analysis: Part 1 Physical and Mineralogical Methods* 5 (1986): 331-362.

[18] Als-Nielsen, Jens, and Des McMorrow. *Elements of modern X-ray physics*. John Wiley & Sons, 2011.

[19] Shi, Hai-Min, Zhi-Chao Sun, and Fang-He Ju. "Recommendations for reducing exposure to medical X-ray irradiation." *Medicine International* 2.4 (2022): 1-7.

مدى معرفة العاملين غير المتخصصين في الأشعة بسلامة الإشعاع

المستخلص

إن استخدام الإشعاعات المؤينة لأغراض تشخيصية وعلاجية أثبت فائدته لعدد كبير من الأفراد. يمكن الوصول إلى طرق الإشعاع المختلفة، مثل الأشعة السينية. في حين أن الإشعاع يوفر فوائد في إدارة الحالات الطبية المختلفة والكشف عنها، فإنه يرتبط أيضًا ببعض المخاطر التي يمكن تجنبها للمرضى ومتخصصي الرعاية الصحية والفنيين. ومع ذلك، فمن الممكن الحد من المخاطر المرتبطة بالإشعاع وضمان سلامة كل من المرضى والعاملين. هدفت هذه الدراسة إلى تقييم مستوى المعرفة بين الأفراد غير المتخصصين في الأشعة فيما يتعلق بالوقاية من الإشعاع.

Single Nucleotide Polymorphism in IL-18 Gene in Iraqi Patients With Inflammatory Bowel Disease

Ruaa Maan[1*], Hameed Majid[2], Sahar Medhat[3], Elham Abdel-Hadi[4]

1. University of Mashreq, College of Medical Sciences Technologies, Department of Medical Physics, Baghdad, Iraq.

2. Al- Nahrain University, College of Biotechnology, Department of Molecular and Medical Biotechnology, Baghdad, Iraq.

3. Al-Razi Center for Research and Medical Kit Production, Baghdad, Iraq.

*Corresponding author: Ruaa Maan Attallah

E-mail: **ruaamaan@gmail.com**

Single Nucleotide Polymorphism in IL-18 Gene in Iraqi Patients With Inflammatory Bowel Disease

Ruaa Maan[1*], Hameed Majid[2], Sahar Medhat[3], Elham Abdel-Hadi[4]

1. University of Mashreq, College of Medical Sciences Technologies, Department of Medical Physics, Baghdad, Iraq.

2. Al- Nahrain University, College of Biotechnology, Department of Molecular and Medical Biotechnology, Baghdad, Iraq.

3. Al-Razi Center for Research and Medical Kit Production, Baghdad, Iraq.

*****Corresponding author: Ruaa Maan Attallah

E-mail: **ruaamaan@gmail.com**

Abstract

Inflammatory Bowel Disease (IBD) is a chronic inflammatory disease of the gastrointestinal tract, traditionally divided into Crohn's disease (CD) and ulcerative colitis (UC). UC is restricted to the colon while CD is can affect any part of the entire gastrointestinal tract from the mouth to the anus. Interleukin-18 is a pro-inflammatory cytokine It plays an important role in the development of chronic inflammatory diseases such as IBD genetic variation within IL18 altered transcriptional activity in Crohn's disease and patients with ulcerative colitis.

Aim of this research is to investigate the relationship between single nucleotide polymorphisms in Exon 1 of IL-18 and the susceptibility to IBD disease.

Patients and Methods: In total, 110 blood samples were collected 50 from IBD patients 40 of them were ideal for this research divided to 21 UC and 19 CD with 60 blood samples from healthy individuals only 40 of them included genomic DNA were extracted from peripheral blood samples by DNA extraction kit then the DNA samples were amplified by PCR technique using specific primers. The final products were sent to be sequenced for SNPs investigation.

Results: Two SNPs have been indicated in samples under study rs360717 (+127 C/T) and a novel SNP (T/G). Comparing genotypes frequency of polymorphic homozygous genotypes between patients and control in total and between each group (UC, CD) and control, no significant difference was found, also

polymorphic heterozygous genotype between patients and control in total and between each group (UC, CD) and control, no significant difference was found.

In conclusion: the +127 (C/T) and the novel SNP (T/G) in Exon 1 at IL-18 are not susceptible factor for inflammatory bowel disease in Iraqi population.

Keywords: Interleukin-18, ulcerative colitis, Crohn's disease, IBD, SNPs

1. Introduction

Inflammatory bowel disease (IBD), which includes Crohn's disease and ulcerative colitis, is a recurrent condition known for chronic inflammation at various sites in the gastrointestinal tract, causing abdominal pain and diarrhea. Crohn's disease and Ulcerative Colitis are differentiated by their clinical manifestations and pathogenic mechanisms [1]. UC involves the rectum and colon, which primarily affect the mucous and submucosal layers, CD it is widely known to involve in any part of the GI tract from mouth to rectum [2,3]. The inflammation results from a cell-mediated immune response in the mucosa of the gastrointestinal tract. The exact etiology of the inflammation is unknown, but evidence suggests that normal gut flora triggers an abnormal immune response (possibly abnormal epithelial barriers and mucosal immunity) in patients with genetic causes or infectious reasons. The immune reaction includes the discharge of inflammatory mediators inclusive of cytokines, interleukin and tumor necrosis factor. Although Crohn's disorder and ulcerative colitis are similar, they may be outstanding in maximum instances [4]. The human Interleukin -18 genes consists of five introns and six exons, and has been found on chromosome 11q23.1, with length of nearly 20 kb [5]. Interleukin-18 is a pro-inflammatory mediator produced by a different cell types including lymphocytes, epithelial cells and myeloid cells [6], it is also expressed by intestinal epithelial cells under normal physiological conditions, it has been suggested that it play a key role in mucosal immunity. any alteration found in the Interleukin-18 gene including single nucleotide polymorphisms have been reported to have a an effect in regulation of intestinal immune responses which may cause IBD [7]. Genetic analysis is a suitable method for recognize a small number of loci with high penetrance, and this is limited to identifying IBD-associated genes.

2. Material and method

in total, 110 blood samples were collected, 50 from IBD patients 40 of them were ideal for this research, divided to 21 UC (18 M, 3 F) and 19 CD (11 M, 8 F) with 60 blood samples from healthy individuals only 40 of them included, divided into 20 males and 20 females. the diagnosis of the disease was made in hospital by doctors based on clinical and endoscopic findings in AL-Yarmouk teaching hospital at Baghdad, Iraq. This study was performed according to the declaration of Helsinki. Information were obtained from all subjects after their permeation.

DNA extraction

Genomic DNA were extracted from peripheral blood samples by DNA extraction kit, the results of extraction showed a clear band of extracted genomic DNA, also there was a high concentrations and purity of DNA solutions. The DNA concentration was ranged between 7.0 and 106 ng/µl, while the purity was ranged between 1.8 and 2.0. This purity and concentration are suitable, recommended and reliable for further genetic analysis by using PCR technique [8].

PCR amplification

To determine the genetic polymorphism in Exon 1 in IL-18 and the susceptibility to IBD the site of polymorphisms were amplified by using specific primers Forward:5'-AAGAGGTACAGGTTTTGGAAGGCA-3' and Reverse:5'-TCCCGAAGCTGTGTAGACTGCA-3'. under the optimal conditions then all products appeared as single and clear band after electrophoresis on agarose gel (1%) in presence of 100 bp DNA ladder marker for patients and controls. which give a product with a band of 350 bp in size and that confirmed by Aizawa and his colleagues whose have the same size of band [9].

genotyping of Exon 1 in IL-18 gene

All amplified products were set to sequencing by Macrogen®-Korea, to investigate for genetic polymorphisms in IL-18 gene with in IBD in Iraqi patients. The sequences were analyzed by aligned with the reference sequence. The ref. seq. recorded in (NCBI) by blast data also the Iraqi patients and Iraqi controls were compared and aligned using BioEdit and Mega programs, the programs also used for further analysis and detection for SNPs. Alignment

showed that the location of extracted SNP within the nucleotide sequence matched with the reference sequence (http://www.ncbi.nlm.nih.gov) of IL-18 gene mentioned in NCBI.

Statistical analysis

The Statistical Package for Social Sciences SPSS (2016) [10] and Statistical Analysis System SAS (2018)[11] programs were used to detect the difference between study parameters T-test and Chi-square were used to significant compare between The variances in gender, age, disease types and between percentage genotypes of The (+127 C/T and novel SNP (T/G) polymorphisms between patients and controls statistical significance at (0.01 and 0.05 probability) in this study.

3. Results and Discussion

Gender distribution and the mean age among disease types and controls showed in [Table 1]. Distribution of genotypes and allele frequency of IL-18 gene polymorphism +127 C/T in Exon 1 in IBD patients and healthy controls are illustrated in [Table 2] and [Table 3] respectively, there were no significant differences in distribution of genotypes between the two disease types and between patients in total and controls.

Table1: Patients and healthy controls category according to their age and gender for inflammatory bowel disease.

Characteristics	Patients (n =40)				Controls (n =40)			
	Male		**Female**		**Male**		**Female**	
Number (%)	29 (72.5%)		11 (27.5%)		20 (50%)		20 (50%)	
Mean age ± SD	33±13.24		40.9±13.33		40.2±13.20		41.25±12.50	
Disease type %	**UC**	**CD**	**UC**	**CD**	-	-	-	-
	18 (62%)	11(38%)	3 (27%)	8 (73%)	-	-	-	-

UC= Ulcerative colitis, CD= Crohn’s disease

Table2: Distribution of genotype and allele frequency of IL-18 gene polymorphism +127 C/T in Exon 1 in total IBD patients and control

Genotype	IBD patients No. (%)	Healthy control No. (%)	P-value	O.D. (C.I. 95%)
CC	40 (100)	38 (95)	0.820 NS	**0.19** (0.008-4.08)
CT	0 (0)	0 (0)	1.00 NS	**1.0** (0.01-51.63)
TT	0 (0)	2 (5)	0.188 NS	**5.26** (0.24-113.11)
Total	40	40	----	----
Allele Frequency				
C	1.00 (80)	0.95 (76)	0.0428 *	**0.10** (0.005-1.99)
T	0.00 (0)	0.05 (4)	0.0428 *	9.4706 (0.50-178.87)
Genotype	**UC Group No. (%)**	**Healthy control No. (%)**	**P-value**	**O.D. (C.I. 95%)**
CC	21 (100)	38 (95)	0.026 *	**0.35** (0.01-7.81)
CT	0 (0)	0 (0)	1.00 NS	**1.88** (0.03-98.29)
TT	0 (0)	2 (5)	0.188 NS	**2.79** (0.13-60.87)
Total	21	40	---	---
Allele Frequency				
C	1.00 (42)	0.95 (76)	0.140 NS	**0.2** (0.01-3.81)
T	0.00 (0)	0.05 (4)	0.140 NS	**5.0** (0.26-95.13)
Genotype	**CD Group No. (%)**	**Healthy control No. (%)**	**P-value**	**O.D. (C.I. 95%)**
CC	19 (100)	38 (95)	0.073 NS	**0.39** (0.01-8.63)
CT	0 (0)	0 (0)	1.00 NS	**2.07** (0.03-108.62)
TT	0 (0)	2 (5)	0.188 NS	**2.53** (0.11-55.37)
Total	19	40	---	---
Allele Frequency				
C	1.00 (38)	0.95 (76)	0.160 NS	**0.22** (0.01-4.21)
T	0.00 (0)	0.05 (4)	0.160 NS	**4.53** (0.23-86.31)
UC / CD (P-value)				
CC		0.892 NS		
CT		1.00 NS		
TT		1.00 NS		
*: Significant (P≤0.05); NS: Non-Significant.				

Table 3: Distributi of genotype on and allele frequency of IL-18 gene polymorphism of Exon 1: T > G in total IBD patients and control

Genotype	IBD patients No. (%)	Healthy control No. (%)	P-value	O.D. (C.I. 95%)
TT	38 (95)	40 (100)	0.820 NS	**0.19** (0.008-4.08)
TG	0 (0)	0 (0)	1.00 NS	**1.0** (0.01-51.63)
GG	2 (5)	0 (0)	0.188 NS	**5.26** (0.24-113.11)
Total	40	40	----	----
Allele Frequency				
T	0.95 (76)	1.00 (80)	0.0428 *	**0.10** (0.005-1.99)
G	0.05 (4)	0.00 (0)	0.0428 *	**9.47** (0.5014-178.8771)
Genotype	**UC Group No. (%)**	**Healthy control No. (%)**	**P-value**	**O.D. (C.I. 95%)**
TT	20 (95.2)	40 (100)	0.179 NS	**0.16** (0.0066-4.32
TG	0 (0)	0 (0)	1.00 NS	**1.88** (0.03-98.29)
GG	1 (4.8)	0 (0)	0.163 NS	**5.92** (0.23-152.01)
Total	21	40	---	---
Allele Frequency				
T	0.95 (40)	1.00 (80)	0.385 *	**0.10** (0.004-2.14)
G	0.05 (2)	0.00 (0)	0.385 *	**9.93** (0.46-211.92)
Genotype	**CD Group No. (%)**	**Healthy control No. (%)**	**P-value**	**O.D. (C.I. 95%)**
TT	18 (94.7)	40 (100)	0.166NS	**0.15** (0.005-3.91)
TG	0 (0)	0 (0)	1.00 NS	**2.07** (0.03-108.62)
GG	1 (5.3)	0 (0)	0.194 NS	**6.56** (0.25-168.9)
Total	19	40	---	---
Allele Frequency				
T	0.95 (36)	1.00 (80)	0.385 *	**0.09** (0.004-1.93)
G	0.05 (2)	0.00 (0)	0.385 *	**11.02** (0.51-235.54)
UC / CD (P-value)				
TT		0.817 NS		
TG		1.00 NS		
GG		1.827 NS		
* (P≤0.05), NS: Non-Significant.				

There is a type of mutations that may strongly have a little or no effect on gene regulation and protein activity. Synonymous or silent mutation it's a type of variant that found in the coding region of every human genome that have no effect on the resulting product protein sequence. Silent mutation is the output of the genetic code degeneracy, where more than one codon can encoded the amino

acids [12]. However, some research claim that silent mutation are possible to be pathogenic like the non-synonymous variants, silent mutation have been implicated in many diseases [13,14]. Synonymous variations can disturb splicing [15], transcription [16], mRNA stability [17], co-translational folding [18], and cause an increase of other functionally related changes. In addition to this, silent mutation can change splicing regulatory factors and transcription in protein coding regions thus, modulating gene expression [19,20, 21].

Non-synonymous SNPs, in particular it's a type of SNP found in protein coding regions change the resulting amino acid at the alteration site and can cause functional and structural changes in the changed protein But, not all functional and structural changes due to non-synonymous SNPs are possibly harmful. Various non-synonymous SNPs affect structural properties, while others may result in functional consequences. Moreover, some of these SNPs can be related with a disease condition while others may not be associated with any disease, therefore, its considered to be un harmful (neutral). The functional outcome of any non-synonymous SNPs to a large extent are based on the attributes of the polymorphisms [22, 23].

Genotyping of Exon 1 of +127 C/T

+127 C/T polymorphism in Exon 1 region of IL-18 was genotyped to determine the association of the site of polymorphism with the incidence of the disease. Results showed that cytosine nucleotide was substituted by thiamine in Exon 1 region of IL-18 in only two subjects of healthy controls and not existence in the DNA sequence of the same region in IBD patients as shown in [Figure 1]. It is a Silent mutation (Point mutation) which the mutated codon gave the same amino acid that resulted from the wild codon (serine).

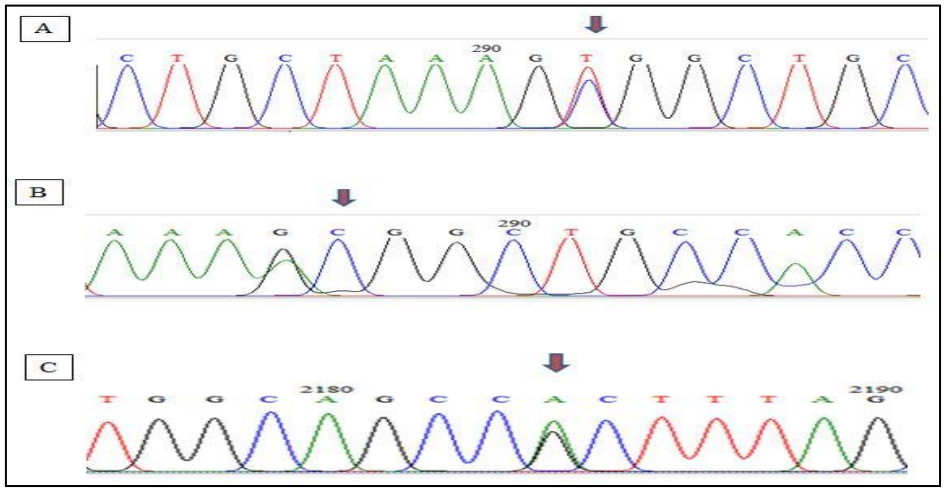

Figure 1: A representative sequence alignment of IL-18 Exon region +127 C/T of healthy control with IBD patients. Red arrow indicate the position of expected SNP. (A): Nucleotide sequence of control using forward primer; (B): IBD patient; (C) Nucleotide sequence of control using reverse primer.

On the other hand, results indicated previously in [Table 2] showed that the percentage of homozygous non-polymorphic genotype (CC), heterozygous polymorphic genotype (CT) and homozygous polymorphic genotype (TT) in IBD patients were 100%, 0% and 0% respectively, while the frequency of these genotypes in healthy controls are 95%, 0% and 5% respectively with no significant difference.

These results also showed that there is no relationship between rs360717 polymorphism and the susceptibility to IBD as C allele was the dominant (OR=0.79 ; 95% C.I.= 0.016-9.83), while the recessive model of inheritance T allele was non-significantly different in both groups, and was not associated with the increased risk to IBD (OR=1.0 ; 95% C.I.=0.01-51.63).

On the other hand, results indicated in [Table 2] showed that the frequency of CC, CT and TT genotypes in UC and crohn's disease are 100%, 0% and 0% respectively compared to the same genotypes in healthy controls (95%, 0% and 5% respectively) with no significant different in distribution of TT homozygous genotype between both UC and crohn's disease, and healthy controls which refer to a non- significant association between Exon 1 rs360717 polymorphism and the incidence of ulcerative colitis or crohn's disease. The odd ratio for recessive TT vs CC and CT was 0.40; 95% C.I.= 0.03-7.87 in UC patients, and 0.36; 95%

C.I.= 0.01-7.79 in CD patients compared to healthy controls. According to these results homozygous polymorphic TT was not a risk factor in etiology of IBD.

These results are not similar to a study mentioned by [9], who found that in Japanese population rs360717 is closely associated with IBD, especially with CD with a significantly higher frequency of T allele in patients with CD compared to UC and control.

Genotyping of Exon 1 novel SNP T/G

A novel SNP (T>G) polymorphism in Exon 1 region was genotyped and to determine the association of the site of polymorphism with the incidence of the disease. results showed that thiamine nucleotide was substituted by guanine at the site of polymorphisms in Exon 1 region of IL-18 in IBD patients which was not existence in the DNA sequence of the same region in healthy subjects as shown in [Figure 2]. It is a Missense mutation (point mutation) which the mutated codon gave different amino acid (lysine) that differ from the wild codon (tryptophan).

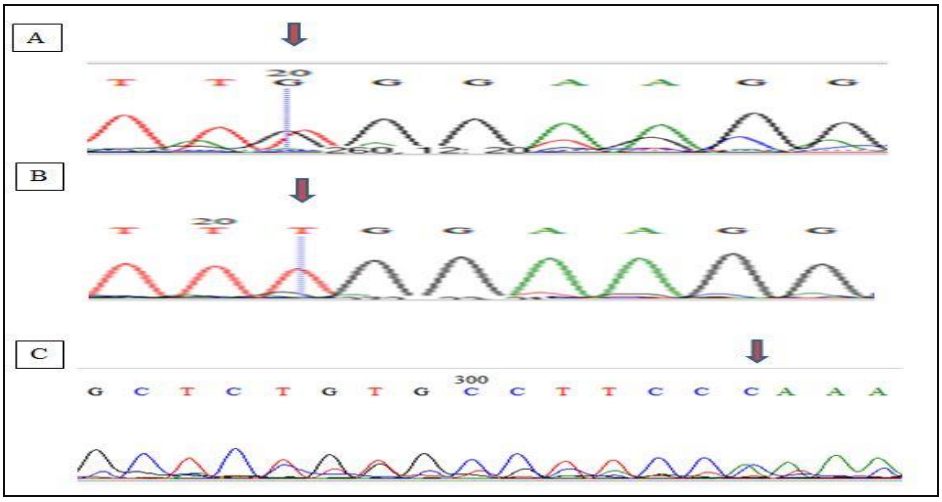

Figure 2: A representative sequence alignment of IL-18 Exon region novel SNP T/G of IBD patients with healthy control. Red arrow indicate the position of expected SNP. (A): Nucleotide sequence of patient using forward primer; (B): control; (C) Nucleotide sequence of patients using reverse primer.

On the other hand, result indicated in [Table 3] showed that the frequency of homozygous non-polymorphic genotype (TT), heterozygous polymorphic genotype (TG) and homozygous polymorphic genotype (GG) in IBD patients are

95%, 0% and 5% respectively, while the frequency of these genotypes in healthy controls are 100%, 0% and 0% respectively. These results showed that GG polymorphic genotype in IBD patients was non-significantly different than in healthy control group.

These results show a non-significant relationship between Exon 1 the novel polymorphism T>G and susceptibility to IBD in a dominant G allele (OR=5.26 ; 95% C.I.= 0.24-113.11), and the recessive model of inheritance allele was non-significantly different in both groups, and was not associated with the increased risk to IBD (OR=1.0 ; 95% C.I.=0.01-51.63).

On the other hand, results indicated in [Table 3] showed that the frequency of TT, TG and GG genotypes in UC are 95.2%, 0% and 4.8% respectively while in CD are 94.7%, 0% and 5.3% respectively compared to these genotypes in healthy controls (100%, 0% and 0% respectively) with no significant different in distribution of GG homozygous genotype between UC and controls which refer to a non- significant association between Exon 1 polymorphism and the incidence of ulcerative colitis. The odd ratio for recessive GG vs TT and TG was 5.92; 95% C.I.=0.23-152.01 in UC patients compared to healthy controls.

Furthermore, results indicated showed that the frequency of TT, TG and GG genotypes in patients with crohns disease are 94.7%, 0% and 5.3% respectively compared with (100%, 0% and 0% respectively) in healthy controls. The odd ratio for recessive GG vs TT and TG was 6.56; 95% C.I.= 0.25-168.9 in CD patients compared to healthy controls. In this study, results showed that the homozygous gg was not a risk factor in etiology of IBD.

Conclusions

In conclusion, +127 C/T and the novel SNP T/G Exon 1 of IL-18 polymorphisms are not considered as a risk factor for IBD in Iraqi population understudy. However, we can’t exclude the possibility of other SNPs in IL-18 gene that may affect the disease susceptibility. Its recommended to study a larger population from different region and the effect of environment and diet on the susceptibility and severity of the disease.

References

[1] Baumgart DC, Sandborn WJ. Inflammatory bowel disease: clinical aspects and established and evolving therapies. Lancet. 2007;369(9573):1641-57.

[2] Colombel JF, Shin A, Gibson PR. AGA Clinical Practice Update on Functional Gastrointestinal Symptoms in Patients With Inflammatory Bowel Disease: Expert Review. Clin Gastroenterol Hepatol. 2019;17(3):380-390.e1.

[3] Oliver BJ, Kennedy AM, van Deen WK, Weaver SA, Heller C, Holthoff MM, Bank J, Melmed GY, Siegel CA, Nelson EC. Development of Balanced Whole System Value Measures for Inflammatory Bowel Disease Care in the IBD Qorus Collaborative Using a Modified Delphi Process. Inflamm Bowel Dis. 2022;28(3):327-336.

[4] Hassan JT, Delmany AS. Epidemiological and clinical characteristics of patients with inflammatory bowel disease in Erbil City. Med J Babylon 2018;15:281-5

[5] Hirooka Y, Nozaki Y. Interleukin-18 in Inflammatory Kidney Disease. Front Med (Lausanne) 2021;8:639103.

[6] Dinarello CA, Novick D, Kim S, Kaplanski G. Interleukin-18 and IL-18 binding protein. Front Immunol. 2013;4:289.

[7] Senhaji N, Diakité B, Serbati N, Zaid Y, Badre W, Nadifi S. Toll-like receptor 4 Asp299Gly and Thr399Ile polymorphisms: New data and a meta-analysis. BMC Gastroenterol. 2014;14:206.

[8] Boesenberg-Smith KA, Pessarakli MM, and Wolk DM. Assessment of DNA yield and purity: an overlooked detail of PCR troubleshooting Clinical Microbiology Newsletter. 2012;34(1), 1-6.

[9] Aizawa Y, Sutoh S, Matsuoka M, Negishi M, Torii A, Miyakawa Y, et al. Association of interleukin-18 gene single-nucleotide polymorphisms with susceptibility to inflammatory bowel disease. Tissue Antigens 2005;1:88-92.

[10] IBM Corp. IBM SPSS Statistics for Windows. Armonk, NY: IBM Corp. Version 24.0. Released 2016.

[11] SAS. Statistical Analysis System, User's Guide. Statistical. Inst. Inc. Cary. N.C. USA. Version 9.6th ed. SAS 2018.

[12] Shen H, Li J, Zhang J, Xu C, Jiang Y, Wu Z, Zhao F, Liao L, Chen J, Lin Y, Tian Q, Papasian CJ, Deng HW. Comprehensive characterization of human genome variation by high coverage whole-genome sequencing of forty four Caucasians. PLoS One. 2013;8(4):e59494.

[13] Sauna ZE, Kimchi-Sarfaty C. Understanding the contribution of synonymous mutations to human disease. Nat Rev Genet. 2011;12(10):683-91.

[14] Supek F, Miñana B, Valcárcel J, Gabaldón T, Lehner B. Synonymous mutations frequently act as driver mutations in human cancers. Cell. 2014;156(6):1324-1335.

[15] Pagani F, Raponi M, Baralle FE. Synonymous mutations in CFTR exon 12 affect splicing and are not neutral in evolution. Proc Natl Acad Sci U S A. 2005;102(18):6368-72.

[16] Stergachis AB, Haugen E, Shafer A, Fu W, Vernot B, Reynolds A, Raubitschek A, Ziegler S, LeProust EM, Akey JM, Stamatoyannopoulos JA. Exonic transcription factor binding directs codon choice and affects protein evolution. Science. 2013;342(6164):1367-72.

[17] Presnyak V, Alhusaini N, Chen YH, Martin S, Morris N, Kline N, Olson S, Weinberg D, Baker KE, Graveley BR, Coller J. Codon optimality is a major determinant of mRNA stability. Cell. 2015;160(6):1111-24.

[18] Pechmann S, Frydman J. Evolutionary conservation of codon optimality reveals hidden signatures of cotranslational folding. Nat Struct Mol Biol. 2013;20(2):237-43.

[19] Plotkin JB, Kudla G. Synonymous but not the same: the causes and consequences of codon bias. Nat Rev Genet. 2011;12(1):32-42.

[20] Shabalina SA, Spiridonov NA, Kashina A. Sounds of silence: synonymous nucleotides as a key to biological regulation and complexity. Nucleic Acids Res. 2013;41(4):2073-94.

[21] Boël G, Letso R, Neely H, Price WN, Wong KH, Su M, Luff J, Valecha M, Everett JK, Acton TB, Xiao R, Montelione GT, Aalberts DP, Hunt JF. Codon influence on protein expression in E. coli correlates with mRNA levels. Nature. 2016;529(7586):358-363.

[22] Dobson RJ, Munroe PB, Caulfield M J, Saqi MAS. Predicting deleterious nsSNPs: an analysis of sequence and structural attributes. BMC Bioinformatics 2006;7, 217.

[23] Venkata SH, Ramesh BP, Subbiah U. In silico analysis of non-synonymous single nucleotide polymorphisms of human DEFB1 gene. Egypt J Med Hum Genet 2020;21 , 66.

الخلاصة :

الأهداف: صممت هذه الدراسة للتحري عن العلاقة بين التباينات الوراثية في جين IL-18 وهي (rs360717) وقابلية الاصابة بمرض التهاب الامعاء لدى المرضى العراقيين

المرضى و الطرق المستعملة: في هذه الدراسة جمعت ١١٠ عينات الدم ٥٠ عينة من مرضى التهاب الامعاء في مستشفى اليرموك التعليمي ببغداد (٤٠ عينة كانت مناسبة لإجراء الدراسة) بالاضافة الى ٦٠ عينة من الاصحاء (٤٠ عينة منهم اختيرت لإجراء الدراسة) تم استخلاص الحمض النووي من عينات الدم بواسطة مجموعة استخراج الحمض النووي ثم تم تضخيم عينات الحمض بواسطة تقنيةPCR باستخدام بادئات محددة . تم إرسال المنتجات النهائية لمعرفة تسلسلها وللتحقيق من SNPsالنووي

تمت الإشارة إلى اثنين من SNPs في العينات قيد الدراسة rs360717 (+127 C / T) وSNP جديد (T / G). بمقارنة للأنماط الجينية متماثلة الزيجوت متعددة الأشكال بين مجموعة المرضى ومجموعة السيطرة وبين كل مجموعة (UC، CD) ومجموعة السيطرة، لم يتم العثور على اختلاف كبير

في الختام: إن rs360717 (+127 C / T) و SNP (T/G)الجديد في Exon 1 عند IL-18 ليسا عاملين قابلين للإصابة بمرض التهاب الأمعاء لدى السكان العراقيين.

Analytical Solution of the Klein-Gordon Coupled Equations via the Homotopy Perturbation Method

Asal B. Saleh[1, a)] and, Abdulghafor M. Al-Rozbayani[2 b)]

[1, 2] *Department of Mathematics*
College of Computer Science and Mathematics
University of Mosul,
Mosul – Iraq
[a)]*asal.23csp19@student.uomosul.edu.iq*
[b)] *abdulghafor_rozbayani@uomosul.edu.iq*

Analytical Solution of the Klein-Gordon Coupled Equations via the Homotopy Perturbation Method

Asal B. Saleh[1, a)] and, Abdulghafor M. Al-Rozbayani[2 b)]

[1, 2] *Department of Mathematics*
College of Computer Science and Mathematics
University of Mosul,
Mosul – Iraq
[a)]*asal.23csp19@student.uomosul.edu.iq*
[b)] *abdulghafor_rozbayani@uomosul.edu.iq*

ABSTRACT

The fundamental equations in physical applications are the Klein-Gordon equation, which gives a description of scalar particles in the fields of quantum and quantum mechanics, by using the homotopy perturbation method (HPM) and combining it with the Adomian method (ADM), to provide an integrated method for solving this equation, and it has been widely used to solve the system of partial differential equations, to eliminate nonlinear terms and complex terms by combining these two methods, which led to reducing the error and thus increasing the efficiency and accuracy of the solution using these numerical methods and theoretical analysis of the method. Researchers can learn more about the dynamics of the quantum field using our method, which facilitates the study of a wide range of physical phenomena including standard particles. In addition to improving the computational toolkit in relativistic quantum mechanics, this work provides a useful basis for investigating fundamental interactions in the field of particle physics and other fields.

Keywords :Partial Differential equation, Klein-Gordon Equations, Homotopy Perturbation Method, Adomian Decomposition Method

1. Introduction

One of the branches of applied mathematics that fall under important fields is partial differential equations (PDE), which in turn form the cornerstone of the core of mathematical applications, whether engineering or scientific, through understanding and analyzing physical and natural phenomena. Partial differential equations are defined as the coupling between variables of the independent and dependent types. They participate in modeling scientific mathematical systems and their applications by providing representation and modeling for applications in space-time, such as issues of heat transfer, wave motion, fluid motion in pipes and channels, etc [1-3] .In physical applications in general and quantum theory in particular, there are equations that govern these applications. Among these equations and systems are the Klein-Jordan equations, which give a descriptive modeling of the dynamic motion of particles such as mesons. Since these equations are closer and closer to the basic concepts of relativity and the quantum physical field, they also describe the motion and nature of these particles that are characterized by zero spin, and as a result, physical phenomena have

developed in the theory of relativity over time. They also give an impression of the motion and behavior of physical components. It also gives researchers the opportunity to understand these particles in terms of properties and dynamic motion, which in turn facilitates the process of understanding quantum physical phenomena according to the components of matter and its general structure[4-6] .

The principle of analytical methods is to provide a mathematical model for analyzing functions in order to find solutions with an error close to zero, using the basic principles of differential and integral calculus. Expressions such as constants and variables can be determined using various solution methods, including differential and integral calculus for calculating derivatives and integrals, solving differential equations using methods of separation of variables or numerical solution, and numerical analysis such as the Newton-Raphson method for solving nonlinear equations and its mathematical applications such as engineering applications and physics in pure and applied mathematics.

The use of mathematical theories does not find solutions to differential equations and ink and values of integrals and analysis of mathematical functions all generate accurate solutions in these areas, thanks to the systematic and analytical method used [7].

The homotopy Perturbation, Method (HPM) is classified as one of the advanced and reliable methods for finding solutions to differential equations, especially nonlinear ones. This method has gained wide popularity, especially in recent years, thanks to its ability to display satisfactory and accurate results and solutions in various engineering, physical and mathematical fields[8] . It also addresses most mathematical problems and difficulties that cannot be solved by traditional methods. This method is characterized by its spread due to its ability to interact with difficulties and problems known for their complexity and instability, as this method depends on the concept of combining the concept of perturbation and the concept of homotopy. The strategy of this method works to transform nonlinear equations into simple and easy linear equations that can be solved with high efficiency. the homotopy perturbation method (HPM) is also characterized by its great flexibility, or may be somewhat complex[9] .In this method, approximate solutions close to the exact solution can be found, and the efficiency of the approximate solution can be increased through some simple variables of the problem. This method is a flexible and effective tool and has useful results for researchers.

The Adomian Decomposition Method (ADM) is a scientific mathematical method. The main benefit of this method is that it provides an effective way to analyze and solve nonlinear differential equations, which facilitates the solution of complex equations without the need for traditional numerical iterations. It divides mathematical solutions into several small partial solutions, and deals with each solution separately until the problem is solved, by finding solutions from the partial solutions iteratively, which makes mathematical solutions improve. After hybridizing the Adomian Decomposition Method (ADM) with the homogeneous perturbation method, the HPM method became more useful in dealing with complex problems represented by the nonlinear part of differential equations, as the homogeneous perturbation method [10, 11] , Method (HPM) facilitates finding solutions to differential equations by converting them into mathematical equations. Which in turn has become a powerful and effective basic technique for solving complex mathematical problems in many different sciences[12] .

1. Homotopy Perturbation Method (HPM)

HPM is a semi-analytical approach to solve many differential equations[13] , whether linear or nonlinear, This method can also solve systems of linear and nonlinear equations. Jihuan [14] introduced the HPM method in 1999. This approach was developed using Physical parameter [15] .

Most traditional perturbation techniques assume small parameters, however, most nonlinear problems lack small parameters, which causes their determination to be highly skilled and efficient and requires unique methods and techniques, as small parameters are very accurate and sensitive and may directly affect the results even if the change in the parameter value is slight. The accuracy in choosing the optimal and correct small factors leads to good and ideal results, and on the contrary, choosing the wrong small parameters may lead to dire consequences. Liao[16] described the artificial parameter technology at the time. He used the homogeneous analysis method to reduce the assumptions of small parameters[17] . where he proposed two successful methods, namely the variable iteration method (VIM) and the HPM method, which does not need to assume small parameters.

This section provides some explanations of the concept and underlying strategy behind the HPM method, taking into account the following differential equation[18] .

$$\Delta(u) - f(r) = 0 \, , r \in \Omega \tag{1}$$

where Δ represents a general differential operator, f (r) is a known analytic function and defined in the domain Ω , The Δ operator may be split into linear (L) and nonlinear (N) components .

$$\mathcal{L}(u) + \mathrm{N}(u) - f(r) = 0 \tag{2}$$

Equation (2) can be modified to include an artificial parameter q in the following way:

$$\mathcal{L}(u) + q[\mathrm{N}(u) - f(r)] = 0 \tag{3}$$

where $0 \leq q \leq 1$ is an artificial parameter[16, 17] .We build a symmetrical model:

$$\mathrm{H(v,q)} = (1 - \mathrm{q})[\mathcal{L}(\mathrm{v}) - \mathcal{L}(\mathrm{u_0})] + \mathrm{q}[\mathcal{L}(\mathrm{v}) + \mathrm{N(v)} - \mathrm{f\,(r)}] = 0 \tag{4}$$

where $\mathrm{u_0}$ is a function in terms ofand represents the initial condition of the problem x

$$\mathrm{H(v,0)} = [\mathcal{L}(\mathrm{v}) - \mathcal{L}(\mathrm{u_0})] + \mathrm{q}[\mathcal{L}(\mathrm{v}) + \mathrm{N(v)} - \mathrm{f\,(r)}] = 0 \tag{5}$$

$$\mathrm{H(v,1)} = [\mathcal{L}(\mathrm{v}) + \mathrm{N(v)} - \mathrm{f\,(r)}] = 0 \tag{6}$$

$$\mathrm{H(v,1)} = \Delta(u) - f(r) = 0 \tag{7}$$

The value of $\mathrm{v(r,q)}$ shifts from $\mathrm{u_0(r)}$ to $\mathrm{u(r)}$ when q grows from 0 to 1. Deformation is the term used in topology to describe this, and the functions $\mathcal{L}(\mathrm{v}) - \mathcal{L}(\mathrm{u_0})$ and $\Delta(\mathrm{v}) - \mathrm{f\,(r)}$ are homotopic to one another. The solution of Equation (7) is taken into consideration as a power series in q as shown below since $\mathrm{q} \in [0, 1]$ is a tiny parameter.

$$\mathrm{v} = \mathrm{v_0} + \mathrm{q\,v_1} + \mathrm{q^2\,v_2} + \mathrm{q^3 v_3} + \cdots \tag{8}$$

Then, the close answer to equation (8) can be found as

$$u = \lim_{q \to 1} v = v_0 + v_1 + v_2 + v_3 + \cdots \quad (9)$$

2. Application Method

(The Klein-Gordon system) Consider the following [19] .

$$u_{xx} - u_{tt} - u + 2u^3 + 2uv = 0 \quad (10)$$

$$v_x - v_t - 4uu_t = 0 \quad (11)$$

Having exact solution defined by :

$u(x,t) = \sqrt{3}\ sech\ (\frac{2x-t}{\sqrt{3}})$,

$v(x,t) = -2\, sech^2(\frac{2x-t}{\sqrt{3}})$

The initial conditions of the Klein-Gordon system are:

$$u(x,0) = \sqrt{3}\, sech\left(\frac{2x}{\sqrt{3}}\right) \quad (12)$$

$$v(x,0) = -2\, sech^2\left(\frac{2x}{\sqrt{3}}\right) \quad (13)$$

The nonlinear partial differential system was solved using HPM method enhanced by Adomian method ADM and the obtained results were compared with the exact solution. And to facilitate the solution, we will impose the value of $\alpha = \text{sech}\left(\frac{2x}{\sqrt{3}}\right)$ and $\beta = \tanh\left(\frac{2x}{\sqrt{3}}\right)$ in the equation 8 and 9 such that α and β are functions of x .

$$u(x,0) = \sqrt{3}\ \alpha \quad (14)$$

$$v(x,0) = -2\alpha^2 \quad (15)$$

Where the value of ψ is defined and the solution formula is

$$\psi_n = \begin{cases} 0 & n \le 1 \\ 1 & n > 1 \end{cases}$$

and the solution formula is

$$f_m(x,t) = \psi_{n-1}\, f_{m-1}(x,t) + h \int \int H_m(f_{m-1}(x,t)) \quad (16)$$

From equation (8) and (9) initial conditions we get u_0 , v_0 :

$$u_0(x,t) = \sqrt{3}\ \alpha + \frac{\alpha\beta}{\sqrt{3}} t \quad (17)$$

$$v_0(x,t) = -2\ \alpha^2 \quad (18)$$

To find the limits u_1, v_1 we need to apply the adomian method to find the nonlinear limits that we will represent with numbers.

$$A_0 = u_0^3 = \left(\sqrt{3}\alpha + \frac{\alpha\beta}{\sqrt{3}}t\right)^3;$$

$$B_0 = u_0 v_0 = -2\left(\sqrt{3}\alpha + \frac{\alpha\,\beta}{\sqrt{3}}t\right)\alpha^2;$$

$$C_0 = u_0\, u_{0t} = \frac{\left(\sqrt{3}\alpha + \frac{\alpha\beta)}{\sqrt{3}}t\right)\alpha\beta}{\sqrt{3}};$$

Substituting these formulas into general formula (16), we get:

$$u_1 = (h\,(\int_0^t\int_0^t((u_0)_{xx} - ((u_0)_{xx} - u_0 + 2A_0 + 2B_0)dt\,dt) \qquad (19)$$

$$u_1 = \frac{h\alpha^3\beta^3}{30\sqrt{3}}t^5 + \frac{h\,\alpha^3\beta^2}{2\sqrt{3}}t^4 + \frac{4\,h\,\alpha\beta^3}{3\sqrt{3}}t^3 - \frac{23\,h\,\alpha\beta}{18\sqrt{3}}t^3 + \frac{7\,h\,\alpha^3\beta}{9}t^3 + \frac{4h\,\alpha\beta^2}{\sqrt{3}}t^2 - \frac{7\,h\,\alpha}{2\sqrt{3}}t^2 + \sqrt{3}\,h\,t^2\,\alpha^3$$

$$v_1 = (h\left(\int_0^t\int_0^t((v_0)_x - ((v_0)_t) - 4C_0)\,dt\,dt\right) \qquad (20)$$

$$v_1 = -\frac{2\,h\beta^2\alpha^2}{9}t^3 + \frac{4h\,\alpha^2\beta}{\sqrt{3}}t^2 - 2\,h\,t^2\alpha^2\beta$$

To find the limits u_2 , v_2 we need to apply the adomian method to get rid of the non-linear limits which we will represent with the limits:

$$A_1 = 3u_0^2\,u_1 3\left(\sqrt{3}\,\alpha + \frac{\alpha\beta}{\sqrt{3}}t\right)^2\left(\frac{h\alpha^3\beta^3}{30\sqrt{3}}t^5 + \frac{h\,\alpha^3\beta^2}{2\sqrt{3}}t^4 + \frac{4\,h\alpha\beta^3}{3\sqrt{3}}t^3 - \frac{23\,h\,\alpha\beta}{18\sqrt{3}}t^3 + \frac{7\,h\,\alpha^3\beta}{3\sqrt{3}}t^3 + \frac{4\,h\alpha\beta^2}{\sqrt{3}}t^2 - \frac{7\,h\,\alpha}{2\sqrt{3}}t^2 + \sqrt{3}h\,t^2\,\alpha^3\right)$$

$$\begin{aligned} B_1 = u_0\,v_1 + u_1\,v_0 &= \left(\sqrt{3}\alpha + \frac{\alpha\beta}{\sqrt{3}}t\right)\left(-\frac{2\,h\beta^2\alpha^2}{9}t^3 + \frac{4\,h\,\alpha^2\beta}{\sqrt{3}}t^2 - 2ht^2\beta\alpha^2\right) \\ &- 2\alpha^2\left(\frac{h\alpha^3\beta^3}{30\sqrt{3}}t^5 + \frac{h\alpha^3\beta^2}{2\sqrt{3}}t^4 + \frac{4h\,\alpha\beta^3}{3\sqrt{3}}t^3 - \frac{23h\,\alpha\beta}{18\sqrt{3}}t^3 + \frac{7\,h\;\alpha^3\beta}{3\sqrt{3}}t^3\right. \\ &\left. + \frac{4\,h\alpha\beta^2}{\sqrt{3}}t^2 - \frac{7\,h\;\alpha}{2\sqrt{3}}t^2 + \sqrt{3}h\,\alpha^3t^2\right) \end{aligned}$$

$$C_1 = u_0\, u_{1t} + u_1\, u_{0t}$$
$$= \left(\sqrt{3}\alpha + \frac{\alpha\beta}{\sqrt{3}}t\right)\left(\frac{h\alpha^3\beta^3}{6\sqrt{3}}t^4 + \frac{2\,h\,\alpha^3\beta^2}{\sqrt{3}}t^3 + \frac{4\,h\,\alpha\beta^3}{\sqrt{3}}t^2 - \frac{23\,h\,\alpha\beta}{6\sqrt{3}}t^2 + \frac{7\,h\;\alpha^3\beta}{\sqrt{3}}t^2 + \frac{8h\,\alpha\beta^2}{\sqrt{3}}t - \frac{7\,h\,\alpha}{\sqrt{3}}t + 2\sqrt{3}h\,t\,\alpha^3\right)$$
$$+ \frac{1}{3}\left(\left(\frac{h\alpha^3\beta^3}{30\sqrt{3}}t^5 + \frac{h\,\alpha^3\beta^2}{2\sqrt{3}}t^4 + \frac{4\,h\,\alpha\beta^3}{3\sqrt{3}}t^3 - \frac{23\,h\,\alpha\beta}{18\sqrt{3}}t^3 + \frac{7\,h\,\alpha^3\beta}{3\sqrt{3}}t^3 + \frac{4\,h\,\alpha\beta^2}{\sqrt{3}}t^2 - \frac{7\,h\;\alpha}{2\sqrt{3}}t^2 + \sqrt{3}h\,t^2\,\alpha^3\right)\sqrt{3}\alpha\beta\right)$$

$$u_2 = (u_1 + h\,(\int_0^t\int_0^t((u_1)_{xx} - ((u_1)_{xx} - u_1 + 2A_1 + 2B_1)dt\,dt) \qquad (21)$$

$$u_2 = \frac{h\alpha^3\beta^3}{30\sqrt{3}}t^5 + \frac{h\,\alpha^3\beta^2}{2\sqrt{3}}t^4 - \frac{23\,h\,\alpha\beta}{18\sqrt{3}}t^3 + \frac{4\,h\,\alpha\beta^2}{\sqrt{3}}t^2 + \frac{34\;h^2\alpha^3\beta^5}{315\sqrt{3}}t^7 + \frac{2\;h^2\,\alpha^3\beta}{315\sqrt{3}}t^7$$
$$+ \frac{167\;\alpha^5\beta^3\;h^2}{630\sqrt{3}}t^7 - \frac{229\;\alpha^3\,h^2\beta^2}{180\sqrt{3}}t^6 + \frac{22\;h^2\alpha^3\beta^4}{15\sqrt{3}}t^6 - \frac{2\,\alpha^3\beta^3\;h^2}{135\sqrt{3}}t^6$$
$$+ \frac{41\;\alpha^5\,h^2\beta^2}{30\sqrt{3}}t^6 - \frac{14\;h^2\alpha\beta^3}{5\sqrt{3}}t^5 + \frac{16\;h^2\alpha\beta^5}{9\sqrt{3}}t^5 + \frac{221\;h^2\alpha\beta}{216\sqrt{3}}t^5 - \frac{217\;h^2\,\alpha^3\beta}{45\sqrt{3}}t^5$$
$$- \frac{4\;\alpha^3\,h^2\beta^2}{15\sqrt{3}}t^5 + \frac{103\,\alpha^5\,h^2\,\beta}{30\sqrt{3}}t^5 - \frac{62\;h^2\alpha\beta^2}{9\sqrt{3}}t^4 + \frac{16\;h^2\alpha\beta^4}{3\sqrt{3}}t^4 - \frac{h^2\,\alpha^3\beta}{\sqrt{3}}t^4$$
$$+ \frac{577\,h^2\alpha^3\beta^3}{90\sqrt{3}}t^5 + \frac{49\,h^2\alpha^3\beta^2}{6\sqrt{3}}t^4 - \frac{4\,h^2\,\alpha\beta^3}{3\sqrt{3}}t^3 + \frac{23\,h^2\,\alpha\beta}{18\sqrt{3}}t^3 - \frac{7\,h^2\;\alpha^3\beta}{3\sqrt{3}}t^3$$
$$- \frac{4\,h^2\alpha\beta^2}{\sqrt{3}}t^2 + \frac{\alpha^5\beta^5\;h^2}{1080\sqrt{3}}t^9 + \frac{\alpha^5\beta^4\,h^2}{40\sqrt{3}}t^8 - \frac{389\;\alpha^3\beta^3\,h^2}{3780\sqrt{3}}t^7 + \frac{2\,t^4\alpha^3\;h^2\beta}{3}$$
$$- \frac{16\;h^2\;\alpha^3}{3\sqrt{3}}t^4 + \frac{7\,\alpha^5\,h^2}{2\sqrt{3}}t^4 + \frac{113\;h^2\,\alpha}{72\sqrt{3}}t^4 + \frac{2\;h^2\,\alpha^3}{45\sqrt{3}}t^6 + \frac{2\,t^5\alpha^3\beta^2\,h^2}{15}$$
$$+ \frac{7\,h^2\;\alpha}{2\sqrt{3}}t^2 - h^2\,t^2\sqrt{3}\alpha^3 - \frac{7h\;\alpha}{2\sqrt{3}}t^2 + \frac{7\,h\,\alpha^3\beta}{3\sqrt{3}}t^3 + \frac{4\,h\,\alpha\beta^3}{3\sqrt{3}}t^3 + h\,t^2\sqrt{3}\alpha^3$$

$$v_2 = (v_1 + h\left(\int_0^t\int_0^t((v_1)_x - ((v_1)_t) - 4c_1)\,dt\,dt\right) \qquad (22)$$

$$v_2 = -\frac{2\,h\alpha^2\beta^2t^3}{9} + \frac{4\,h\,\alpha^2\beta}{\sqrt{3}}t^2 - 2\,h\,t^2\alpha^2\beta - \frac{2\alpha^4\beta^4\,h^2}{315}t^7 - \frac{2\alpha^4\beta^3\,h^2}{15}t^6 - \frac{46\;\alpha^4\,h^2\beta^2}{45}t^5$$
$$- \frac{16\;\alpha^2\beta^4\,h^2}{45}t^5 + \frac{46\;h^2\alpha^2\beta^2}{135}t^5 - \frac{11\;h^2\alpha^2\beta^2}{18}t^4 + \frac{2\;h^2\alpha^2}{9}t^4 + \frac{h^2\alpha^2\beta^2}{\sqrt{3}}t^4$$
$$- \frac{h^2\alpha^2}{3\sqrt{3}}t^4 - \frac{8\;\alpha^2\,h^2\beta^3}{3}t^4 + \frac{22\;h^2\alpha^2\beta}{9}t^4 - \frac{10\;\alpha^4\,h^2\beta}{3}t^4 - \frac{4\;h^2\alpha^2\beta}{3\sqrt{3}}t^3$$
$$+ \frac{2\;h^2\alpha^2\beta}{3}t^3 - \frac{16\,h^2\alpha^2\beta^2}{3}t^3 + \frac{14\;h^2\alpha^2}{3}t^3 - 4\,t^3\alpha^4\,h^2$$

In the same way, the series for the term $u_3\ and\ v_3$ can be found.

$$u_3 = (u_2 + h\,(\int_0^t\int_0^t((u_0)_{xx} - ((u_2)_{xx} - u_2 + 2A_2 + 2B_2)dt\,dt) \qquad (23)$$

$$v_3 = (v_2 + h\left(\int_0^t \int_0^t ((v_2)_x - ((v_2)_t) - 4C_2)\, dt\, dt\right) \quad (24)$$

After expanding the last two series with additional terms, we can deduce the approximate solution series for u, v by adding the partial series of the series u, v, using the formula:

$$u = u_0 + u_1 + u_2 + u_3 + \cdots$$

$$v = v_0 + v_1 + v_2 + v_3 + \cdots$$

By replacing the values of x and t by fixing one of them and changing the other with some selected values in the system domain, we find the results that we will mention later. Table (1) and (2) also show the absolute error between the exact solutions and the solutions that we obtained from the series. We can obtain high accuracy in the solutions by entering a number of components to find the solution to the series, as Figure (1) and (2) show the solutions to the series for u(x, t), Also, the average square error for the u-series was calculated, as shown in Table 5.

Table1: Numerical values of the u-series at t=0.05

	Error results for a series u			
	x	HPM(x)	EXACT(x)	*Error*
$t = 0.05$	-0.5	1.466767858	1.456181903	$1.06\ E-2$
	-0.4	1.552467428	1.542544789	$9.92\ E-3$
	-0.3	1.625664240	1.616854796	$8.81\ E-3$
	-0.2	1.682425861	1.675194259	$7.23\ E-3$
	-0.1	1.719389579	1.714163912	$5.23\ E-3$
	0	1.734214919	1.731329370	$2.89\ E-3$
	0.1	1.725931338	1.725575852	$3.55\ E-4$
	0.2	1.695089465	1.697279932	$2.19\ E-3$
	0.3	1.643673490	1.648250876	$4.58\ E-3$
	0.4	1.574799886	1.581458003	$6.66\ E-3$
	0.5	1.492284019	1.500617286	$8.33\ E-3$
MSE-Error		$4.69\ E-5$		

Table2 :Numerical values of the u -series at t=0.01

	Error results for a series u			
$t = 0.01$	x	HPM(x)	EXACT(x)	*Error*
	-0.5	1.476149364	1.474224790	1.92 E − 3
	-0.4	1.560211549	1.558500144	1.71 E − 3
	-0.3	1.631332395	1.629919506	1.41 E − 3
	-0.2	1.685667487	1.684632228	1.04 E − 3
	-0.1	1.719992246	1.719397745	5.94 E − 4
	0	1.732137408	1.732021940	1.15 E − 4
	0.1	1.721310472	1.721681631	3.71 E − 4
	0.2	1.688218615	1.689052126	8.34 E − 4
	0.3	1.634958857	1.636202352	1.24 E − 3
	0.4	1.564706111	1.566286817	1.58 E − 3

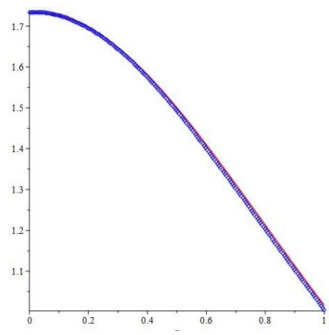

u_{exact}) Solution with approximate solution (**Figure 1**: using Homotopy Perturbation Method at $t = 0.05$

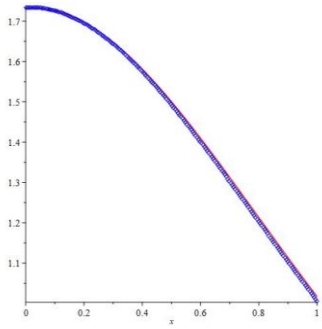

u_{exact}) Solution with approximate solution using (**Figure 2:** Homotopy Perturbation Method at $t = 0.01$

Table (3) and (4) show the absolute error between the exact solutions and the solutions we obtained from the series, and we can obtain high accuracy in the continuous solutions. A number of other elements of the solution to the series, as Figure (3) and (4) show the solutions to the series for v (x,t), Also, the average square error for the v-series was calculated, as shown in Table 6.

Table3: Numerical values of the v -series at t=0.05

	Error results for a series v			
	x	HPM(x)	EXACT(x)	*Error*
$t = 0.05$	-0.5	-1.457033646	-1.413643823	$4.34\ E-2$
	-0.4	-1.626815705	-1.586296284	$4.05\ E-2$
	-0.3	-1.777444645	-1.742812954	$3.46\ E-2$
	-0.2	-1.896603740	-1.870850538	$2.58\ E-2$
	-0.1	-1.973310050	-1.958905278	$1.44\ E-2$
	0	-1.999916480	-1.998334258	$1.58\ E-3$
	0.1	-1.973665210	-1.985074682	$1.14\ E-2$
	0.2	-1.897277532	-1.920506112	$2.32\ E-2$
	0.3	-1.778371748	-1.811153967	$3.28\ E-2$
	0.4	-1.627914766	-1.667339611	$3.94\ E-2$
	0.5	-1.458221065	-1.501234827	$4.30\ E-2$
MSE-Error		$9.77\ E-4$		

Table4: Numerical values of the v-series at t=0.01

	Error results for a series v			
	x	HPM(x)	EXACT(x)	*Error*
$t = 0.01$	-0.5	-1.457642358	-1.448892488	$8.75\ E-3$
	-0.4	-1.627394115	-1.619281801	$8.11\ E-3$
	-0.3	-1.777952572	-1.771091732	$6.86\ E-3$
	-0.2	-1.897000476	-1.891990496	$5.01\ E-3$
	-0.1	-1.973560912	-1.970885738	$2.68\ E-3$
	0	-1.999999333	-1.999933334	$6.60\ E-5$
	0.1	-1.973574977	-1.976125093	$2.55\ E-3$
	0.2	-1.897027161	-1.901931390	$4.90\ E-3$
	0.3	-1.777989296	-1.784772091	$6.78\ E-3$
	0.4	-1.627437659	-1.635502929	$8.07\ E-3$
	0.5	-1.457689412	-1.466421778	$8.73\ E-3$
MSE-Error		$4.00\ E-5$		

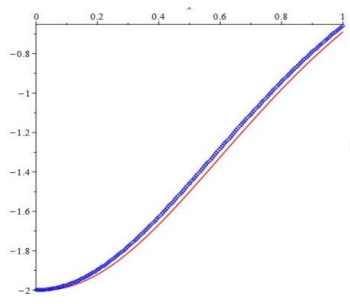

v_{exact}) Solution with approximate solution (**Figure 3:** :
using Homotopy Perturbation Method at $t = 0.05$

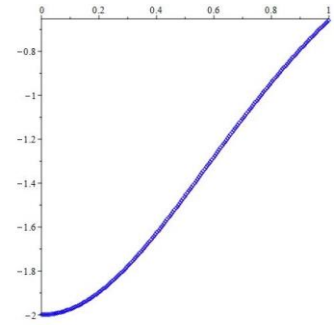

v_{exact}) Solution with approximate solution (**Figure 4**:
using Homotopy Perturbation Method at $t = 0.01$

Table5: Average square error (AVG) for the u-series

t	MSE u	(AVG)
0.05	$4.69\ E-5$	$2.43E-5$
0.01	$1.66\ E-6$	

Table6: Average square error (AVG) for the v -series

t	MSE v	(AVG)
0.05	$9.77\ E-4$	$5.08\ E-4$
0.01	$4.00\ E-5$	

3. Conclusions

The Adomian decomposition method (ADM) and the Homotopy Perturbation Method (HPM) together provide a powerful approach to solve the Klein-Gordon system equation. Our research has demonstrated the effectiveness of this integrated method in solving complex differential equations governing standard particle dynamics efficiently and accurately. The nonlinearities and bounds in the Klein-Gordon system equation have proven to be formidable obstacles, but we have overcome them by combining the two approaches, and the results are robust and reliable. By the proposed method, an

approximate solution close to the exact solution for the u and v series is obtained. These results are considered acceptable based on the calculation of the mean square error for the values $t = 0.01$ and $t = 0.05$, as shown in Tables 1, 2, 3, and 4. In addition, the mean square error (AVG) for the series u and v for all values of t taken in solving this system was calculated and compared with each other, as shown in Tables 5 and 6.

The behavior of standard particles in relativistic quantum mechanics can be better understood with the help of this comprehensive methodology, which also improves computational efficiency. HPM is a powerful and flexible tool for academics in many fields, including applied mathematics, particle physics, and quantum field theory, as our results demonstrate. The future looks bright for tackling more complex systems and improving our understanding of fundamental physical processes as we continue to investigate and develop this integrated approach.

References

[1] G. Evans, J. Blackledge, and P. Yardley, *Analytic methods for partial differential equations*: Springer Science & Business Media, 2012.

[2] M. Schechter, *Modern methods in partial differential equations*: Courier Corporation, 2014.

[3] E. Zauderer, *Partial differential equations of applied mathematics*: John Wiley & Sons, 2011.

[4] C.-Y. Wong, "Klein–gordon equation in hydrodynamical form," *Journal of mathematical physics,* vol. 51, 2010.

[5] M. Dehghan and A. Shokri, "Numerical solution of the nonlinear Klein–Gordon equation using radial basis functions," *Journal of computational and Applied Mathematics,* vol. 230, pp. 400-410, 2009.

[6] A. R. Kanth and K. Aruna, "Differential transform method for solving the linear and nonlinear Klein–Gordon equation," *Computer Physics Communications,* vol. 180, pp. 708-711, 2009.

[7] C. M. Bender and S. A. Orszag, *Advanced mathematical methods for scientists and engineers I: Asymptotic methods and perturbation theory*: Springer Science & Business Media, 2013.

[8] G. O. Ebenezer, "The Application of Homotopy Perturbation Method to the Solution of Non-Linear Partial Differential Equations," *arXiv preprint arXiv:2310.19525,* 2023.

[9] M. Ganjiani, "Solution of nonlinear fractional differential equations using homotopy analysis method," *Applied Mathematical Modelling,* vol. 34, pp. 1634-1641, 2010.

[10] A. Opanuga, E. Owoloko, O. Agboola, and H. Okagbue, "Application of homotopy perturbation and modified Adomian decomposition methods

for higher order boundary value problems," in *Proceedings of the World Congress on Engineering, London, UK*, 2017.

[11] L. Riabi, K. Belghaba, M. H. Cherif, and D. Ziane, "Homotopy perturbation method combined with ZZ transform to solve some nonlinear fractional differential equations," *International Journal of Analysis and Applications,* vol. 17, pp. 406-419, 2019.

[12] F. Soltanian, M. Dehghan, and S.-M. Karbassi, "Solution of the differential algebraic equations via homotopy perturbation method and their engineering applications," *International Journal of Computer Mathematics,* vol. 87, pp. 1950-1974, 2010.

[13] A. K. Farhood and O. H. Mohammed, "Homotopy perturbation method for solving time-fractional nonlinear Variable-Order Delay Partial Differential Equations," *Partial Differential Equations in Applied Mathematics,* vol. 7, p. 100513, 2023.

[14] J.-H. He, "Homotopy perturbation technique," *Computer methods in applied mechanics and engineering,* vol. 178, pp. 257-262, 1999.

[15] G. Liu, "New research directions in singular perturbation theory: artificial parameter approach and inverse-perturbation technique," in *Conference of 7th modern mathematics and mechanics, Shanghai*, 1997, pp. 47-53.

[16] S.-J. Liao, "An approximate solution technique not depending on small parameters: a special example," *International Journal of Non-Linear Mechanics,* vol. 30, pp. 371-380, 1995.

[17] J.-H. He, "Variational iteration method–a kind of non-linear analytical technique: some examples," *International journal of non-linear mechanics,* vol. 34, pp. 699-708, 1999.

[18] J. Biazar and P. S. Derakhsh, "Equivalence of (ADM, HPM, APM) for solving functional equations," *Univ J Eng Sci,* vol. 2, pp. 1-5, 2014.

[19] K. Khan, M. A. Akbar, and S. R. Islam, "Exact solutions for (1+ 1)-dimensional nonlinear dispersive modified Benjamin-Bona-Mahony equation and coupled Klein-Gordon equations," *SpringerPlus,* vol. 3, pp. 1-8, 2014.

Enhance Penetration Testing Techniques to Improve Cybersecurity with NetLogo, Nmap, and Wireshark

Huthaifa Mohammed Kanoosh[1] Mohammed Muayad Sultan[2] Ammar Farooq Abbas[3]

[1,3] Department of Computer Science, College of Computer Science and Mathematics, Tikrit University, Tikrit, Iraq.

[2] Mathematics Department, Tikrit University, College of Education of Girls, Tikrit University, Tikrit, Iraq.

[1]E-mail: huthife@tu.edu.iq, [2] E-mail: Mmsultan@tu.edu.iq, [3] E-mail: ammar.abbas@tu.edu.iq

Enhance Penetration Testing Techniques to Improve Cybersecurity with NetLogo, Nmap, and Wireshark

Huthaifa Mohammed Kanoosh[1] Mohammed Muayad Sultan[2] Ammar Farooq Abbas[3]

[1,3] Department of Computer Science, College of Computer Science and Mathematics, Tikrit University, Tikrit, Iraq.

[2] Mathematics Department, Tikrit University, College of Education of Girls, Tikrit University, Tikrit, Iraq.

[1]E-mail: huthife@tu.edu.iq, [2] E-mail: Mmsultan@tu.edu.iq, [3] E-mail: ammar.abbas@tu.edu.iq

Abstract

This study will try to address the complex network security dimensions using a multidimensional approach involving a NetLogo simulation, Nmap scanning, and Wireshark analysis. The NetLogo simulation model ensures an accurate insight into the dynamics of penetration testing and defense strategies of networks thereby allowing a better understanding of interactions amongst different elements in the network and how they affect security from practice (defensive and offensive) to comprehensive security. Information provided by Nmap scanning is used for hosts and services on the network in detail these aid in identifying and assessing potential vulnerabilities as well as enhancement of security strategies. Wireshark analysis focuses on packet transfer behaviors, describing ways communication patterns are identified as well as how to detect suspicious activities: and possible intrusions. At its core, findings accentuate network security as complex, digital assets needing protection through robust defense mechanisms.

Keywords: Cybersecurity, Ethical hacking, Network Security, NetLogo, Nmap, and Wireshark.

1. Introduction

In the modern digital age, our daily life and business continuity highly depend on interconnected systems and electronic platforms. Due to this increasing dependence on technology, new advanced cyber threats have evolved that can harm data security and system integrity. Cybersecurity is the practice of protecting information and systems from these digital attacks which could cause large financial losses as well as damage the reputation of organizations, or even governments. Ethical hacking has now become one of the most important tools in cybersecurity by which security vulnerabilities in systems are identified before they are attacked by a hacker so that such operations are performed with the permission network or system owner to enhance security by managing networks to find vulnerabilities early [1][2]. The study is based on how well-advanced tools can be used in the operation of ethical hacking, specifically NetLogo, Nmap, and Wireshark. NetLogo contributes to capturing a vision of systems' behavior and pre-visioning how various systems will act in response to different conditions, thus shedding light on potential vulnerabilities. Nmap proves to be a robust network finding and auditing tool that aids in listing down all connected devices as well as open services that would be possible targets for attacks. However, in this paper, we used Wireshark as a tool to help view data packets as they move across the network and identify any malicious activity that could be an attempt to hack [3]. The widespread use of sensitive data in networks has highlighted the difficulties faced by cybersecurity researchers, especially in defending against cyberattacks on their systems, which have been increasing in recent years. For this reason, experts have had to implement complex, adaptable, and changeable defense plans to keep up with the threats [4]. The process of integrating ethical hacking with advanced technologies can greatly

help organizations secure their data and systems. This paper aims to provide comprehensive insights into enhancing cybersecurity with the aforementioned tools and guide researchers and professionals to adopt more adaptable and efficient tactics to confront the growing threats [5].

2. Research Problem

Cyberattacks pose a real and growing threat to information infrastructure in all sectors. The number of cyberattacks has reportedly increased significantly [6]. The company said in its study that cybercrime growth in some countries around the world exceeded 50% between 2016 and 2023, and pointed out the prevalence of cyberattacks, especially ransomware attacks, in its published research. The study showed that the number of ransomware attacks in 2021 increased by 64% compared to the previous year [7]. This growth is because it is becoming easier to carry out these attacks and the availability of attack tools on the dark web at reasonable prices, which has led to a very rapid growth in such attacks. Organizations have suffered significant financial losses due to these attacks. This problem is compounded by the inadequacy of traditional tools and strategies in the face of these sophisticated attacks. This is where the role of ethical hackers proves to be an effective tool in identifying security vulnerabilities before attackers exploit them [8].

3. Research Objectives

This research delves into facets of network security. It centers on three tools: NetLogo, for simulating networks, Nmap for scanning networks and detecting vulnerabilities, and Wireshark for analyzing network traffic. The study investigates the security hurdles faced by networks and aims to offer insights

and actionable approaches to enhance network security. Furthermore, it assesses the efficiency of the tools employed. Offers suggestions, for enhancing security protocols.

4. Previous Studies

Mirjalili et al. (2021) explored the concept of penetration testing, in web development underscoring the significance of identifying security weaknesses in web applications to safeguard data. They also pointed out methods like SQL injection and cross-site scripting (XSS). How they can be used to exploit vulnerabilities in web apps. The findings of this research help shed light on the importance of penetration testing in web applications ensuring an environment for users. This study extends its focus beyond web development to networking aspects by utilizing tools, like Nmap and Wireshark [9]. Zhang et al. (2021) researchers examined the vulnerabilities in industrial control systems (ICS) and highlighted the unique challenges these systems face due to their sensitive nature. The study proposed models and techniques to assess and enhance the security of these systems. Through analyzing real-world cases the study showcased how cyberattacks can lead to harm to industrial control systems. It underscores the importance of conducting security assessments for intricate systems. Subsequent research has leveraged these insights to expand security evaluations to enterprise networks offering an understanding of security risks and diverse preventive measures [10]. Saravanan et al. (2021), A research study delved into how mobile technology affects security emphasizing that mobile devices serve as targets for cyberattacks. The research revealed the vulnerabilities of applications to attacks when lacking proper security measures. Ongoing investigations address these risks. Employ tools, like Wireshark to

scrutinize transmission patterns and detect any dubious activities potentially stemming from mobile devices [11]. Yunita et al. (2022), examined soil resilience in the context of infrastructure development and pointed out the importance of improving security in digital infrastructure projects. Although the focus was on physical infrastructure, the study highlighted the need for strong security in all aspects of large projects. Although the research primarily addresses infrastructure its principles are also relevant, to infrastructure. Recent studies utilize these findings to strengthen security measures, in networks emphasizing the significance of implementing comprehensive defense tactics [12]. Altulaihan et al. (2023), Explored the significance of safeguarding web applications. Highlighted the growing vulnerabilities stemming from input verification. The research outlined methods to mitigate these weaknesses and enhance security an aspect of networks. Building upon these tactics the ongoing study extends their application to enhance network security overall by leveraging tools, like Nmap and Wireshark [13]. Leroy (2024), The article discusses the expanding role of intelligence, in cybersecurity. It focuses on introducing ReaperAI, an AI agent created to simulate and carry out cyberattacks. Developed with the help of language models like GPT 4, it showcases its capability to independently identify, exploit, and assess vulnerabilities. The study also introduces methods to enhance the effectiveness and performance of this agent including utilizing task-oriented testing frameworks AI-powered command generation and enhanced prompting techniques. Testing conducted on platforms like Hack the Box has revealed ReaperAIs proficiency in exploiting known vulnerabilities underscoring its potential, in cybersecurity [14].

5. Conclusion of Previous Studies

Prior research has highlighted the significance of cybersecurity, across domains spanning from web apps to platforms and mobile devices. Building upon this existing knowledge the present study introduces an approach that incorporates tools, for evaluating and bolstering network security. The findings derived from these investigations offer insights aimed at enhancing measures and mitigating cyber risks effectively.

6. Research Methodology

The research process involves planning how the study will be conducted, gathering data in ways analyzing the data collected, considering aspects, and acknowledging any limitations, in the research. Tools like NetLogo, Nmap, and Wireshark are used to help achieve research goals. NetLogo is utilized for simulating network behavior, Nmap for identifying vulnerabilities in networks, and Wireshark for analyzing transmissions. Data is gathered through simulations, network scans, and direct observations with precision. Statistical and qualitative analysis methods are applied to uncover patterns and connections, among factors while upholding standards by ensuring data confidentiality and privacy protection.

7. Tools Used in the Current Research

a. NetLogo

NetLogo serves as a versatile simulation platform enabling users to construct and execute models that mimic the behaviors of systems. It is utilized for developing models offering users the ability to directly modify and interact with models fostering an engaging learning experience that aids in deepening comprehension of scientific concepts. Additionally, it facilitates the creation of an

interactive and adaptable learning environment. Known for being user-friendly and open-source, NetLogo empowers researchers to tailor models to explore scenarios. Researchers can adjust variables within the model or network such, as the rate of news dissemination, credibility fact-checking probability, and user (agent) forgetfulness rate [15].

b. Nmap

Nmap, also known as Network Mapper, is a tool that helps in exploring networks and recognizing both hosts and security weaknesses within the network. It can conduct security scans, locate devices, on the network uncover open ports, and reveal services accessible through those ports. Additionally, this tool offers flexibility by enabling users to tailor scans according to their requirements either through commands or by creating scripts, to automate the process entirely [16]. Nmap sends data packets to designated targets, within the network assessing the ensuing responses to extract details about said targets. This tool proves valuable and user-friendly for conducting network security analysis and monitoring emphasizing its importance, as a component of organizations' information security strategies [17].

c. Wireshark

Wireshark is a tool that allows for the examination and monitoring of data transmitted through network packets. It is instrumental in analyzing the behaviors of transfers including details like source, destination, and the type of protocol utilized thereby aiding in the detection of suspicious activities. The tool proves beneficial in identifying and studying attacks associated with protocols enabling users to filter, search, and generate statistics for an analysis of captured data. Being source and user-friendly Wireshark supports network

protocols and seamlessly integrates with systems, like intrusion detection systems to pinpoint potential threats and enhance network security [18][19][20].

8. Methods Generally Used Currently and Previously

a. Traditional methods of penetration testing

At times penetration testing methods depend a lot on tools and basic techniques to discover vulnerabilities. Testers had to scan networks and search for vulnerabilities without the aid of advanced tools to make the process easier.

b. Modern and advanced tools

With the progress of technology, new and improved tools for penetration testing and security analysis like Metasploit, Nessus, and Burp Suite have been developed. These tools offer enhanced functionalities to detect vulnerabilities and conduct network analysis, with precision and efficiency. Their capabilities encompass identifying vulnerabilities, scanning networks, and performing automated penetration tests.

9. Research Results

a. Network simulation using NetLogo:

- The simulation illustrated the interactions, among network components. Highlighted the impact of security measures on network security. Through this simulation, valuable insights were gained on enhancing network infrastructure, for security. Based on Figure 1, we have a space filled with creators of red and blue characters.

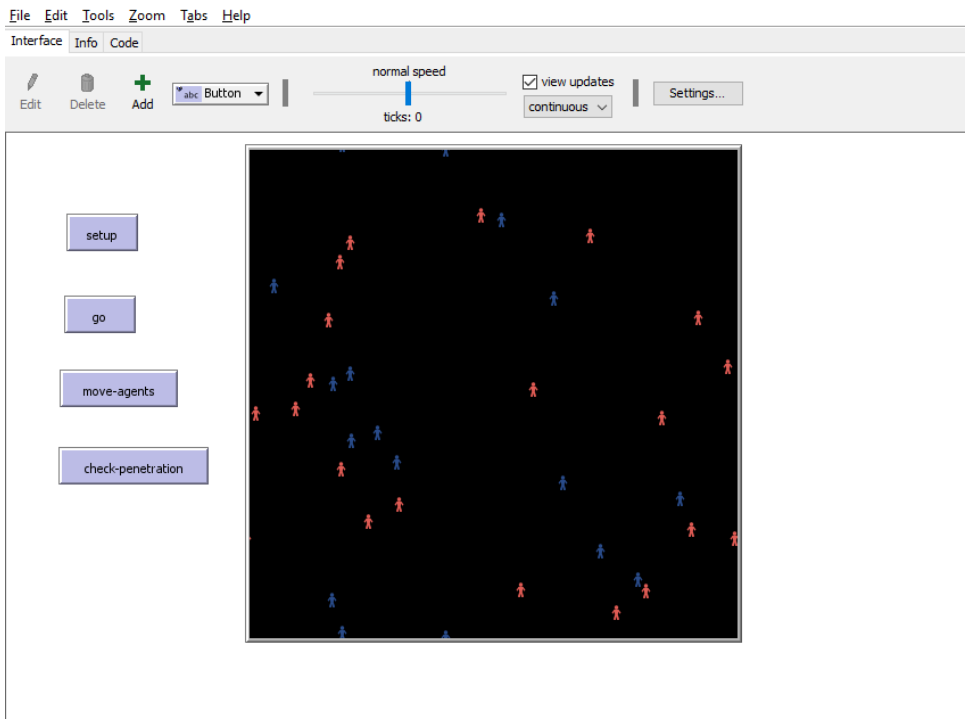

Figure 1 ***Error! No text of specified style in document.*** **Netlogo space and User-**

Red characters refer to the attackers on the network, while the blue refer to the defenders of the network is:

1. **Global Variables**:
    - **hackers**: This variable stores the number of hacker turtles (Software objects, virtual elements, or the basic element used in the simulation environment) in the simulation.
    - **defenders**: This variable stores the number of defender turtles in the simulation.
2. **Setup Procedure (setup)**:
    - **Clear All: Clear the current state of the world.**

- **Set Default Turtle Shape to "Person": Set the default turtle shape to "Person".**
- **Set Intruders 20**: Set the number of Intruders to 20.
- **Set Defenders 15**: Set the number of Defenders to 15.
- **Create Hacker Turtles [...]**: Creates Hacker Turtles based on the value stored in the Hacker variable. Each Hacker Turtle is assigned a red + 1 color and placed in a random location in the world.
- **Create Defender Turtles [...]**: Creates Defender Turtles based on the value stored in the Defenders variable. Each Defender Turtle is assigned a blue color − 1 and placed in a random location in the world.
- **Reset Marks**: Resets the mark counter to zero, indicating that the simulation has started.

3. **Go action**:

• **Move-Agents**: Call the move-agents procedure to move all turtles.

• **Check-Penetration**: Call the check-penetration procedure to detect and handle hacking attempts.

• **Tick**: Increments the tick counter by one, which advances the simulation by a one-time step.

4. **Move-Agents**: Call the move-agents action to move all turtles.

- This action is responsible for moving all turtles (intruders and defenders) randomly.

- Each turtle rotates at a random angle between 0 and 50 degrees (rt random 50) and moves forward by one step (fd 1).

5. **Check Penetration Procedure (check-penetration):** Call the check-penetration action to detect and handle hacking attempts.
    - This procedure is called to check if the intruders are within range to attack the defenders.
    - It first selects all the intruder turtles as red + 1.
    - For each intruder turtle, it selects potential defender targets within a radius of 3.
    - If there are potential targets, it randomly selects one target using one of them and calls the attack procedure on that target.
    - **Tick:** Increment the tick counter by one, which advances the simulation by a one-time step.

6. **Attack Procedure (attack):**
    - This procedure is called to simulate an attack by a hacker on a defender.
    - It takes the target defender turtle as a parameter (**[target]**).
    - It kills the target defender turtle by calling the **die** procedure on it.

7. **Set Hackers and Set Defenders Procedures:**

These procedures allow you to dynamically change the number of hackers and defenders during the simulation by setting the values of the **hacker's** and **defender's** global variables.

The global variables for attackers and defenders act as parameters that define the initial conditions of the simulation. These variables determine the number of attackers and defenders in the environment. The setup process begins by initializing the simulation environment by scanning the world and setting the default appearance of the turtles to “person”. It then determines the initial number of attackers and defenders using global variables. Attackers and defenders are generated and randomly distributed across the world.

Once setup is complete, the move action governs the progress of the simulation over time. It calls two sub-actions: move agents and check attack, before advancing the simulation time with a single click. The move agent's action determines the movement behavior of the turtles in the simulation. Each turtle, whether attacker or defender, rotates randomly at a specified angle (between 0 and 50 degrees) and moves forward one step. This random movement creates dynamic interactions between agents in the environment.

The optional hack maneuver is, in charge of spotting attacks that assailants could carry out against protectors. Initially, it pinpoints all assailants. Then locates targets for protectors within a designated range. If potential targets are discovered one target is chosen randomly. The assault maneuver is executed. This maneuver imitates an attack by a hacker on a protector. Upon activation, it utilizes the target turtle, as input. Eliminates it from the simulation by executing the dice move.

Finally, the set penetration maneuvers and designated defenders offer the ability to adapt the quantity of hackers and defenders in time during the simulation. This functionality enables users to experiment with scenarios and tactics, within the simulated setting. Essentially the code manages the

engagement between hackers and defenders, in an environment, where hackers strive to breach and assail defenders while defenders work to safeguard themselves. The actions defined for each entity drive their behavior leading to an understanding of penetration testing dynamics.

a. Scan the network using Nmap:

Network scanning revealed multiple security vulnerabilities in corporate networks. The results showed the importance of using advanced tools such as Nmap to identify and remediate these vulnerabilities before they can be exploited by attackers.

As shown in Figure 2 The results of the Nmap scanning reveal detailed information about the network hosts and the services running on them. Here's a breakdown of the findings:

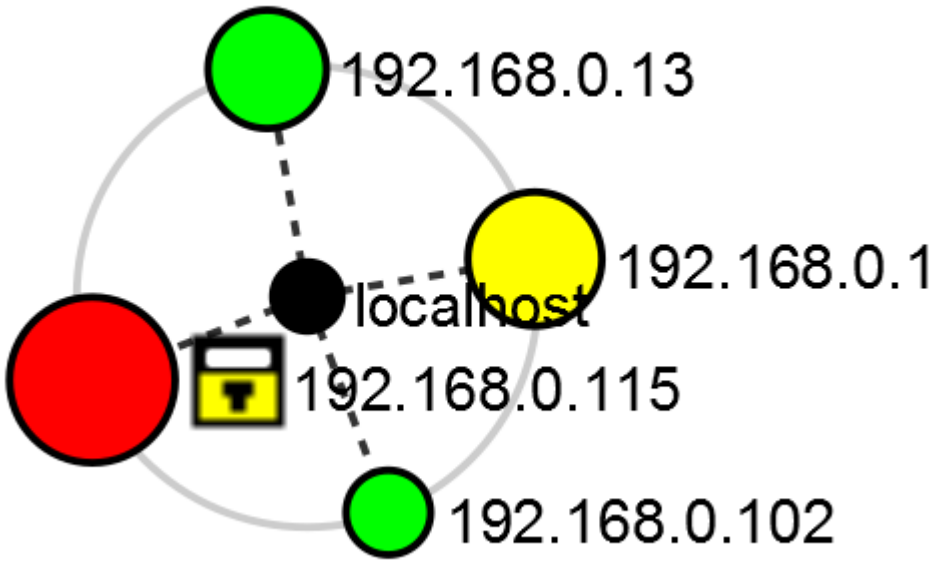

Figure 2 Nmap network Topology Detected over network Scan

1. **192.168.0.1**
    - Host is up with low latency (0.0100s).
    - Open ports:
        - 22/tcp: SSH
        - 53/tcp: Domain
        - 80/tcp: HTTP
        - 1900/tcp: UPnP
    - MAC Address: D8:47:32:04:EA:C6 (TP-Link Technologies)
2. **192.168.0.13**

- Host is up with low latency (0.010s).
- Open ports:
  - 22/tcp: SSH
  - 80/tcp: HTTP
- MAC Address: B0:4E:26:7D:15:7E (TP-Link Technologies)

3. **192.168.0.102**
   - Host is up with low latency (0.011s).
   - All 100 scanned ports are in ignored states.
   - MAC Address: 42:5C:A9:A0:B5:1F (Unknown)

4. **192.168.0.115**
   - Host is up with extremely low latency (0.000020s).
   - Open ports:
     - 135/tcp: MSRPC
     - 139/tcp: NetBIOS-SSN
     - 445/tcp: Microsoft-DS
     - 1433/tcp: MS-SQL-S

The Nmap scan results provide insightful details about the network hosts and the services they provide. Across the scanned IP addresses, several notable findings emerged. First, at 192.168.0.1, the scan detected an active host with minimal latency, revealing open ports for SSH, Domain, HTTP, and

UPnP services, along with the MAC address associated with TP-Link technologies. Similarly, 192.168.0.13 showed a response with open ports for SSH and HTTP services, also associated with TP-Link technologies via its MAC address. However, at 192.168.0.102, despite the host responding immediately, all scanned ports were in the Ignore state, indicating potential security configurations or firewall restrictions. Finally, 192.168.0.115 showed a fast response and revealed open ports for MSRPC, NetBIOS-SSN, Microsoft-DS, and MS-SQL-S services, highlighting a variety of network functions. Overall, the Nmap scan provided basic insights into the network topology, helping administrators assess vulnerabilities, improve security configurations, and strengthen network defenses against potential threats.

b. Analysis of packet transmission using Wireshark:

- Packet transfer analysis helped identify suspicious activities and potential threats within the network. The results showed how Wireshark can be used to detect and combat threats in real-time.

In Figure 3 of the Wireshark results a series of TCP acknowledgments (ACKs) is captured from the source IP address 192.168.0.115 to the destination IP address 104.18.103.100, through port 443. The sequential acknowledgments indicate that the sender received the data packets successfully. Each packet is 54 bytes in size suggesting small data transfers

took place. The consistent pattern of acknowledgments with increasing acknowledgment numbers (Ack) and window sizes (Win) suggests communication between the source and destination hosts. The timestamps show an exchange of packets within a period underscoring the efficiency of the data transfer process. In summary insights from Wireshark results shed light on network traffic dynamics and communication trends, between the source and destination hosts during a timeframe.

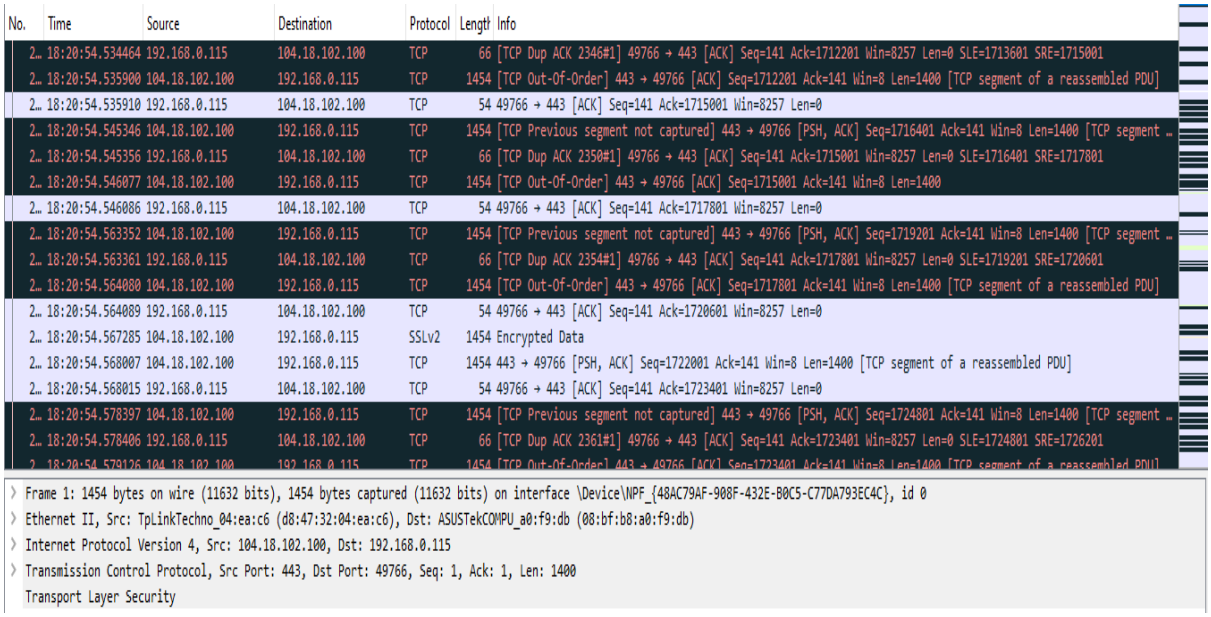

Figure *3* Discover Transmitted Packets Over the Network Using Wireshark

10. Summary of the Results

The results obtained from the NetLogo simulation, Nmap scanning, and Wireshark analysis offer comprehensive insights into different aspects of network behavior, penetration testing, and packet transmission dynamics.

- NetLogo Simulation Results:

- The simulation orchestrates interactions between hackers and defenders within a simulated environment.
- Global variables define the initial conditions, including the number of hackers and defenders.
- The setup procedure initializes the simulation environment, creating and distributing turtles randomly.
- The go procedure governs the simulation progression over time, invoking sub-procedures for movement and penetration checks.
- Movement procedures dictate random movement behaviors for turtles.
- Penetration check procedures assess potential attacks and simulate hacker-defender interactions.
- Dynamic adjustment procedures allow for real-time changes to hacker and defender counts, facilitating scenario exploration.

- Nmap Scanning Results:

Detailed data on network hosts and the services they offer was revealed. The analysis also noted the responsiveness and open ports, along with MAC addresses. Key discoveries include hosts providing services possibly restricted ports and overlooked ports suggesting security setups.

- Wireshark Analysis Results:

- Captured TCP acknowledgments between specific source and destination IPs over port 443.
- Sequential acknowledgments with consistent packet lengths indicate ongoing data exchanges.
- Timestamps reveal rapid packet exchange within a short timeframe, suggesting efficient communication.

In summary, the NetLogo simulation helps us understand how hackers and defenders interact while Nmap scanning uncovers network structure and service specifics. Wireshark analysis illuminates the dynamics of transmission. When combined these findings give us an understanding of network behavior assisting in evaluating vulnerabilities optimizing security and developing defense tactics.

11. Conclusion and Recommendations

This paper delves into the intricacies of network security by taking an approach that leverages tools, like NetLogo for simulating networks, Nmap for vulnerability scanning and Wireshark for analyzing packets. The main goal was to grasp the complexities of cyber threats and devise strategies to bolster cybersecurity in networks. This study offers a framework for scrutinizing and boosting network security through penetration testing and network analysis tools. The insights gained offer guidance for organizations looking to safeguard their data and systems against evolving cyber threats. By implementing these recommendations organizations can strengthen their defense mechanisms. Ensure the safety of their networks, in todays landscape.

Based on the findings, the following recommendations can be made to enhance cybersecurity in enterprise networks:

1. Adoption of advanced penetration testing tools: organizations are encouraged to use penetration testing tools, like NetLogo, Nmap, and Wireshark for analyzing networks and identifying vulnerabilities.

2. Employee cybersecurity training: training employees on cybersecurity best practices and how to use advanced tools can reduce the risk of cyberattacks.

3. Develop advanced defense strategies: organizations must develop and update their defense strategies regularly to keep pace with growing and evolving cyber threats.

4. Conduct periodic security reviews: conducting periodic security reviews of networks and infrastructure can help uncover and address security vulnerabilities before they are exploited.

12. Acknowledgements

We are very pleased to present this work on improving penetration testing techniques to improve cybersecurity, and we would like to express our deep gratitude to those who offered their valuable time and guidance in my time of need. It is a great honor to do this work in the esteemed Department of Computer Science, College of Computer Science and Mathematics, Tikrit University, Iraq.

References

[1] R. Shandler and M. A. Gomez, “The hidden threat of cyber-attacks–undermining public confidence in government,” Journal of Information Technology and Politics, vol. 20, no. 4, pp. 359–374, 2023, doi: 10.1080/19331681.2022.2112796.

[2] U. Inayat, M. F. Zia, S. Mahmood, H. M. Khalid, and M. Benbouzid, “Learning-Based Methods for Cyber Attacks Detection in IoT Systems: Methods, Analysis, and Future Prospects,” May 01, 2022, MDPI. doi: 10.3390/electronics11091502.

[3] B. Huang, Y. Li, F. Zhan, Q. Sun, and H. Zhang, “A Distributed Robust Economic Dispatch Strategy for Integrated Energy System Considering Cyber-Attacks,” IEEE Trans Industr Inform, vol. 18, no. 2, pp. 880–890, Feb. 2022, doi: 10.1109/TII.2021.3077509.

[4] Ö. Aslan, S. S. Aktuğ, M. Ozkan-Okay, A. A. Yilmaz, and E. Akin, “A Comprehensive Review of Cyber Security Vulnerabilities, Threats, Attacks, and Solutions,” Mar. 01, 2023, MDPI. doi: 10.3390/electronics12061333.

[5] W. Duo, M. Zhou, and A. Abusorrah, “A Survey of Cyber Attacks on Cyber Physical Systems: Recent Advances and Challenges,” IEEE/CAA Journal of Automatica Sinica, vol. 9, no. 5, pp. 784–800, May 2022, doi: 10.1109/JAS.2022.105548.

[6] A. Kuzior, I. Tiutiunyk, A. Zielińska, and R. Kelemen, “Cybersecurity and cybercrime: Current trends and threats,” JOURNAL OF INTERNATIONAL STUDIES, vol. 17, no. 2, pp. 220–239, Jun. 2024, doi: 10.14254/2071-8330.2024/17-2/12.

[7] S. Temara, “Article no.AJARR.112469 Review Article Temara,” Asian Journal of Advanced Research and Reports, vol. 18, no. 3, pp. 1–16, 2024, doi: 10.9734/ajarr/2024/v18i3610ï.

[8] C. Bain and U. Wilensky, “Sorting Out Algorithms: What Makes One Better than Another?,” in Proceedings of the 50th ACM Technical Symposium on Computer Science Education, New York, NY, USA: ACM, Feb. 2019, pp. 1278–1278. doi: 10.1145/3287324.3293856.

[9] M. Mirjalili, A. Nowroozi, and M. Alidoosti, “A survey on web penetration test.” [Online]. Available: https://www.researchgate.net/publication/270523617

[10] Y. Zhang, J. Wu, D. Wang, and S. zhang, “Research and application of penetration testing method in industrial control system,” SPIE-Intl Soc Optical Eng, Dec. 2021, p. 43. doi: 10.1117/12.2624840.

[11] D. Saravanan and D. Stalin David, “Portable Appliance Penetration Testing and Susceptibility Assessment,” Artech Journal of Effective Research in Engineering and Technology (AJERET), vol. 2, pp. 7–12, 2021, [Online]. Available: http://www.csoonline.com/article

[12] H. Yunita et al., “Spatially Distribution of Soil Ultimate Bearing Capacity at Singkil-Aceh Based on a Static Cone Penetration Test,” Aceh International Journal of Science and Technology, vol. 11, no. 1, pp. 1–11, Apr. 2022, doi: 10.13170/aijst.11.1.23287.

[13] E. A. Altulaihan, A. Alismail, and M. Frikha, “A Survey on Web Application Penetration Testing,” Mar. 01, 2023, MDPI. doi: 10.3390/electronics12051229.

[14] L. J. Valencia, “Artificial Intelligence as the New Hacker: Developing Agents for Offensive Security,” May 2024, [Online]. Available: http://arxiv.org/abs/2406.07561

[15] E. Sulis and M. Tambuscio, “Simulation of misinformation spreading processes in social networks: an application with NetLogo.” [Online]. Available: https://el.media.mit.edu/logo-foundation/

[16] S. Stošović, N. Vukotić, D. Stefanović, and N. Milutinović, “Automation of Nmap Scanning of Information Systems,” in 2024 23rd International Symposium INFOTEH-JAHORINA (INFOTEH), IEEE, Mar. 2024, pp. 1–5. doi: 10.1109/INFOTEH60418.2024.10496014.

[17] D. Bayu Rendro and W. Nugroho Aji, “ANALISIS MONITORING SISTEM KEAMANAN JARINGAN KOMPUTER MENGGUNAKAN SOFTWARE NMAP (STUDI KASUS DI SMK NEGERI 1 KOTA SERANG),” vol. 7, no. 2, 2020.

[18] G. Jain and Anubha, “Application of SNORT and Wireshark in Network Traffic Analysis,” IOP Conf Ser Mater Sci Eng, vol. 1119, no. 1, p. 012007, Mar. 2021, doi: 10.1088/1757-899x/1119/1/012007.

[19] R. Afzal and R. K. Murugesan, “Implementation of a Malicious Traffic Filter Using Snort and Wireshark as a Proof of Concept to Enhance Mobile Network Security,” Journal of Telecommunications and Information Technology, vol. 2022, no. 1, pp. 64–71, 2022, doi: 10.26636/jtit.2022.155821.

[20] N. Alsharabi, M. Alqunun, and B. A. H. Murshed, “Detecting Unusual Activities in Local Network Using Snort and Wireshark Tools,” Journal of Advances in Information Technology, vol. 14, no. 4, pp. 616–624, 2023, doi: 10.12720/jait.14.4.616-624.

تعزيز تقنيات اختبار الاختراق لتحسين الأمن السيبراني باستخدام NetLogo و Nmap و Wireshark

المستخلص

تقدم هذه الورقة طريقة لمعالجة أبعاد أمن الشبكات المعقدة وذلك من خلال استخدام ادوات متعددة لتحقيق النهج المطلوب، وذلك باستخدام NetLogo لمحاكاة بيانات الشبكة ومسحها من خلال Nmap واستخدام Wireshark لتحليل البيانات. يضمن نموذج محاكاة NetLogo نظرة ثاقبة دقيقة لديناميكيات اختبار الاختراق واستراتيجيات الدفاع للشبكات مما يتيح فهم أفضل للتفاعلات بين العناصر المختلفة في الشبكة وتئثيرها على امن الشبكة من الممارسة (الدفاعية والهجومية) للوصول إلى الأمن الشامل لها. تم استخدام جيمع تفاصيل بيانات الشبكة اثناء عملية المسح من خلالNmap ، مما ساعد في تحديد وتقييم نقاط الضعف المحتملة في الشبكة و تحديد الإضافات المناسبة لتعزيز استراتيجيات الأمان. اما Wiresharkفركز على تحليل سلوكيات نقل الحزم، ووصف الطرق التي يتم بها تحديد أنماط الاتصال بالإضافة إلى كيفية اكتشاف الأنشطة المشبوهة والاختراقات المحتملة. اكدت نتائج البحث على أمن الشبكة كأصول رقمية معقدة تحتاج إلى الحماية من خلال آليات دفاع قوية, ووضع رؤية شاملة حول جوانب مختلفة من سلوك الشبكة واختبار الاختراق وديناميكيات نقل الحزم من خلال تنظم المحاكاة و تحليل التفاعلات بين المتسللين والمدافعين داخل بيئة محاكاة.